In situ, time-resolved, and mechanistic studies of metal-organic framework nucleation and growth

Mary J. Van Vleet, Tingting Weng, Xinyi Li, and J.R. Schmidt*

Theoretical Chemistry Institute and Department of Chemistry, University of Wisconsin–Madison, Madison, Wisconsin, 53706, United States

E-mail: schmidt@chem.wisc.edu

Abstract

The vast chemical and structural diversity of metal-organic frameworks (MOFs) opens up the exciting possibility of "crystal engineering" MOFs tailored for particular catalytic or separation applications. Yet the process of reaction discovery, optimization, and scale-up of MOF synthesis remains extremely challenging, presenting significant obstacles to the synthetic realization of many otherwise promising MOF structures. Recently, significant new insights into the fundamental processes governing MOF nucleation and growth, as well as the relationship between reaction parameters and synthetic outcome, have been derived using powerful in situ, time-resolved and/or mechanistic studies of MOF crystallization. This Review provides a summary and associated critical analysis of the results of these and other related "direct" studies of MOF nucleation and growth, with a particular emphasis on the recent advances in instrument technologies that have enabled such studies and on the major hypotheses, theories, and models that have been used to explain MOF formation. We conclude

with a summary of the major insights that have been gained from the work summarized in this Review, outlining our own perspective on potential fruitful new directions for investigation.

Mary Van Vleet Mary J. Van Vleet is a Visiting Assistant Professor of Chemistry at Harvey Mudd College, from which she also received her B.S. in 2012. She has a Ph.D. in Physical Chemistry from the University of Wisconsin–Madison (with J.R. Schmidt) in 2017, focusing on methodological advances in first-principles force field development. Prof. Van Vleet's current research interests involve simultaneously expanding the accuracy and broad applicability of force fields to model traditionally challenging functional groups in organic chemistry.

Tingting Weng Tingting Weng received her B.S. in chemistry in 2014 from USTC in Hefei, China. She is currently a Ph.D. student under the supervision of Prof. J.R. Schmidt, at the University of Wisconsin–Madison. Her research is focused on the simulation studies of the nucleation and growth of metal-organic framework materials, with an initial goal of developing flexible force field for zeolitic imidazolate frameworks.

Xinyi Li Xinyi Li earned his B.S. in chemical physics in 2015 from University of Science and Technology of China. He is currently a Ph.D. student under the supervision of J. R. Schmidt, at University of Wisconsin–Madison. His research interests include the simulation of crystallization of electrolytes in dilute solution, with a particular focus on the nucleation of metal-organic frameworks.

J.R. Schmidt J. R. Schmidt is an Associate Professor of Chemistry at the University of Wisconsin–Madison, and a member of the Theoretical Chemistry Institute. He earned his B.S. from Hope College in 2001, and a Ph.D. in Physical Chemistry from the University of Wisconsin (with Jim Skinner) in 2006, focusing on simulations of the dynamics and non-linear spectroscopy of aqueous solutions. After postdoctoral work at Yale (with John Tully), he returned to UW in 2008, becoming an Associate Professor in 2015. Prof. Schmidt's research

interests include developing accurate, first-principles force fields, nano-porous materials, and computational heterogeneous catalysis.

Contents

1 Introduction

Metal-organic frameworks (MOFs) are a class of nanoporous materials, popularized over the past 20 years, that have shown great promise in a host of industrial, synthetic, and even biomedical applications.[1–10] MOFs are defined by their characteristic nanoporous lattice built of inorganic nodes (metal cations or oxide clusters) bridged by organic linkers, and within this general motif a vast amount of structural and chemical diversity has be found.[7] Exploration of this MOF diversity, not only with regards to their practical applications, but also with respect to the types of network topologies and chemical compositions that might be synthesizable, has been and continues to be a major research focus. It now appears that hundreds of thousands[11] of distinct MOF materials are possible, and this vast materials space opens up the exciting possibility of generating tailored MOF materials for a wide range of applications via a rational 'crystal engineering' approach.[6]

Unfortunately, the process of reaction discovery, optimization, and scale-up of MOF synthesis remains extremely challenging, presenting significant obstacles to the synthetic realization of many otherwise promising MOF structures. For most MOFs, the relationship between reaction parameters (reagent concentrations, time, temperature, etc.) and synthetic outcome is hard to predict, such that reaction discovery and optimization is typically accomplished on the basis of trial and error, chemical intuition, and/or large-scale screenings, rather than by rational design.[5,9] Strikingly, such brute force synthetic efforts are often required even to generate families of isostructural MOFs from known parent phase(s). Indeed, syntheses that differ only in the nature of the metal and/or ligand building blocks can either fail entirely or lead to undesirable products of different topologies.[12] Similarly, scaled-up syntheses (a necessary prerequisite for industrial application) can fail even for MOFs that

have been obtained under laboratory-scale conditions.[9,13] In these and other situations where trial-and-error syntheses fail, it can often be difficult to determine why the targeted MOF was not produced or to identify (a priori) alternative synthetic strategies that might lead to a successful synthetic outcome.

As a consequence of these synthetic challenges, a better understanding of the link between reaction parameters and synthetic outcome is needed to enable targeted MOFs synthesis. Steps towards such a predictive understanding have advanced greatly over the past decade, due primarily to an abundance of work involving either screenings of MOF reaction parameters, or alternately time-resolved and/or in situ studies of MOF crystallization and growth. In the former case, compositional (reagent concentrations, solvent, etc.) and/or process (time, temperature, heating method, etc.) parameters are systematically varied, noting the resulting changes in MOF composition, structure, and/or crystal morphology.[9] Both serial and high-throughput studies have been instrumental in reaction discovery and optimization, and have, for select MOFs, identified dominant reaction trends and the significant reaction parameters that are required for optimal synthesis of particular MOFs or MOF families.[9] For further detail on the results and conclusions from such screening studies, the reader is referred to several recent reviews.[5–7,9,10]

Despite their utility, systematic investigations of reaction parameters provide little direct or generalizable information on the reaction mechanism(s) and intermediate(s) that underlie MOF nucleation and growth.[9,11,14,15] An alternative approach is to investigate the process of MOF crystallization itself, using one of a large variety of time-resolved and/or in situ experimental observation methods. This more 'direct' approach offers a number of exciting opportunities. First, understanding nucleation and growth is a central challenge in chemical and materials science; consequently, fundamental insights into MOF crystallization may offer a window into related crystal growth processes in other chemical, biological, and/or material systems.[16] In addition, direct studies of MOF nucleation and growth provide a detailed picture of the underlying MOF reaction mechanism(s), thus lending microscopic insight into crucial synthetic reaction parameters and hopefully reducing the reaction parameters space that must be explored to yield a successful synthesis. Such a reduction is crucial, as the amount of screening required to sufficiently explore reaction parameter space for the vast number of conceivable MOFs is intractably large.[17] As such, direct studies of MOF crystallization open up the exciting prospect of crystal engineering MOFs via methods grounded in fundamental principles rather than high-throughput empirical screening.[6,11,15,17]

This Review provides a comprehensive overview (as of mid 2016) of studies that in-

vestigate MOF nucleation and growth mechanisms using this latter 'direct' approach. In particular, we restrict our scope to experimental and computational studies which have focused either on the mechanisms or reaction intermediates involved in MOF crystallization, often via time-resolved in situ or ex situ investigation; it does not, in general, include systematic investigations of reaction parameters, as these studies offer less direct insight into the mechanisms of MOF formation. Ours is certainly not the first review to discuss this burgeoning field, and we note here the several recent reviews and perspectives that have also focused on time-resolved and/or in situ characterizations of the MOF crystallization process.[6,9,14,15,17] We begin the Review with a conceptual introduction to the major hypotheses, theories, models, and techniques that have been used to explain MOF formation. Next, we critically summarize, on a technique-by-technique basis, what has been learned from such 'direct investigations of MOF crystallization. This structure has been chosen, first and foremost, to highlight (vide infra) the many critical advances in instrument technology that have recently[9] enabled new types of (often time-resolved) in situ and/or ex situ investigations of MOF crystallization. This structure also facilitates a clear perspective regarding the scope and complimentary utility of each experimental technique for addressing fundamental questions regarding the mechanisms of MOF nucleation and growth. Lastly, we conclude with a critical analysis of the major insights that have been gained from the work summarized in this Review, outlining our own perspective on directions for potential future investigations.

2 Conceptual Overview of MOF Crystallization

Crystallization is a long-standing challenge in chemistry and materials science, with a large number of theories, hypotheses, and models applicable to various chemical / materials systems. We thus begin with an overview of these models, focusing on those that are most relevant to the nucleation and growth of MOFs and related porous materials. In particular, because many hypotheses regarding MOF formation have their origins in the zeolite and/or zeotype literature (zeolites sharing many structural similarities to MOFs), specific emphasis is given to pertinent zeolite crystallization hypotheses. For clarity, nucleation and growth hypotheses are discussed separately; nevertheless, in practice these processes may sometimes exhibit significant temporal overlap.

2.1 Nucleation

2.1.1 Classical Theories

Homogeneous nucleation is the initial process of crystal formation whereby a small number of ions, atoms or molecules rearrange into crystalline nuclei sufficiently large to allow for further irreversible growth into a well-faceted macroscopic crystal. Homogeneous nucleation has traditionally been described by classic nucleation theory (CNT), a subject which is reviewed in depth elsewhere (see ref. 18–20 and references therein). Briefly, CNT states that, under supersaturation conditions, where crystallization is thermodynamically favored, the formation of a nucleus gives rise to a free energy change that is dependent on two competing factors: a negative contribution due to the difference in chemical potential per unit volume, $\Delta\mu$, between the crystal phase and the liquid, and a positive contribution arising from the unfavorable interfacial free energy, γ, between the two phases. These two factors lead in turn to a size-dependent free energy of the form

$$\Delta G = 4\pi r^2\gamma - \frac{4}{3}\pi r^3\Delta\mu \tag{1}$$

where r is the radius of the nucleus. Central to the theory, CNT predicts nucleation to be an activated process whose kinetics are determined, in part, by the so-called "critical nucleus size", defined as the size of the nucleus that maximizes the free energy. Importantly, CNT also implicitly assumes that nucleation leads directly to the most thermodynamically-favorable phase, without amorphous or alternative crystalline intermediates. Non-classical nucleation theories, which allow for multi-step nucleation mechanisms and the existence of metastable intermediate phases,[19] are discussed below (see Sections 2.1.3 and 2.2.2) and in detailed reviews elsewhere.[19,21]

2.1.2 Heterogeneous and Secondary Nucleation

In the presence of foreign substrates such as dust, impurities, bubbles, or solid interfaces, many systems crystallize at supersaturation levels much lower than those predicted by CNT and a purely homogeneous nucleation mechanism.[19,20] However, alternate nucleation mechanisms, such as *heterogeneous* nucleation (nucleation onto a foreign substrate) and *secondary* nucleation (nucleation onto pre-existing nuclei and/or crystals of the final product material), can induce nucleation at these experimentally-observed lower supersaturation levels.[18,19,22] Consequently, under industrial conditions, heterogeneous and secondary nucleation are fre-

quently the most important contributors to new particle formation, and classical nucleation theories are frequently modified by a scale factor in order to account for these important substrate-dependent effects.[20,23]

The presence of certain additives — substrates or seed particles, for example — can also influence the rates and mechanisms of heterogeneous and secondary nucleation.[16] These and other additives (such as modulators or capping agents) have become common tools for rationally designing MOFs and other materials, and have already been employed to control crystal sizes and morphologies, generate 2D MOF thin films and/or membranes, or even engineer novel MOF structures at the meso/macroscopic scale.[9,24] The use of additives in MOF synthesis is an ongoing area of research, and mechanistic studies involving these materials will be a major focus of this Review.

2.1.3 Models of Zeolite Nucleation

CNT provides a simple, generic model for nucleation. Nevertheless, many complications arise when dealing with real systems, and alternative conceptual models for both classical and non-classical nucleation have been developed to explain nucleation in specific domains. In particular, a large body of work has been devoted to the development of qualitative hypotheses for the nucleation of zeolites, a class of inorganic compounds composed of metal tetrahedral nodes (Si and/or Al) linked by oxygen atoms. Like MOFs, zeolites exhibit interconnected metal centers, permanent porosity, topological diversity, and similar (solvothermal) synthetic approaches, making them both structurally and conceptually similar (although chemically less diverse) as compared to MOFs.[25] Many of these early zeolite formation hypotheses have had a significant impact on our understanding of MOF crystallization and are thus outlined below.

A consistent nomenclature for zeolite formation is lacking, and we closely follow the terminology of Aerts et al., in which hypotheses can be grouped into three main models: MONOMER, SBU, and NANOSLAB (see Fig. 1). Despite the fact that all three models also describe some elements of growth in addition to nucleation, we presently consider only the MONOMER and SBU nucleation models, and defer discussion of the NANOSLAB model (an aggregation model) until Section 2.2.2. It is important to mention that, for zeolites, and in all models, the fundamental reactions leading to nucleation and growth are the making / breaking of T-O-T (T=Si and/or Al) linkages. The differences between models lie in *how* these bond-making and -breaking reactions occur, and the intermediates and precursors involved in the crystallization process.[27]

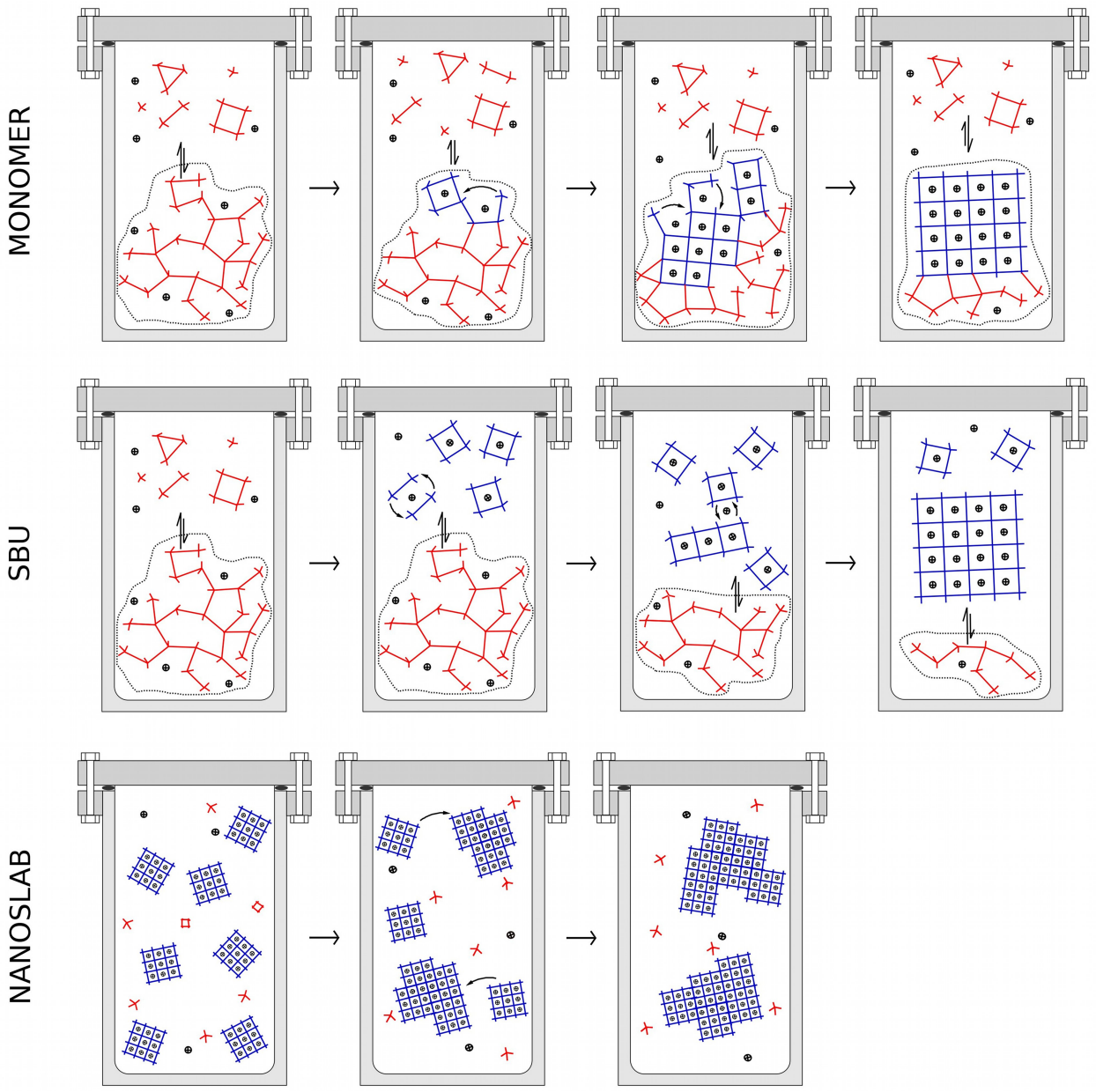

Figure 1: Mechanisms for zeolite crystallization classified according to growth unit. Black dots represent template cations. (top row) Growth from monomers; (middle row) growth from secondary building units (SBUs); (bottom row) growth by oriented aggregation of nanoparticles. Reproduced from ref. 26 with permission of The Royal Society of Chemistry.

Amorphous gel phases have been observed in zeolite formation, and within the MONOMER model (Fig. 1, top panel) crystallization proceeds via local restructuring of this gel phase.[11,26] In particular, the MONOMER model predicts that the unordered T-O-T bonds that form the amorphous gel will reversibly break and reform to yield a thermodynamically stable crystal corresponding to a particular zeolite framework. Note that, because this transformation takes place within a pre-existing amorphous gel and thus does not rely on the addition of new monomeric units, the MONOMER model is in significant contrast to the classical picture of nucleation described in Section 2.1.1.[16] Put differently, whereas CNT would predict that nucleation occurs at the interface between the solution and growing crystalline phases via addition of simple monomer units, the MONOMER model postulates that nucleation is better described as a local *restructuring from within* a solid amorphous phase to yield a crystalline product.

A more classical picture of zeolite nucleation is given by the secondary building unit (SBU) model (Fig. 1, middle panel), which derives its name from the nomenclature of the crystallographic community, wherein SBUs are defined as the smallest structural unit of the product crystal.[28] Under the SBU model, zeolite formation proceeds via monomer addition, in particular SBU addition, onto a growing nucleus. The amorphous gel phase serves either as a reservoir of SBUs or as a plausible site for heterogeneous nucleation,[11,27] but does not otherwise participate in the formation of the final crystal. Thus in contrast to the MONOMER model, which predicts that nucleation takes place from within the amorphous gel phase, the SBU model envisages nucleation as occurring either homogeneously or heterogeneously at the gel surface.[11,26] Furthermore, and as in CNT, the SBU model assumes that the SBU-based nuclei directly grow into the final crystalline product without passing through metastable intermediate phase(s). Note that, at least within the context of zeolites, the SBU model is under significant debate.[11,26] A variant of the SBU hypothesis was also proposed by Taulelle et al.,[29] involving prenucleation building units (PNBUs) that structurally resemble their SBU counterparts, but are soluble.

2.1.4 Models of MOF Nucleation

We turn now to a discussion of MOF nucleation hypotheses, highlighting some of the key similarities and differences between models for zeolite and MOF nucleation. First, it is important to note that, while much of the zeolite literature focuses on the role of experimentally-observed amorphous gel phase(s) during crystallization, a discussion of such amorphous phases (e.g. MONOMER-like theories) in MOF synthesis seems to be far less

common.[11,27,30,31] On the other hand, SBU-like models are frequently invoked in the MOF community, and have been broadened to encompass other hypothesized building units. For clarity, we will refer to such models as nucleation building unit (NBU) models, emphasizing the variety of building units that may be involved in MOF crystallization. As proposed by Férey, we consider such building units as "the minimum assembly of atoms, ions, or molecules which, by condensation of the group with others (identical or different), gives rise to the final solid".[28]

Several prominent NBU models for MOFs merit particular discussion. One hypothesis is that simple monomeric species (organic linkers and metal ions) participate in the nucleation of MOFs.[15] Other NBU hypotheses involve more complex structures, intermediate in size between bare metal ions and the full SBU. Ramanan and Whittingham, for example, posit NBUs as 'point zero charge molecule(s)' (pzc), defined as soluble metal complexes that undergo condensation with organic linkers at their isoelectric point.[32,33] One or more metal pzcs may participate in each condensation reaction: MOF-5, for instance, requires condensation of four zinc pzcs to form the final product. Note that this 'pzc' hypothesis is similar to other models developed in the context of supramolecular self-assembly, namely Brunet et al.'s 'tecton' and Desiraju's 'supramolecular synthon'.[33,36]

Similar to the pzc hypothesis, Férey et al. has suggested that pre-nucleation building units (PNBUs) can act as important precursors in the nucleation of certain MIL MOFs. These PNBUs are structurally similar to subunits of the SBU and can react with other PNBUs and/or metal monomers in solution to form new PNBUs and eventually the final SBU. Note that, in Ferey's terminology, neutral soluble metal complexes that otherwise resemble the full SBUs are referred to as neutral molecular building units (MBUs) rather than PNBUs. As with Ramanan's model, it is critical that the PNBUs be electrically neutral so as to be capable of approaching one another to undergo reaction instead of being driven apart by electrostatic repulsion.[37]

2.2 Growth

There exists a wealth of models explaining the transformation of nucleated particles into a stable crystalline product. We present several major theories relevant to zeolite and MOF crystallization, beginning with classic theories of crystal growth, which are particularly relevant under thermodynamically-controlled conditions, and ending with some alternative crystallization hypotheses that may be especially predominate under kinetic control. Once again, it is important to note that, even under a single set of synthetic conditions, a system may

exhibit features from multiple modes of growth,[16] all of which may overlap spatially and/or temporally with each other and with various nucleation processes.

2.2.1 Classical Growth Models

Under supersaturation, crystal growth is thermodynamically favored, and under equilibrium conditions proceeds so as to yield morphologies that minimize the total Gibbs surface free energy (the bulk energy contribution being identical between morphologies with constant volume). Under these conditions, the final shape of the crystal can be determined from the 'Wulff construction'.[38] Additionally, at equilibrium larger particles (which further minimize unfavorable surface energies) are favored, leading to dissolution of smaller particles and deposition on the surface of larger particles in a process known as Ostwald ripening.[39] Following Ostwald ripening, MOF product crystals in the nano- to micro-meter diameter regime are typical, though exact sizes and morphologies are highly dependent on synthesis conditions.[9,40,41] Fig. 10 provides a graphical example of such growth and Ostwald ripening processes in the case of ZIF-8, a prototypical MOF.

To move beyond thermodynamic considerations and predict the kinetics of crystal growth, classical growth theories rely on the assumption that growth from solution occurs via the diffusion and subsequent incorporation of small monomeric units onto the crystal surface.[16,20,22,23,42] Classical growth can be either diffusion-limited or controlled by the rate of surface integration, and theories exist to treat both regimes.[20] (Alternate theories, some of which additionally describe nucleation processes, have been used to describe crystallization in the specific case of MOFs, and these models are discussed in detail in Section 4.3.1.) Surface integration may involve multiple steps, and the exact mechanism of surface integration is largely dependent on the level of supersaturation (see Fig. 2). Briefly, at lower supersaturation, the crystal surface is typically smooth, and growth tends to proceed via the attachment of adsorbed growth units into energetically-favorable sites. At the lowest supersaturation levels, these sites are postulated to be self-perpetuating steps in the crystal surface that originate from dislocations in the crystal,[43] and this mechanism of surface growth is referred to as either 'spiral growth' or 'screw dislocation' (Fig. 2, left panel). At slightly higher supersaturations, 2D nucleation becomes possible, and growth units can attach to so-called 'step' and 'kink' sites via a 'birth and spread' mechanism (Fig. 2, center panel). Finally, as the supersaturation level increases and driving forces for growth become larger, growth units begin to integrate into the surface at any site irrespective of attachment energy (Fig. 2, right panel),[23] leading to adhesive (also referred to as continuous or rough) growth, and ultimately

producing crystals with spherulitic, fractal, and/or dendritic patterns.[23]

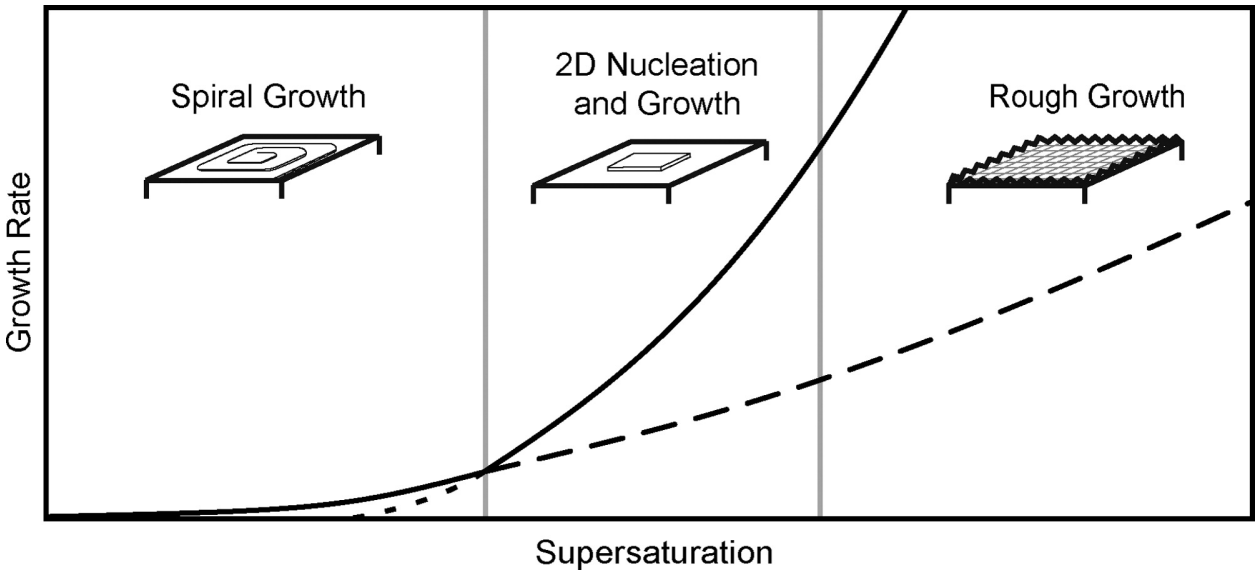

Figure 2: Growth mechanisms for a flat face, as a function of supersaturation. The solid line is the growth rate. The short dashed lines are the growth rates if two-dimensional nucleation continues to be dominant below its applicable supersaturation range. The long dashed line is the rate if spiral growth was the persistent mechanism above its applicable supersaturation range. Reproduced with permission from ref. 44. Copyright 2008 American Chemical Society.

2.2.2 Non-classical Growth Models

In the words of Cölfen and Mann, the aforementioned classical crystallization theories treat growth as "an *amplification* process in which stable nuclei are simply enlarged by unit-cell replication without incurring structural changes in the bulk or at the surface".[45] This definition highlights two major assumptions of classical crystallization: 1) that the growing nuclei maintain the same crystalline phase as the final product throughout growth, and 2) that growth proceeds via attachment of small (relative to the nuclei size) growth units rather than by aggregation of large pre-formed building blocks. Unsurprisingly, and especially under kinetically-controlled conditions, both of these assumptions can be violated.

Polymorphism and Ostwalds Step Rule In many multi-component systems, a variety of intermediates, ranging from amorphous gels to metastable crystalline phases, are possible, and this type of supramolecular isomerism (or polymorphism) has also been observed in MOFs.[11,46] The existence of supramolecular isomers has twofold impact on the crystal growth

process. First, polymorphism opens up the possibility that, depending on the relative free energy barriers towards formation of the various isomers, different (and possibly competing) products may crystallize under similar synthetic conditions. In such cases, reaction parameters such as solvent, heating method, and the presence of additives, can all have a significant impact on crystallization mechanisms and/or the observed product. However, even given the same final crystalline product, crystallization may proceed via sequential precipitation rather than via a one-step process (see Fig. 3). In fact, many systems *do* seem to crystallize via sequential, rather than one-step, pathways, an empirical observation known as Ostwald's Rule of Stages.[16,19,47] According to Ostwald's conjecture, which can be rationalized on the basis of entropic considerations,[48] it is the phase with the lowest free energy barrier (relative to the solution) that first nucleates and grows, rather than the thermodynamically most stable phase, with further transformations required to yield the thermodynamically-stable product.

Ostwald's Rule shows that, contrary to the simple amplification process proposed by classical growth theories, many sequential transformations (any of which might individually follow a classical model of growth) may be required to crystallize the final MOF product. Elsewhere we discuss several such transformations between intermediates: the MONOMER model of zeolite formation, for instance, falls under the broad umbrella of amorphous-to-crystalline transformations,[49] and some of the various aggregation theories discussed below in Section 2.2.2 provide viable mechanisms whereby low-dimensionality MOF intermediates can transform into more complex 2D and 3D crystalline materials.[50] Structural transformations between solid MOF phases are typically assumed to proceed via either dissolution-recrystallization or solid-phase rearrangement (the latter sometimes referred to as solid-state or single-crystal-single-crystal) transformations.[27,51] Dissolution-recrystallization involves the dissolution of a reactant phase, ultimately resulting in the release of reactive solution species to form a more thermodynamically stable product phase. Because a solution-phase intermediate is involved, dissolution-recrystallization reactions often give rise to dramatic structural differences between the reactant and product phases. By contrast, solid-phase rearrangements, whereby a solid interconverts without involving a solution-phase intermediate, are less common and typically require that the reactant(s) and final product(s) be structurally related and with identical building units (since dissolution processes cannot be used to generate new SBUs).[51] X-ray techniques are often applied to detect structural differences between phases, with a rearrangement mechanism assigned based on the magnitude of the difference.[52–55]

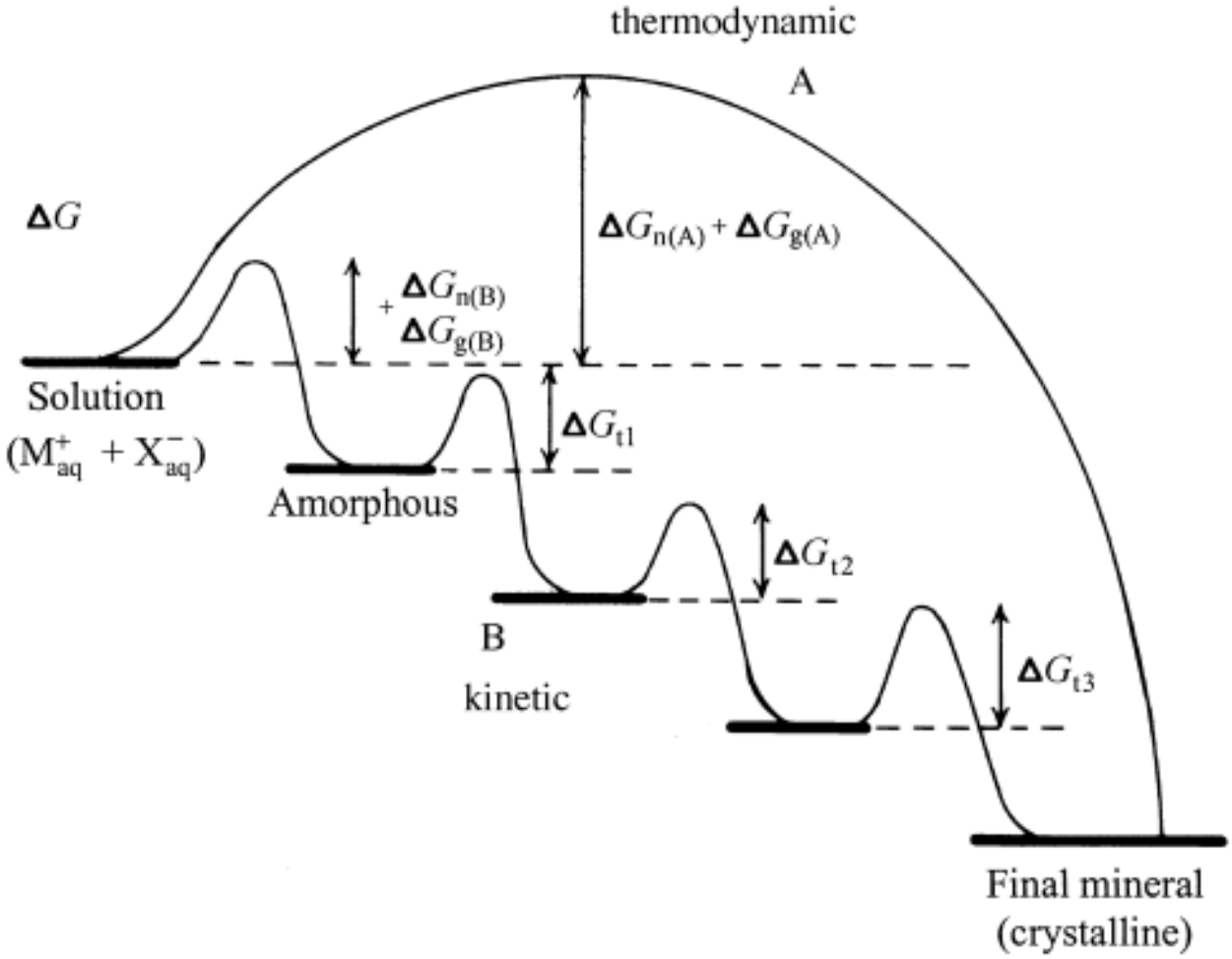

Figure 3: Crystallization pathways under thermodynamic and kinetic control. Whether a system follows a one-step route to the final mineral phase (pathway A) or proceeds by sequential precipitation (pathway B), depends on the free energy of activation (ΔG) associated with nucleation (n), growth (g), and phase transformation (t). Amorphous phases are common under kinetic conditions. Reproduced from ref. 45 with permission from John Wiley and Sons.

Aggregation The second assumption of classical growth theory, that of small growth unit attachment, also bears scrutiny. This assumption is addressed by many experimental and theoretical studies probing the role of aggregation in crystallization, and a complete review of aggregation in solids is given by Cölfen and Mann and by De Yoreo et al..[16,45] In aggregation-mediated pathways of crystal growth, which typically predominate under kinetically-controlled growth conditions, pre-formed crystalline building blocks (sometimes referred to as primary particles) aggregate to form a single crystal and/or iso-oriented crystals whose crystal habit(s) is largely influenced by the morphology of the primary particles. For this reason, crystals grown through aggregation-mediated pathways can exhibit morphologies contrary to the surface energy minimization principles of classical growth theory.

Several aggregation-type models of porous material crystallization are prevalent within the literature. In particular, the NANOSLAB model of zeolite synthesis (Fig. 1, bottom panel) is an aggregation hypothesis proposed on the basis of TEM studies (see ref. 26 and refs therein) in which transient nanoparticles (commonly referred to as 'nanoslabs' on account of their morphology) were experimentally observed during crystallization. Thus the NANOSLAB model proposes that zeolite crystallization occurs via the oriented aggregation of either amorphous or crystalline nanoparticles.[6,9,26]

Within the context of open-framework metal phosphate structures, Rao et al. proposed an aufbau, or "building-up" principle, whereby 0D monomeric units first assemble into 1D chains and subsequently (either via self-assembly, aggregation, condensation/hydrolysis, and/or dissolution-recrystallization) form higher dimensional 2D and 3D structures.[56,57] Note that, though the aufbau terminology is Rao's, earlier work by Oliver et al. also proposes a building-up mechanism for aluminum phosphate structures.[58] A subset of transformations in Rao's aufbau principle, such as the condensation of 1D chains/wires to form 2D sheets or 3D architectures, are best thought of as aggregation-mediated pathways.[58] Aggregation of 1D chains has been observed in several MOF syntheses,[6] and has been implicated in the formation of complex meso- or macroscale MOF superstructures.[24]

3 Techniques

Experimental studies of MOF crystallization have greatly benefited from the use of a broad range of complementary techniques, and Fig. 16 summarizes the major experimental and computational techniques discussed in this Review. Most techniques fall into one of four categories — scattering methods, microscopy, spectroscopy, and simulation/modeling —

with each type of technique providing complementary insight into the MOF crystallization process. Scattering methods (XRD, DLS/SLS, SAXS/WAXS, etc.), for example, are spatially-averaged, and thus are frequently used to provide quantitative insight into crystallization kinetics (e.g. reaction rate constants and activation energies) and bulk crystal properties (e.g. sizes and structural parameters). By contrast, microscopy techniques (AFM, SEM, TEM, etc.) are typically spatially-*localized*, and are instead used in imaging and to characterize crystal morphology, inhomogeneities and defects.

Aside from the unique types of information each time-resolved technique can provide regarding the MOF crystallization process (as summarized in Fig. 16, vide infra), the utility and efficacy of each technique depends significantly on (i) the phase regime(s) to which the technique is sensitive and (ii) the extent to which the technique is noninvasive and capable of probing the system under synthetically-relevant conditions. Regarding the first point, and as shown in Fig. 16, no single technique is capable of probing the full range of phases (nor length/time scales) represented in MOF crystallization.[59] As such, many of the conclusions from studies in this Review depend on information gathered from multiple techniques, performed either via simultaneous[60] or sequential experiments.

Furthermore, not all experimental techniques are noninvasive, nor can the experimental setups for all techniques exactly replicate the reaction conditions typically employed in MOF synthesis. Thus, although time-resolved ex situ experiments of MOF crystallization are often more straightforward to conduct as compared to their in situ counterparts (vide infra), such ex situ experiments require periodic quenching of the reaction, and consequently induce (sometimes large) perturbations on the system of interest.[9,61] In order to overcome the limitations of quenching experiments, the past decade has seen ongoing growth in instrument technology facilitating noninvasive, in situ characterization of solvothermal reactions.[9,17] In particular, considerable effort has gone into the development of sealed reaction vessels that are transparent to diffraction and/or spectroscopy experiments. Moreover, these vessels can withstand high heat and pressure, support relatively large volumes so as to avoid reaction container effects, and allow for sub-second to minute time resolution.[17] However, in situ x-ray studies frequently require intense synchrotron radiation and must be carried out at special facilities.[9,17,59] The first in situ static light scattering (SLS), atomic force microscopy (AFM), energy-dispersive x-ray diffraction (EDXRD), and angle-dispersive x-ray diffraction (ADXRD) experiments on MOFs were published in 2007, 2008, 2010, and 2015, respectively; many of the in situ studies reviewed herein thus represent some of the first applications of a still-emerging research frontier.[9,53]

Even with current state-of-the-art in situ techniques, subtle experimental limitations may lead to qualitatively-important discrepancies in synthetic conditions between in situ studies and industrially-relevant protocols. For example, MOF crystallization is now known to be (sometimes qualitatively) dependent on stirring effects.[6,9,62] Nevertheless, scattering techniques (such as in situ XRD) usually depend on sample stirring in order to maintain a homogeneous reaction mixture,[55,63–65] and most microscopy studies are carried out under static conditions; consequently, and depending on the desired synthetic conditions, both types of techniques can introduce unwanted perturbations on the system of interest. In general, and for both ex situ and in situ techniques, caution may be warranted when drawing mechanistic conclusions about a particular MOF synthesis from a time-resolved study which utilizes disparate reaction (e.g. reagent concentration, solvent) and/or process (e.g. temperature, pressure, stirring conditions) parameters.

Bearing in mind these broad conceptual and technical issues, we now turn to a critical analysis of how various experimental and computational techniques have contributed to our understanding of the mechanisms of MOF nucleation and growth.

4 X-ray Approaches

4.1 Overview

X-ray diffraction (XRD), scattering, and absorption approaches have all been utilized in a wide variety of in situ, ex situ, and/or time-resolved studies of MOF nucleation and growth, with XRD approaches being particularly dominant. XRD data is collected on the basis of Bragg scattering, which in turn relies upon on the long-range crystalline order of the MOF sample. As such, XRD is a spatially averaged technique (in contrast to microscopy methods). Furthermore, XRD is not well suited to probing the very earliest stages of MOF nucleation, as it is insensitive to sub-nanometer crystallites, and is also blind to the presence of non-crystalline intermediates or products. (The limitation on long-range order could be relaxed by examining instead the total/diffuse — as opposed to Bragg — scattering over a wide range of wavevectors, thus providing information regarding *local* order via the pair distribution function (PDF). Although such PDFs have not yet been commonly measured for MOF formation,[66] a similar approach was recently used to probe the nucleation and growth of inorganic nanoparticles.[67,68]) Despite these limitations, XRD offers many exciting opportunities for both in situ as well as well as time-resolved ex situ applications,[60] each of which has been applied extensively to monitor both zeolite[69] and MOF nucleation and

growth.

A particular challenge for in situ XRD studies is the need for a reactor that can withstand the rigors of a typical solvothermal reaction environment (elevated temperatures and pressures) while maintaining sufficient x-ray transparency.[69] High intensity synchrotron sources not only mitigate the latter concern, but also offer improved time resolution via the increased signal. Specifically, the vast majority of time-resolved x-ray studies of MOF crystallization have utilized energy-dispersive x-ray diffraction (EDXRD) to achieve increased time resolution. EDXRD employs a polychromatic source at fixed scattering angle, measuring signal as a function of scattered energy. EDXRD facilitates the rapid collection of XRD patterns in minutes or seconds, and the experimental geometry allows the diffraction volume to be focused inside the reaction volume, thus avoiding diffraction from the surrounding reaction vessel. Yet these advantages come at the expense of decreased spatial resolution as compared to conventional XRD approaches. Consequently, most time-resolved XRD experiments do not yield atomically-resolved crystal structures. More recently, time-resolved angle-dispersive x-ray diffraction (ADXRD), measuring multiple scattering angles, has demonstrated the possibility of extracting detailed diffraction patterns,[17,53] with recent experimental advances now yielding synchrotron ADXRD acquisition times of $\sim$1 frame/second.[12] Both EDXRD and ADXRD have been used to measure MOF "crystallization curves" by monitoring specific crystallographic reflections over the course of the synthesis. Coupled with analyses based on one or more analytical crystallization models (e.g. Avrami, Gualteri – vide infra), these crystallization curves can be used to provide insight into the kinetics of MOF crystallization and the associated activation energies.

Small angle x-ray scattering (SAXS) provides complementary measurements of MOF particle growth in a size regime of 1-100 nm. By measuring x-ray scattering at low angles, SAXS provides a probe of particle size and shape. Since it does not rely upon Bragg scattering off of lattice planes, SAXS is also sensitive to non-crystalline or amorphous particles that may be present in the initial stages of MOF nucleation and growth. Via incorporation of additional information at larger scattering angles via wide-angle x-ray scattering (WAXS), this combination has been utilized to probe the growth of MOF particles over a wide variety of length scales.

Select examples of **x-ray absorption spectroscopies** have also been applied to MOF nucleation and growth. In particular, extended x-ray adsorption fine structure (EXAFS) exploits the scattering and interference of electrons excited from the atomic core into continuum states off of the neighboring atoms. By measuring the constructive and destructive

interference of the emitted electrons as a function of energy, information about the number, type, and distances of the neighboring atoms can be obtained. EXAFS thus provides a detailed probe of the local chemical environment, applicable to both crystalline or amorphous samples. As such, EXAFS has been used to probe the chemical environments that are present in the very earliest stages of MOF nucleation, providing insights that are generally inaccessible via other x-ray approaches.

4.2 Historical Development: Inorganic-Organic Coordination Polymers

Many of the earliest in situ or time-resolved XRD studies of MOF-like compounds focused on inorganic-organic coordination polymers (CPs). Although many of these CPs lack the porosity of traditional MOF materials and lie outside the explicit scope of this review, these studies nonetheless illustrate many of the same phenomenon identified in later studies of prototypical MOFs, including a sensitivity of nucleation and growth kinetics to the heating method utilized during synthesis and the the observation of metastable crystalline intermediates that may form prior to the final crystalline product.

A number of the earliest studies of hybrid CP nucleation and growth under solvothermal conditions were conducted by Stock and coworkers, primarily utilizing EDXRD.[70–72] Notably, they examined the solvothermal synthesis of a series of isostructural rare-earth isophosphonatosulfonates, employing both conventional and microwave heating.[70] The crystallization was observed to involve an intermediate phase via a two-step process, with the activation energy of the second step exhibiting a strong dependence method of applied heating. In a subsequent study, many of the same authors also identified and characterized a series of intermediates during the crystallization of a related copper phosphonatoethanesulfonate compound, some of which could only be isolated and characterized by quenching.[71]

Such studies are not restricted to solvothermal, or even solution-phase, reactions. Kojima, Choi, and Kawano examined the synthesis of a Zn-tripyridyl-containing CP from the gas-phase reaction of ZnI_2 and 2,4,6-tris(4-pyridyl)triazine (TPT) via time-resolved XRD.[73] The products included a mixture of three crystalline structures, varying with synthesis temperature and reaction stoichiometry and evolving into more thermally stable structures with increasing reaction time.

4.3 Mechanistic Analyses

More recently, many of the same approaches utilized in time-resolved studies of CPs have also been applied to porous MOF structures. These studies not only allow for a quantitative determination of MOF nucleation / growth kinetics, but also provide insight into the mechanistic pathways and structural evolution (including intermediate amorphous or crystalline phases) that precede the final observed MOF product. In the first application of EDXRD to MOFs, Millange et al. demonstrated in situ monitoring of the solvothermal synthesis of two carboxylate-based MOFs (HKUST-1 and MIL-53(Fe)) with ∼1 minute time resolution.[52] Interestingly, the authors found evidence for two distinct crystallization scenarios, with HKUST-1 synthesis proceeding via classical nucleation and growth, and MIL-53(Fe) crystallizing via a transient intermediate structure in line with Ostwalds Rule of Stages (see Fig. 4). Since this initial application, EDXRD and other in situ and ex situ x-ray approaches have been utilized to study crystallization mechanisms for a wide variety of MOFs.

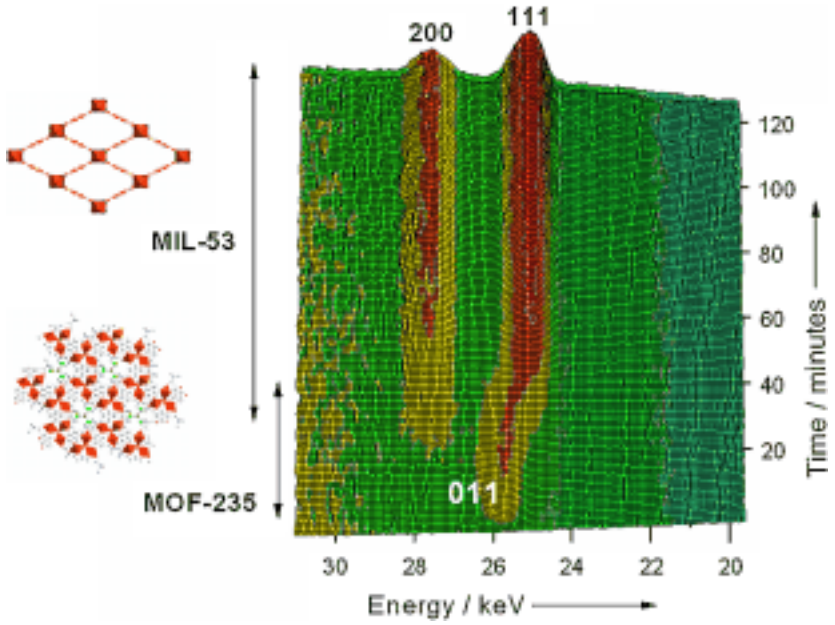

Figure 4: Time-resolved EDXRD measured during the crystallization of MIL-53 at 150 ^{o}C, with a crystalline transient phase seen at short reaction times. Reproduced from Millange et al.[52] with permission from John Wiley and Sons.

4.3.1 Quantitative Kinetic Modeling of MOFs

Crystallization Models The extraction of both quantitative kinetic and qualitative mechanistic insight from XRD-measured crystallization curves is reliant upon the fitting of the

measured data to one or more underlying physical models. Amongst the earliest of these models is the Avrami (or Avrami-Erofeev) model,[74–76] originally formulated to describe solid-state phase transformations. Despite its origin, the Avrami model remains one of the most frequently utilized approaches to describe *solvothermal crystallization* of various materials, including MOFs. The Avrami-Erofeev (AE) equation may be expressed as

$$\alpha = 1 - \exp[-(kt)^n] \tag{2}$$

where α is the extent of crystallization, k is the crystal growth rate constant, t is the reaction time, and n is Avrami exponent, described below.

A significant limitation of the AE model is that it does not distinguish between nucleation and growth processes; rather, the AE model assumes that crystallization occurs via stepwise addition of individual molecules at a constant rate.[77] In principle, the Avarmi exponent contains information about the dimensionality and mechanism of growth. Three regimes are often distinguished: diffusion mechanisms (n = 0.54-0.62), first-order or phase boundary mechanisms (n = 1.0-1.24), and nucleation or growth mechanisms (n = 2.0-3.0).[60,78] Note that since the AE model was originally formulated for solid state reaction, the interpretation of these parameters within the context of solvothermal MOF synthesis can be challenging.

In contrast to the AE model, the Gualtieri model was explicitly constructed to describe solution-mediated transformations. The Gualtieri model treats nucleation and crystal growth as separate events with distinct rate constants, with the dimensionality of crystal growth as a model parameter:

$$\alpha = \frac{1}{1 + \exp\left[-\left(\frac{t-a_N}{b_N}\right)\right]}\{1 - \exp\left[-(k_G t)^{n_G}\right]\}, \tag{3}$$

where n_G is the dimensionality of crystal growth (1, 2 and 3 for needles, plates and 3D particles, respectively),[79] k_G is the rate constant of crystal growth, a_N is the reciprocal of the nucleation rate constant k_N, and b_N is the variance of the nucleation probability distribution. The relative magnitudes of k_G and k_N can then be used to infer the rate-determining process in crystallization. The value of b_N also contains information about the nature of nucleation, with $b_N < 15$ indicating heterogeneous nucleation, $b_N \approx 20$ homogeneous nucleation, and $b_N > 20$ autocatalytic nucleation.

Although both the AE and Gualtieri models have been extensively applied to the crystallization of MOFs, the latter is likely more appropriate for describing conventional solvother-

mal MOF nucleation and growth.[17,80,81] In particular, while the AE model is extremely generic and has been applied to a wide variety of crystallization phenomenon, the model does not provide a detailed description of the "physics" governing MOF crystallization — including the separation of nucleation and growth phases. In contrast, the Gualtieri model was original derived for the analysis of hydrothermal zeolite synthesis, a closely related application which likely exhibits similar nucleation and growth phases.[17]

Summary of Nucleation and Growth Rates A recurring theme in XRD studies of MOF nucleation and growth is the analysis of crystallization kinetics via Avrami or Gualtieri models to yield rate constants for growth and/or nucleation and associated activation energies, the results of which are summarized in Table 1; a more detailed discussion of the associated studies and their qualitative conclusions is given in the subsequent subsections. Several conclusions can be drawn from examination of Table 1. First, the measured nucleation/growth rate constants for a wide variety of MOFs span a relatively modest range of $\sim 10^{-3}$ to 10^{-1} min^{-1}. Nevertheless, this observation likely reflects the adjustment of experimental conditions (e.g. temperature, supersaturation) to yield rates that are conducive to time-resolved XRD measurements, rather than any fundamental physical significance. Gualtieri analysis facilitates separate assignments of rates for nucleation and growth, and comparison of the associated rates yields information about which of these processes may be rate limiting. However, at least under conditions associated with such time-resolved XRD measurements, most systems do not show dramatic differences between nucleation and growth rates (i.e. no clear separation of timescales), which in most cases agree within a factor of 5-10.

Table 1: Summary of quantitative nucleation and growth kinetic data extracted from time-resolved XRD experiments.

Ref.	System	Model	K_n min^{-1}	K_g min^{-1}	Av. Exp. unitless	A_n min^{-1}	A_g min^{-1}	$E_{a,n}$ kJ/mol	$E_{a,g}$ kJ/mol	Heating Method	Exp. Conditions
53	$(H_2NMe_2)_2$ $[Co_3(BDC)_4]\cdot$ yDMF	Gualtieri	5.10×10^{-2}	4.80×10^{-2}						Solvothermal	250C, resin assisted
82	2D Cobalt MOF	First-order rxn	4.70×10^{-4}					1.60×10^{2}			25 C
83	CAU–1–$(OH)_2$	Avrami	9.18×10^{-2}		6.60×10^{-1}			1.31×10^{2}		Microwave	125 C, MeOH
83	CAU–1–$(OH)_2$	Avrami	3.88×10^{-2}		1.10			1.36×10^{2}		Solvothermal	125 C, MeOH
65	CAU–1–NH_2	Avrami	2.53×10^{-1}		6.70×10^{-1}			1.36×10^{2}		Microwave	125 C, MeOH
65	CAU–1–NH_2	Avrami	2.70×10^{-2}		1.14			1.36×10^{2}		Solvothermal	125 C, MeOH
84	CAU–13	Gualtieri	4.00×10^{-2}	5.94×10^{-2}		7.90×10^{8}	9.60×10^{8}	7.70×10^{1}	7.60×10^{1}	Solvothermal	115C
85	Ce–BTC	Misc	1.00	5.00×10^{-1}						Ultrasound	25 C, DMF/H2O
86	Co-NDC-DMF	Avrami	8.10×10^{-2}		7.40×10^{-1}					Solvothermal	200C, resin assisted
87	CPO–27(Co)	Misc	6.96×10^{-3}							Microwave	70 C, DMF
87	CPO–27(Co)	Misc	7.33×10^{-4}							Solvothermal	70 C, DMF
87	CPO–27(Co)	Misc	2.11×10^{-2}							Ultrasound	70 C, DMF
87	CPO–27(Ni)	Misc	5.65×10^{-3}							Ultrasound	70 C, DMF
87	CPO–27(Zn)	Misc	8.22×10^{-2}							Ultrasound	70 C, DMF
88	CPO–27(Co)	Gualtieri						8.36×10^{1}	4.84×10^{1}	Microwave	80 C, H2O
88	CPO–27(Co)	Gualtieri	2.29×10^{-1}	1.05×10^{-1}				6.65×10^{1}	9.04×10^{1}	Solvothermal	80 C, H2O
88	CPO–27(Ni)	Gualtieri						7.28×10^{1}	6.38×10^{1}	Microwave	90 C, H2O
88	CPO–27(Ni)	Gualtieri	8.79×10^{-2}	8.00×10^{-2}				1.32×10^{2}	9.23×10^{1}	Solvothermal	110 C, H2O
89	Cu–BTC	Misc	1.43×10^{-2}	2.04×10^{-3}		5.70×10^{23}	1.00×10^{17}	1.83×10^{2}	1.41×10^{2}	Microwave	100 C, H2O/EtOH
89	Cu–BTC	Misc	2.08×10^{-3}	1.22×10^{-3}		4.20×10^{13}	4.40×10^{15}	1.16×10^{2}	1.33×10^{2}	Solvothermal	100 C, H2O/EtOH
52	HKUST–1	Avrami			1.50				73.3	Solvothermal	125C
90	HKUST–1	Gualtieri	3.78×10^{-2}	1.18×10^{-1}				7.16×10^{1}	6.38×10^{1}	Solvothermal	105C
55	indium imidazolate	Gualtieri	1.71×10^{-2}	1.81×10^{-2}		3.22×10^{9}	2.51×10^{8}	9.40×10^{1}	9.40×10^{1}	Ionothermal	160 C

Table 1: Summary of quantitative nucleation and growth kinetic data extracted from time-resolved XRD experiments.

Ref.	**System**	**Model**	K_n min^{-1}	K_g min^{-1}	**Av. Exp.** unitless	A_n min^{-1}	A_g min^{-1}	$E_{a,n}$ kJ/mol	$E_{a,g}$ kJ/mol	**Heating Method**	**Exp. Conditions**
91	layered lithium carboxylate, $Li_4[C_4H_2S(CO_2)_2]_2[C_3H_7NO]_2$	Gualtieri	2.80×10^{-2}	1.52×10^{-2}		2.76×10^{14}	9.72×10^{11}	1.33×10^{2}	1.15×10^{2}	Solvothermal	160C
92	MIL–127(Fe)	Gualtieri	1.59×10^{1}	8.02				1.16×10^{2}	5.50×10^{1}	Solvothermal	175C, DMF
92	MIL–127(Fe)	Avrami	2.98×10^{-1}		6.10×10^{-1}	2.16×10^{11}	2.16×10^{11}	1.02×10^{2}	1.02×10^{2}	Solvothermal	175C, DMF
92	MIL–127(Fe)	Gualtieri	2.27	3.24				9.20×10^{1}	1.06×10^{2}	Solvothermal	80C, proppan-2-ol
92	MIL–127(Fe)	Avrami	4.86×10^{-2}		8.10×10^{-1}	5.28×10^{11}		9.20×10^{1}		Solvothermal	80C, proppan-2-ol
93	MIL–47(V)	Misc	3.13×10^{-3}	3.02×10^{-4}				6.18×10^{1}	8.44×10^{1}	Microwave	135 C
93	MIL–47(V)	Misc	1.91×10^{-3}	1.41×10^{-4}						Solvothermal	125 C
94	MIL–47(V)	Misc	1.91×10^{-3}	1.41×10^{-4}		2.48×10^{5}	1.75×10^{7}	6.18×10^{1}	8.44×10^{1}	Hydrothermal	125 C, H2O
93	MIL–53(Al)	Misc	2.47×10^{-3}	2.17×10^{-4}				7.52×10^{1}	9.53×10^{1}	Microwave	150 C
93	MIL–53(Al)	Misc	1.52×10^{-3}	1.32×10^{-4}						Solvothermal	140 C
94	MIL–53(Al)	Misc	1.52×10^{-3}	1.32×10^{-4}		4.78×10^{6}	1.40×10^{8}	7.52×10^{1}	9.53×10^{1}	Hydrothermal	140 C, H2O
93	MIL–53(Cr)	Misc	1.52×10^{-3}	2.71×10^{-4}				1.74×10^{2}	1.87×10^{2}	Microwave	175 C
93	MIL–53(Cr)	Misc	3.97×10^{-4}	8.40×10^{-5}						Solvothermal	165 C
94	MIL–53(Cr)	Misc	3.97×10^{-4}	8.40×10^{-5}		2.28×10^{17}	1.57×10^{18}	1.78×10^{2}	1.87×10^{2}	Hydrothermal	165 C, H2O
95	MIL–53(Fe)	Misc	5.00×10^{-2}	2.08×10^{-2}		1.19×10^{10}	1.23×10^{12}	7.48×10^{1}	9.06×10^{1}	Microwave	70 C, DMF
95	MIL–53(Fe)	Misc	3.23×10^{-3}	3.78×10^{-4}		3.05×10^{3}	4.78×10^{6}	3.92×10^{1}	6.64×10^{1}	Solvothermal	70 C, DMF
95	MIL–53(Fe)	Misc	1.67×10^{-1}	9.89×10^{-2}		3.57×10^{11}	8.03×10^{14}	8.11×10^{1}	1.04×10^{2}	Ultrasound	70 C, DMF
96	Mn–MIL–100	Avrami	1.10×10^{-1}		1.77 / 0.91					Solvothermal	135C
96	Mn–MIL–100	Gualtieri	1.16×10^{-1}	2.03×10^{-1}				1.27×10^{2}	9.89×10^{1}	Solvothermal	135C
90	MOF–14	Gualtieri	4.80×10^{-2}	1.28×10^{-1}				1.14×10^{2}	8.28×10^{1}	Solvothermal	120C
97	NH_2–MIL–101(Al)	Gualtieri	8.40×10^{-2}	3.80×10^{-2}				8.20×10^{1}	9.40×10^{1}	Solvothermal	130 C
97	NH_2–MIL–101(Al)	Gualtieri	3.40×10^{-2}	1.10×10^{-2}				7.50×10^{1}	1.02×10^{2}	Solvothermal	130 C, HPA templated

Table 1: Summary of quantitative nucleation and growth kinetic data extracted from time-resolved XRD experiments.

Ref.	System	Model	K_n min^{-1}	K_g min^{-1}	Av. Exp. unitless	A_n min^{-1}	A_g min^{-1}	$E_{a,n}$ kJ/mol	$E_{a,g}$ kJ/mol	Heating Method	Exp. Conditions
98	NH_2–MIL–53(Al)	Gualtieri	2.70×10^{-1}	7.20×10^{-3}						Solvothermal	130 C, H2O
98	NH_2–MIL–53(Al)	Gualtieri	6.60×10^{-2}	1.60×10^{-2}						Solvothermal	130 C, DMF
85	Tb–BTC	Misc	1.20×10^{-1}	1.40×10^{-1}						Ultrasound	25 C, DMF/H2O
99	UiO–66–NO_2 (and many other UiO-66 variants)	Gualtieri	5.00×10^{-1}	6.00×10^{-1}						Solvothermal	100 C, DMF, HCl
99	UiO–66–NO_2 (and many other UiO-66 variants)	Avrami	1.60		7.80×10^{-1}			1.13×10^{2}		Solvothermal	100 C, DMF, HCl
100	UiO–66(Zr)	Avrami	2.35×10^{-1}		1.18	3.76×10^{2}		2.20×10^{1}		Solvothermal	80 C, DMF, HCl
100	UiO–66(Zr)	Gualtieri	2.41×10^{-1}	4.40×10^{-1}		1.20×10^{1}	2.83×10^{2}	1.10×10^{1}	1.90×10^{1}	Solvothermal	80 C, DMF, HCl
101	UiO–66(Zr)–NH_2	Arrhenius							64.5	Solvothermal	110C
63	UiO–66(Zr)-(COOH)	Avrami	4.60×10^{-2}		1.58					Solvothermal	120 C, H2O
63	UiO–66(Zr)-(COOH)	Gualtieri	1.81×10^{-2}	3.40×10^{-2}				8.60×10^{1}	4.90×10^{1}	Solvothermal	120 C, H2O
63	UiO–66(Zr)-$(COOH)_2$	Avrami	3.60×10^{-2}		8.50×10^{-1}					Solvothermal	120 C, H2O
63	UiO–66(Zr)-$(COOH)_2$	Gualtieri	9.70×10^{-3}	9.00×10^{-2}				8.50×10^{1}	5.60×10^{1}	Solvothermal	120 C, H2O
54	Various lithium tartrate MOFs and intermediates	Varies						2.10×10^{2}	4.10×10^{1}	Solvothermal	Varies
85	Y–BTC	Misc	1.10×10^{-1}	9.00×10^{-2}						Ultrasound	25 C, DMF/H2O
102	$[Yb_2(BDC)_3(DMF)_2(H_2O)_2]$	Gualtieri	2.31×10^{-2}	3.10×10^{-2}						Solvothermal	110 C, H2O/DMF
103	$[Yb_2(BDC)_3(DMF)_2]\cdot H_2O$	Gualtieri	2.55×10^{-2}	1.07×10^{-3}						Solvothermal	110 C, DMF
104	ZIF–67	Avrami	1.37×10^{-4}		3.00						RT, MeOH
79	ZIF–11	Gualtieri	2.80×10^{-3}	2.30×10^{-3}						Ultrasound	100 C, DMF
79	ZIF–20	Gualtieri	3.20×10^{-3}	3.00×10^{-3}						Ultrasound	65 C, DMF
105	ZIF–7	Gualtieri	1.75×10^{-2}	2.80×10^{-2}							25 C, DMF, DEA modulator

Table 1: Summary of quantitative nucleation and growth kinetic data extracted from time-resolved XRD experiments.

Ref.	**System**	**Model**	K_n min^{-1}	K_g min^{-1}	**Av. Exp.** unitless	A_n min^{-1}	A_g min^{-1}	$E_{a,n}$ kJ/mol	$E_{a,g}$ kJ/mol	**Heating Method**	**Exp. Conditions**
106	ZIF–71	Gualtieri	1.47	7.04×10^{-1}							RT, 1-PrOH
107	ZIF–8	Avrami	9.48×10^{-2}		2.20					Mechano-chemical	35 C, liquid assisted grinding
64	ZIF–8	Avrami	2.40×10^{-2}		1.03					Solvothermal	130 C. MeOH
64	ZIF–8	Gualtieri	2.74×10^{-2}	5.90×10^{-2}		2.56×10^{7}	1.31×10^{8}	6.90×10^{1}	7.18×10^{1}	Solvothermal	130 C, MeOH, *isotructural
108	ZIF–8	Avrami	2.38×10^{-4}		1.12					Solvothermal	110C
108	ZIF–8	Gualtieri	2.78×10^{-4}	5.84×10^{-4}				1.15×10^{2}	8.77×10^{1}	Solvothermal	110C, DMF
79	ZIF–8	Gualtieri	2.00×10^{-3}	5.00×10^{-3}						Ultrasound	140 C, DMF
30	ZIF–8	Avrami	2.70×10^{-2}		4.00						25 C, MeOH
109	ZIF–8	Avrami	6.90×10^{-4}		2.70×10^{-1}						25 C, MeOH
110	Zr-furmarate	Gualtieri	1.50×10^{-2}	2.60×10^{-2}				7.10×10^{1}	6.60×10^{1}	Solvothermal	120 C, DMF, formic acid modulator

In addition to data on crystallization rates, the Avrami analyses in Table 1 yield exponents, n, that provide information on the mechanisms and dimensionality of crystal growth. For almost all MOF systems, values between 0.5-1.5 are characteristic, suggesting that diffusion and phase-boundary controlled mechanisms are quite common, although the wide range of these values also confirms the difficulty of generalizing over such a diverse set of materials and conditions. As noted above, the Avrami analysis was originally derived to describe solid-state phase transformations, and its applicability to solution-phase nucleation and growth (and thus the interpretation of the exponent) is questionable.[60]

By examining the temperature-dependence of MOF crystallization kinetics (whether via Gualtieri or Avrami methods), it is possible to extract activation energies associated with the nucleation and/or growth. When these kinetics are modeled via Gualtieri analysis, extraction of separate activation energies for both nucleation and growth is possible. In general, measured activation energies appear to be highly sensitive to not only the MOF system, but also to the details of the synthetic condition (in particular, solvent and heating method). For example, Chevreau et al. showed that the activation energies for MIL-127 differed by ~ 10 kJ/mol between DMF and propanol solvents, with the relative rates of nucleation and growth also changing.[92] Yet clear trends do emerge in rates, activation energies and associated pre factors when comparing syntheses conducted with differing heat methods (e.g. solvothermal vs. microwave vs. ultrasound) and metal ions of differing kinetic lability. These trends are discussed in detail in Sections 4.4.1 and 4.4.3.

Although many MOFs appear to exhibit characteristic activation energies in the range of 60-100 kJ/mol, significantly higher and lower values have occasionally been observed, particularly in conjunction with alternative heating methods (vide infra) or for two-dimensional MOFs (see for example Refs. 82,91). Interestingly, activation barriers for nucleation vs. growth for a given MOF are often of similar magnitudes (within 10-20 kJ/mol), with no clear trends as to which is typically larger. In cases where both Avrami and Gualtieri analyses have been used on the same dataset, the analyses often yield comparable activation energies, likely due to the fact that (in many cases) nucleation and growth steps exhibit similar magnitudes.

Corresponding Arrhenius prefactors for crystallization have also been calculated in many cases, yielding characteristic values of 10^7 – 10^{11} min^{-1}, although in some cases dramatically (and likely unphysically) higher values up to 10^{17} min^{-1} have been reported, in the latter case often coupled with very high activation energies. It thus appears that, at least in some cases, the reported activation energies/prefactors are highly coupled. As such, their absolute

values should likely be utilized with caution, and comparison of trends (and particularly trends within a consistent data analysis procedure) is likely to be more fruitful.

4.3.2 Secondary Building Unit Formation

In addition to providing quantitative kinetic information, time-resolved x-ray based studies can also be used to address challenging mechanistic questions regarding framework and/or SBU formation. For example, during MOF framework formation, are framework metal sites initially solvent-coordinated or, alternatively, already coordinated with the final ligand? To this end, Wu et al. utilized monochromatic ADXRD to extract detailed structural information and accurate time-resolved lattice parameters (via Rietveld refinement) during the crystallization of a rare-earth containing MOF.[103] They observed the exchange of an initially coordinated H_2O solvent for a DMF ligand, strongly suggesting a picture in which the MOF material is "water rich" in the early stages, with coordinated water replaced by DMF at later stages of the reaction.

The formation of MOF SBUs or, more generally, NBUs, also presents several interesting questions in MOF nucleation and growth. Typically, NBUs must assemble in solution from monomeric metal precursors. Alternatively, in a "controlled SBU" approach, metal oxide clusters are utilized directly as a reagent. Surble et al. employed EXAFS to demonstrate that, in the case of MIL-89 synthesis using a trimeric Fe(III) acetate precursor, iron trimers remain intact during all stages of MOF crystallization, including early-stage amorphous intermediates, providing strong support for an NBU-like model of nucleation of related MOFs.[111] In another example, Stock and coworkers examined SBU formation in Mn-MIL-100, whose synthesis involves a Mn(II) reactant that must undergo in situ oxidation to Mn(III) prior to framework formation.[96] Sharp-Hancock analysis of the EDXRD data suggested that crystallization occurs via two dominant mechanisms, initially controlled via nucleation and then later via a first-order mechanism during which the in situ generation of the requisite Mn^{3+} cations may become rate limiting.

4.3.3 Evidence for Non-Classical Growth: Crystalline Intermediates Phases

Many authors have emphasized the important role of thermodynamics in MOF crystallization,[87,112] particularly with high-temperature solvothermal conditions which are (eventually) expected to favor the thermodynamic product. Nonetheless, since the early EDXRD work of Millange and coworkers,[52] and consistent with Ostwald's Rule of Stages, various intermediate (presumably kinetically metastable) products have frequently been observed or isolated in

MOF synthesis. A significant advantage of in situ or time-resolved x-ray approaches is that they provide for the possibility of identifying and probing such crystalline intermediates.

Particularly well-studied examples are NH_2-MIL-53(Al) and NH_2-MIL-101(Al), both of which are synthesized from the same precursors.[97,98,113] Using a combination of SAXS and WAXS, Gascon and coworkers concluded that crystallization in DMF proceeds via the formation of an MOF-235 intermediate phase (whose identity was confirmed via quenching and characterization), which, depending on solvent, converts into either MIL-101 (aprotic solvents) or MIL-53 (protic solvents).[98] Consistent with Ostwald's Rule of Stages, MOF-235 represents the kinetically favored (but unstable) phase, while the latter represent the thermodynamically stable phase. Interestingly, in water, NH_2-MIL-53(Al) can be synthesized without formation of the intermediate phase.[113] Addition of a phosphotungstic acid template stabilizes the MOF-235 intermediate and promotes its formation.[97] Notably, Millange et al. also observed a similar MOF-235-like intermediate in their EDXRD study of MIL-53(Fe) crystallization.[52]

Crystalline intermediates have also been observed in other MOF systems. One rich example comes from Yeung et al., who examined the crystallization of a lithium tartrate MOF involving three competing phases.[54] Using EDXRD, two low-density kinetic intermediates were identified. Analysis of the kinetic data suggested that formation of the thermodynamic product proceeds over a much higher activation energy ($\sim$ 210 kJ/mol) vs. the intermediate / kinetic product ($\sim$ 41 kJ/mol). The large activation energy of the former involves a highly unfavorable change in ligand conformation in the transition from the intermediate to the stable product.

A second illustrative example comes from the synthesis of MOF-5, where disparate crystalline intermediates haven been observed depending on various reaction parameters or even, strikingly, the choice of characterization technique(s).[61,62] An initial ex situ, time-resolved XRD study by McKinstry et al. discovered the presence of at least one crystalline intermediate in the synthesis of MOF-5, whose presence and concentration was found to depend significantly on synthetic parameters such as time, temperature, and stirring.[62] At high synthesis temperatures (140°C), the intermediate phase was identified as MOF-69c(desolv), which was found to convert into MOF-5 via reaction with additional terephthalic acid. In a separate study, Wu et al. used *both* ex situ powder XRD (via quenching and extraction of the solid product) as well as in situ ADXRD to characterize a transient crystalline intermediate formed during the synthesis of MOF-5 at 110°C.[61] Importantly, the quenching experiments yielded a different intermediate, a layered Zn(BDC)(DMF) structure with dimeric SBUs,

compared to the in situ experiments, where the intermediate was characterized as a layered $Zn_3(BDC)_3(H_2O)_2 \cdot 4\,DMF$ compound with trimeric SBUs (see Fig. 5). Neither of these intermediates correspond to the MOF-69c(desolv) structure above, though this discrepancy might be due to differences in synthesis conditions between the two experiments.[61] Overall, these results nicely illustrate the fundamental limitation of ex situ quenching experiments compared to less invasive in situ techniques.

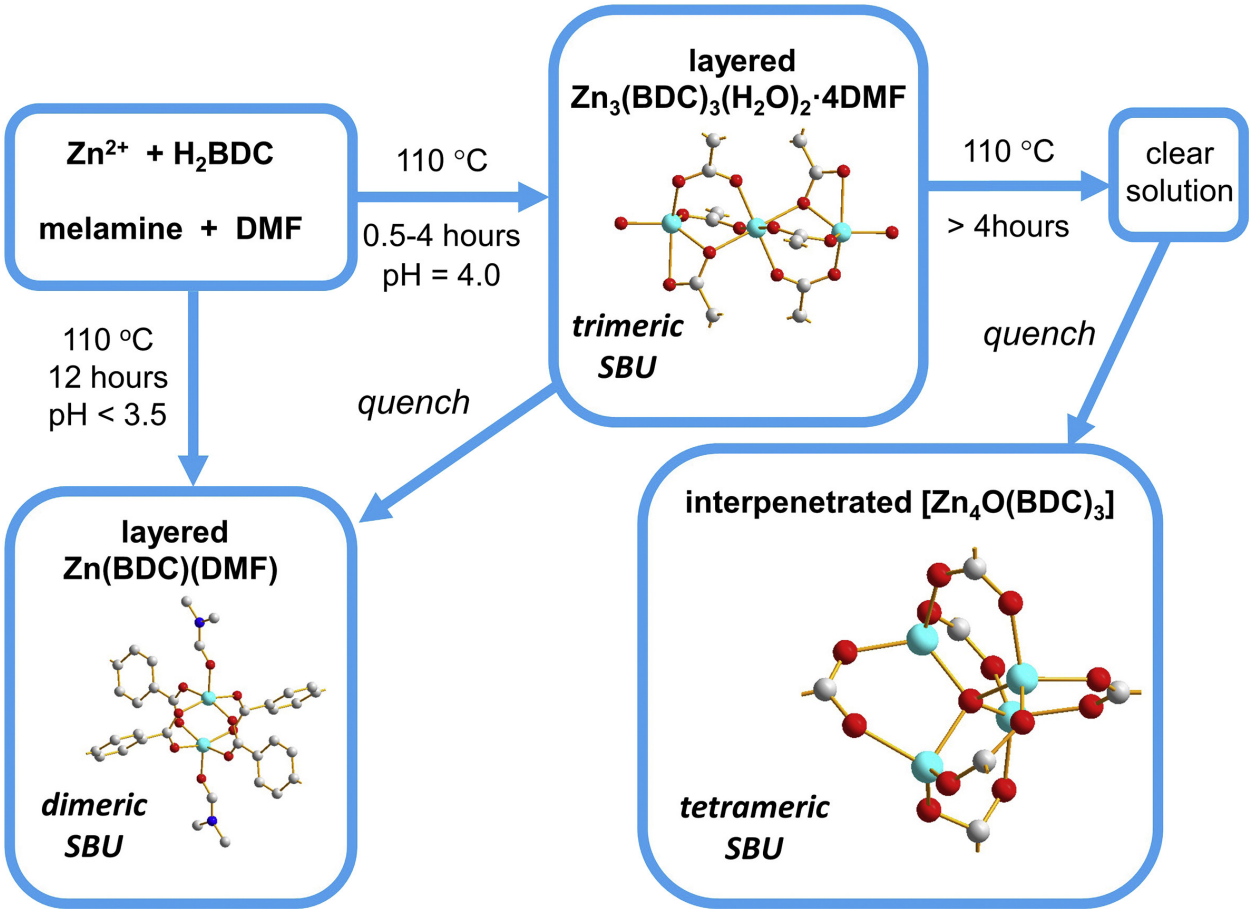

Figure 5: Schematic of reaction pathways leading to the formation of interpenetrated MOF-5 based on results from this work and observations reported by Kim et al.[114]. Reprinted from ref. 61, with permission from Elsevier.

In many cases, including those discussed above, crystalline intermediate phases are believed to convert to the final product via a dissolution-recrystallization mechanism. In contrast, Wu et al. examined the Co-BDC-DMF system, observing crystallization towards the final product via in situ ADXRD.[53] In this case, the authors concluded that the intermediate converts to the final product via a rapid solid-phase rearrangement, basing their conclusion

on the extremely abrupt nature of the transformation and the structural similarity of the phases (which could help facilitate a solid-phase transformation).

Zeolitic imidazolate frameworks (ZIFs) represent a particularly intriguing model system for probing the role of intermediates in MOF crystallization. ZIFs are known to exhibit sometimes significant polymorphism, with (for example) at least nine different polymorphs of $Zn(Im)_2$ [Im = imidazolate] synthesized to date. Wiebce, Leoni, and coworkers have examined the solvothermal synthesis of several ZIFs via EDXRD.[55,115] In the case of $Zn(Im)_2$, crystallization under various conditions yields either the **coi** or **zni** phases, with the former proceeding via an **neb** intermediate via dissolution-recrystallization; the remaining **neb** crystallites are hypothesized to serve as heterogeneous nucleation sites for the final **coi** product.

Interestingly, sometimes even the desired crystalline MOF product can serve as a metastable intermediate to a final (often undesirable) non-porous product, illustrating the frequent extreme sensitivity to reaction conditions that can characterize MOF synthesis. For example, Millange et al. examined copper(II)-based MOF-14, monitoring not only its crystallization to the MOF-14 product, but also its eventual dissolution / collapse into Cu_2O at higher synthesis temperatures and extended reaction times.[90] These observations highlight the importance of tailoring reaction conditions so as to isolate the desired species, which may in some instances actually constitute the kinetic rather than thermodynamic product.

Finally, another recurring paradigm in the crystallization of MOFs is the "building up" of structures / intermediates of increasing dimensionality. Rao and coworkers explored this "aufbau" principle in a series of early manuscripts using time-resolved XRD.[116,117] Heating a zinc oxalate precursor in the presence of piperazine at increasing temperatures yielded a variety of structures of increasing dimensionality – from 1D helical chains, to 2D honeycombs, to 3D pillared layers.[116] At the highest temperatures, their results showed that the 3D structure is formed by the progressive building-up of structures of increasing dimensionality, rather than by decomposition / reformation. Subsequent work on metal-benzene dicarboxylates found evidence for a similar 1D to 3D transformation.[117] Mahta et al. also observed a similar motif of increasing dimensionality in their case of manganese oxy-bis(benzoate) structures.[112,118] Using ex situ time-resolved XRD at increasing temperatures, they found 1D wire-like structures, which transitioned to 2D layered structures and eventually to a 3D network at the highest temperatures. These structures were progressively more dehydrated, possibly driven by the entropy of dehydration. Later, Kondo et al. investigated the crystallization kinetics of a two-dimensional Co-based MOF material $[Co(bpy)_2(OTf)_2]$,

monitoring the various phase transitions via time-resolved XRD.[82] The MOF crystallized via a progression from 0D molecular complexes, which transition under atmospheric conditions to 1D chains via loss of coordinating acetonitrile solvent. Additional heating at elevated temperature in vacuum leads to loss of coordinating water, yielding a 2D stacked structure.

4.3.4 Amorphous to Crystalline Transformations

An open question in studies of MOF crystallization is the extent to which nucleates present during the initial stages of nucleation and growth are actually crystalline. In the specific case of ZIFs, a frequent target for time-resolved XRD probes, there is considerable evidence that the growing ZIF particles may proceed through an amorphous or medium-range order phase that later transitions to the final crystalline product. For example, Carreon and coworkers used a combination of time-resolved XRD and TEM to monitor the room temperature crystallization kinetics of ZIF-8.[30] Based on XRD patterns and TEM images, they identified four different stages of ZIF-8 formation: nucleation, crystallization, growth, and stationary periods. They hypothesized that crystallization proceeds via a gel solution, leading to ZIF-8 crystallites that grow at the expense of the surrounding gel, similar to behavior observed in zeolites (see Section 2.1.3). Crucially, they also proposed the existence of a medium-range ordered ZIF-8 intermediate that eventually develops long-range crystalline order, either via solution- or solid-mediated mechanisms.

The existence of partially ordered intermediates is also supported by subsequent work. In particular, Feng and Carreon examined the kinetics of ZIF-67 nucleation and growth.[104,119] They observed a subset of well-defined XRD peaks, even at very short synthesis times, and suggested that these may result from the evolution of ZIF-67 from a low crystallinity (medium-range order) metastable intermediate phase with an ordered surface. Avrami analysis of the crystallization kinetics suggested heterogeneous nucleation, potentially at grain boundaries or impurities.[104] A comparison of crystallization in both methanol and DMSO showed that the latter yielded smaller crystals, perhaps due to better charge separation (and thus slower crystallization) induced by the higher dielectric constant of DMSO.[119] Interestingly, similar crystallization curves for ZIF-8 measured by Moh et al. were achieved by a very different approach: time-resolved *gravimetric* analysis, using the mass of the isolated product as a function of time.[108] Gualtieri analysis of those results suggests that nucleation extends far into the crystal growth regime, with nucleation typically slower than growth.

As noted earlier, the very earliest stages of nucleation and growth are typically inaccessible via XRD. To this end, Cravillon et al. used time-resolved SAXS/WAXS to monitor this

important regime in ZIF-8 nucleation.[31] This is a unique study because it directly probes the existence of amorphous/primary particles, which few other techniques are able to achieve. By exploiting the high intensity of the x-ray source and utilizing stop flow methods, they were able to achieve a ∼1s time resolution. They found evidence for the nearly immediate formation of small ∼1nm clusters, whose disappearance is coincident with the formation of larger particles. In this case, WAXS data could not determine whether these initial particles were crystalline, or amorphous with subsequent reorganization to yield ZIF-8; nevertheless, similar transformations from amorphous to crystalline have been proposed in zeolites (e.g. the MONOMER model of zeolite nucleation). Analysis of the SAXS data also suggested that ZIF particles may grow by the addition of monomers rather than by coalescence, bearing resemblance to the NBU model of MOF growth discussed in Section 2.1.4. The authors speculated that the initial clusters may serve as either simple reservoirs for monomers for particle growth, or, alternatively, may play a role in nucleation as prenucleation particles that eventually evolve toward the final ZIF-8 structure.

This work was later extended by Saha et al., who employed a combination of light scattering and SAXS/WAXS to probe the early stages of ZIF-71 growth.[106] Their data strongly suggest that growth proceeds first via small clusters, then by the formation of larger amorphous particles. As with ZIF-8, the authors concluded that particle growth takes place via monomer addition, where in this case the 'monomers' may be small clusters, oligomers, or individual metals/linkers. Consistent with the general trends observed for other ZIFs, these particles were eventually found to transform into crystalline ZIF-71 via an amorphous-to-crystalline transformation, possibly involving initially crystalline domains near the particle-solution interface. As such, the totality of these ZIF studies support the contention that the crystallization of ZIFs generally proceeds through an intermediate that lacks long-range order (whether amorphous or semi-crystalline), with subsequent transition(s) yielding the final crystalline product.

Finally, amorphous to crystalline transitions have begun to be observed in MOF materials aside from ZIFs. Using a combination of SAXS/WAXS and DFT calculations, Goesten et al. investigated the time-dependent crystallization behavior of UiO-66.[120] The SAXS/WAXS data revealed the existence of amorphous MOF particles as intermediates followed by a swift reorganization into the final crystalline UiO-66 solid. Interestingly, the complete transformation mechanism (cluster formation followed by condensation and finally crystallization) was shown to be a 'chemical clock' reaction with HCl as an autocatalyst, thus coupling together the condensation and crystallization processes and leading to experimentally-observed

oscillations in the size of the amorphous UiO-66 particles.

4.3.5 Mesoscale Organization

In contrast to the microscopic assembly of MOFs, other studies have probed the assembly of MOFs on the larger mesoscale, examining factors that govern MOF topology and long-range organization. For example, MOF mesoscale assembly was examined by Kitagawa and coworkers, aiming to understand the factors that control domain formation in MOFs composed a mixture of metal precursors.[121] Exploiting the difference in reactivity between precursors, the synthesis of a mixed MOF was monitored with time-resolved XRD. The resulting structure exhibits mesoscopic phase separation with Zn- and Mn-rich domains, and displays unique cooperative gas sorption behavior. Later, Moorhouse, Wu, and O'Hare examined a Co-NDC-DMF (NDC = 2,6-naphthalenedicarboxylate) MOF, which exhibits at least three distinct structures, depending on reaction conditions, and studied the factors which ultimately determine MOF topology.[86] Using a resin-assisted synthesis approach, they were able to synthesize a structure that was inaccessible via traditional bulk synthesis approaches. Avrami analysis of the in situ XRD data suggested that the reaction is primarily diffusion controlled, perhaps associated with the release of metal cations from the metal-exchanged resin, and indicated that slow diffusion of the metal cation may play a role in framework selectivity.

Beyond simple topology, chemically similar MOFs may also exhibit structural variants with interpenetrating sub-lattices, often yielding dense (rather than porous) structures. Ferguson et al. used time-resolved XRD to monitor the degree of interpenetration as a function of heating time for a single-crystal to single-crystal autocatentation transformation (i.e. a transition from an non-interpenetrated to interpenetrated lattice).[122] Their results suggest that MOF interpenetration may occur via either sequential growth of interpenetrating sub lattices or, alternatively, via a thermodynamically metastable non-interpenetrated intermediate followed by subsequent autocatenation.

4.4 Influence of Reaction Parameters

Time-resolved XRD methods have also provided unique insights into the influence of various reaction parameters (e.g. heating method, added promoters) on the resulting MOF nucleation and growth. In particular, the studies reviewed herein exploit their in situ or time-resolved nature to extract information as to the often complex connection between

reaction parameters and the observed MOF product.

4.4.1 Influence of Heating Methods

A number of authors have used time-resolved XRD methods to discern the influence of heating method on the kinetics of MOF synthesis, including some early and extensive work by Jhung and coworkers.[85,87,89,93,95] The influence of these various heating approaches (including ultrasound (US), microwave (MW), and conventional electric (CE)) on the kinetics of nucleation and growth is summarized in Table 1. In the case of MIL-53(Fe), Haque et al. utilized a two-step synthesis procedure to understand, separately, the influence of heating on both nucleation and growth.[95] They found that both nucleation and growth rates decrease in the order US > MW $\gg$ CE. Interestingly, their analysis showed that this trend is dominated by an increase in the pre-exponential factor (up to 8 orders of magnitude!), with US and MW actually *increasing* the measured activation energy. Although acceleration due to US and MW heating has been attributed to phenomenon such as hot spots,[123] there does not appear to be a simple physical explanation for such a dramatic increase in pre-exponential factor, and the observed dominance of the pre-exponential factor is not universal (vide infra). Decoupling the influence of MW heating shows acceleration in both nucleation and growth, but a more substantial influence on growth. Khan, Haque, and Jhung reached very similar conclusions when examining the microwave-assisted growth of HKUST-1.[89] Later, Haque and Jhung examined CPO-27-Co (MOF-74-Co) under the same three heating conditions, once again monitoring with XRD.[87] From the crystallization kinetics, the same broad rate trends arose: US >MW > CE; these results are consistent with the general observation from similar studies on a range of systems, and all indicate that microwave heating or ultrasonication leads to increased crystallization rates at lower temperatures.[79,124] Acceleration of comparable magnitude (10-30x) is observed in both nucleation and crystal growth regimes. Haque et al. later re-examined the nucleation kinetics of a variety of isostructural MIL MOFs using the Erying model, and attributed the acceleration to an entropy increase (which more than counterbalances the associated enthalpy increase) under microwave irradiation,[93] perhaps due to less organized intermediates.

Ahnfeldt et al. found that utilization of MW vs. CE heating not only influenced the synthesis rate, but also the observed induction period prior to crystallization.[83] Using in situ EDXRD to probe the synthesis of CAU-1-$(OH)_2$, they found that the measured induction time decreased with temperature, but considerably more rapidly under MW heating. Avrami analysis also suggested that microwave heating leads to a transition from phase-

boundary controlled (in the case of CE heating) to diffusion controlled growth. In the former case, linker attachment may be rate limiting.[65] Although both heating methods lead to very similar calculated activation energies, the authors speculate that the larger microwave pre-exponential factor may arise from an increased number of nuclei or increased reaction mobility induced by the microwave field. Subsequent work by Ahnfeldt and Stock examined the related amino-functionalized CAU-1-NH_2 MOF, reaching similar conclusions.[65]

It is important to note that not all authors have attributed MW-induced acceleration to an increase in the pre-exponential factor. Using EDXRD, El Osta et al. monitored the crystallization of a two CPO-27/MOF-74 variants (Co^{2+} or Ni^{2+}).[88] In contrast to most of the prior work, they observed a substantial decrease in the activation energies for crystal growth under irradiation from 92.3 (90.4) kJ/mol to 63.8 (48.4) kJ/mol for the Ni- (Co-) containing MOF, and an even more dramatic decrease in the associated nucleation activation energy, particularly for Ni. The authors thus speculated that the use of MW heating may help overcome the lower kinetic lability of the solvated Ni^{2+}.

4.4.2 Mechanochemical MOF synthesis

Mechanochemical synthesis via milling has recently been explored as an environmentally friendly alternative to solution-based MOF synthesis approaches.[125] XRD provides a unique window into the structural transformations that take place during these syntheses, which have often been shown to involve unique pathways/intermediates that differ from their solution-phase counterparts.[126] Friščić and coworkers monitored the solid-state reaction of ZnO and crystalline 2-ethylimidazole to form ZIFs via time-resolved powder diffraction.[107,127] Framework formation was observed to occur via intermediates with **rho**, **ana**, and **qtz** topologies, while, in contrast, mechanochemical synthesis of ZIF-8 (using 2-methylimidazole) proceeded without observable crystalline intermediate. Subsequent work by many of these same authors found that continued milling of the crystalline ZIF-8 led first to amorphization and then to a new metastable phase with **kat** topology.[126] The authors hypothesized that the amorphization may have been induced, at least in part, by an increase in ligand lability due to a mildly acidic environment.

Via in situ XRD, novel intermediates have also been observed for other mechanochemical MOF systems. In one such example, Julien et al. identified two new metastable intermediate phases in the synthesis of Zn-MOF-74.[128] Interestingly, the synthesis was observed to proceed via a close-packed intermediate ($Zn(H_2O)_2(H_2dhta)$) that later transformed into the (open) MOF-74 product (see Fig. 6). Liquid-assisted grinding (LAG) with DMF led

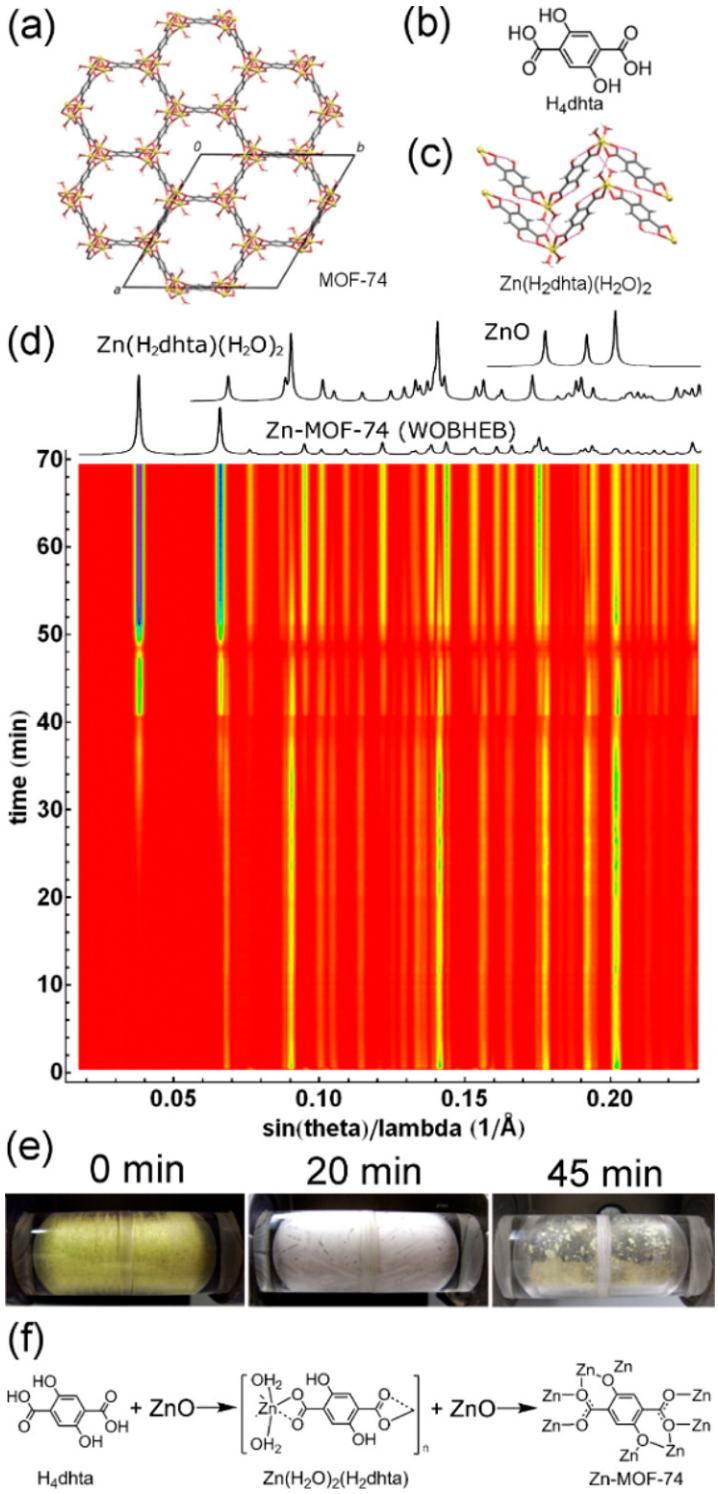

Figure 6: Structures of: (a) Zn-MOF-74 (CCDC WOBHEB); (b) H_4dhta; (c) $Zn(H_2O)_2(H_2$dhta) (CCDC ODIPOH). (d) Time- resolved in situ X-ray powder diffractogram for LAG of ZnO and H_4dhta (stoichiometric ratio 2:1) using water, ($\eta = 0.625$ μL/mg, $\lambda =$ 0.207). Signal losses at 40 and 48 min are artifacts of time-dependent sample distribution during milling. (e) Views of reaction mixture at different milling times and (f) stepwise formation of Zn-MOF-74. Reproduced with permission from ref. 128. Copyright 2016 American Chemical Society.

to an additional short-lived intermediate phase, although the structure of that intermediate could not be determined. In other studies, such liquid additives have also been shown to influence the course of the mechanochemical synthesis. Stolar et al. used in situ XRD to demonstrate that LAG with coordinating additives (DMF, EtOH) led to an intermediate phase prior to HKUST-1 formation.[129] Interestingly, the intermediate was characterized by a mononuclear Cu(II) SBU, in contrast to binuclear HKUST-1. The authors hypothesized that this intermediate eventually reacts with additional metal precursors to form HKUST-1.

Related work on mechanochemical synthesis of coordination polymers provides some potential insights into the mechanisms at play during mechanochemical synthesis. In particular, Užarević et al. showed that the synthesis of a Cd-based coordination polymer displayed a mechanochemical synthesis rate that was a strong function of temperature, with a 6-fold increase in reactivity over only a 45K increase in temperature.[130] This observation calls into question the applicability of "hot spot" models of mechanochemical synthesis for soft materials such as MOFs. Those authors also point out the potential importance of water released during the course of the synthesis reaction, potentially transforming the reaction from "dry" milling into LAG.

4.4.3 Importance of Metal Lability

Several XRD studies have highlighted the importance of metal cation lability in the crystallization of isostructural MOFs differing only in the identity of the metal cation, offering novel insights into the 'synthesizability' challenges that are known to arise in targeted MOF synthesis. For example, in comparing the Co/Ni MOF-74 variants, El Osta et al. found that crystallization of the Co analogue is systematically faster, possibly due to the higher kinetic lability of Co.[88] Gualtieri analysis showed that the two metals exhibit very similar activation energies for growth (∼90 kJ/mol), but much smaller nucleation activation energies for Co vs. Ni. An ex situ time-resolved XRD study by Haque and Jhung on the same M-MOF-74 system (M= Zn, Co, or Ni) also found crystallization rates proportional the the metal's kinetic lability, likely due to the importance of complexation and/or ligand exchange processes during MOF synthesis.[87]

Other MOFs display similar trends regarding the importance of metal lability. Khan et al. synthesized a series of isostructural lanthanide-benzene tricarboxylate MOFs, examining the role of the metal cation on the rates of nucleation and growth under US heating.[85] Crystallization curves obtained from time-resolved XRD show that nucleation and growth rates for a Ce-based MOF were significantly faster (8-9x for nucleation, 3-5x for growth)

as compared to the less reactive Tb and Y variants, consistent with known water-exchange reaction kinetics, thus suggesting a crucial role of metal ion lability. A related study by Haque et al., using metal-substituted MIL variants, reached a similar conclusion.[94] In this case, it was also found that the activation energies for both nucleation and growth varied systematically with metal, with V <Al <Cr, and that both activation energies and reaction rates were correlated with known water exchange rates. Later, Wu et al. examined a series of $M_2(bdc)_2$dabco MOFs, reaching a similar conclusion.[12]

4.4.4 Influence of Linker Functionalization

Functionalization of linkers within an isoreticular series of MOFs can also influence the observed crystallization kinetics, though generalizable trends are not typically as easy to identify as compared to the above cases of metal cation substitution. In one study on linker functionalization, Ahnfeldt and Stock contrasted the synthesis of -OH and -NH_2 functionalized CAU-1 using EDXRD.[65] In the case of CE heating, similar reaction rates were observed, suggesting only a minimal influence from linker acidity or solubility. Later, an extensive EDXRD study of functionalized UiO-66 variants was conducted by Ragon et al.[63,99,100] Those authors probed both the role of linker length and functionalization in UiO-66-like materials, using X-functionalized terephthalates (X = NH_2, NO_2, Br, CH_3), as well as larger linkers (e.g. napthalene dicarboxylate, biphenyl dicarboxylate).[99] Interestingly, crystallization times were seen to decrease with increasing linker length, although the differences were minimal as lower pH. Gualtieri analysis showed that both nucleation and growth steps were significantly faster for the longer vs. shorter linkers in the presence of modest added HCl, with trends reversed at lower pH. Similarly, shorter ligands were observed to crystallize faster at lower temperatures (373 K) and low pH, with smaller differences at higher temperatures (423 K). Estimated activation energies also seemed to scale with linker length, ranging from 22 kJ/mol all the way to 72 kJ/mol. The authors argued that many of these observations can be explained in terms of ligand solubility.

The authors continued by examining the role of linker functionalization,[99] finding that the unfunctionalized, $-CH_3$, and -Br variants all exhibited similar crystallization behavior and almost no induction time, whereas the -NO_2 and -NH_2 variants displayed induction times two and five times longer, respectively. All materials displayed very similar crystallization times, with the exception of UiO-66-NH_2, which was significantly slower at higher temperatures. At these higher temperatures, all materials (with the exception of UiO-66-NH_2) displayed similar crystallization curves and thus similar kinetics, but differed at lower temperatures.

These differences do not generally appear to correlate with linker acidity, and may instead be related to linker solubility, though the unique behavior of the -NH_2 variant can possibly be attributed to the basicity of the functional group. Despite similar reaction times, sharply different activation energies were calculated for each variant: 77, 15, 35, and 113 kJ/mol for -CH_3, -Br, -NH_2, and -NO_2, vs. 22 kJ/mol for unfunctionalized UiO-66. No clear physical explanation for these striking differences was provided.

The kinetics and mechanism(s) of post-synthetic ligand exchange have also been probed via XRD methods. Ban et al. examined the ligand exchange of a parent ZIF-108 MOF, monitoring the structural evolution upon exposure to a solution of an alternate linker.[131] XRD was used to monitor the appearance of peaks corresponding to the final (product) topology and the associated weakening of peaks corresponding to the parent structure, suggest a dissolution-heterogeneous nucleation mechanism, where the underlying ZIF-108 parent acts as a seed. This conclusion was also supported by monitoring of the morphology of the crystals via SEM, which showed a transitions from quasi-spherical ZIF-108 into hexagonal rod-shaped product.

4.4.5 Influence of Crystallization Promoters / Modulators

Modulators are commonly employed to aid in MOF synthesis. These modulators are often monodentate ligands (as opposed to the bi- or multi-dentate ligands used as organic linkers), and various mechanisms for modulation have been proposed, including deprotonation modulation (altering the protonation state of the organic linker) and coordination modulation (competitive coordination of the modulator and metal).[110] In the latter case, the competitive binding of the modulator may slow aggregation processes, and can potentially avoid the formation of undesirable amorphous products. In either case, such modulators can often aid in MOF crystallization and/or alter the morphology of the resulting crystalline product.[132]

A number of studies have supported a deprotonation modulation mechanism for formate and amine modulators during ZIF synthesis. For example, Cravillon et al. used EDXRD to examine the role of added formate on the solvothermal synthesis of ZIF-8.[64] (Importantly, the EDXRD results had to be collected under stirring conditions, whereas most ZIF-8 solvothermal syntheses are performed under static conditions. SEM experiments from the same study, discussed in Section 7.2.1, identified qualitatively different particle morphologies depending on stirring conditions, thus pointing to a possible complication in using EDXRD to investigate traditional ZIF-8 solvothermal synthesis.[64]) EDXRD showed that ZIF-8 emerged rapidly with short induction time when synthesized at 130°C. Avrami analysis suggested that, in-

dependent of the modulator, growth was limited by a "surface reaction". Gualtieri analysis led to somewhat different conclusions, and identified nucleation as rate-limiting with activation energies of 69 and 72 kJ/mol for nucleation and growth, respectively. Insight regarding the role of the modulator was obtained by examining various modulator concentrations. Increased modulator concentration led to decreased induction times and higher nucleation rates, yielding smaller crystal size. In this case, the authors thus concluded that the principle role of the formate modulator was to deprotonate the Hmim ligand, rather than to directly compete for metal binding sites, but emphasized that formate may play a different role in *room temperature* ZIF-8 synthesis.

Later, Goesten et al. used a combination of SAXS/WAXS and quick-scanning EXAFS to probe the synthesis of ZIF-7 under the influence of an amine modulator.[105] Both nucleation and growth rates (obtained from Gualtieri analysis of WAXS data) increased slightly with amine concentration. Interestingly, the amine also favored growth of certain crystallographic planes, and SEM confirmed that particle morphology could also be influenced via the modulator. The authors proposed that the role of the basic amine modulator is to neutralize the acid generated during ZIF synthesis (and thus maintain the proper protonation state of the linker).

In other cases, coordination modulation is likely the principal mode of action for monodentate additives, such as formic acid — with the success of the synthesis sometimes hinging on the additive. Behrens and coworkers examined the crystallization of one such system, Zr-fumarate MOF, using EDXRD.[110] Synthesis was conducted in either water or DMF solvent, and differences in the influence of the formic acid modulator with solvent were noted. In aqueous solution, MOF synthesis was rapid. Under large excesses of modulator (70-150 equivalents), crystallization induction times increased from 2 minutes (in the absence of modulator) up to as high as 86 minutes. This increase in induction time, along with the already acidic conditions, strongly supported a coordination rather than protonation modulation mechanism. (Owing to the topological similarities between Zr-fumarate MOF and UiO-66, this result contrasts somewhat with a previously-mentioned study by Goesten et al. on UiO-66, in which hydrochloric acid was implicated as a *protonation* modulator.[120]) Gualtieri analysis showed that increasing modulator concentration led to decreases in both the nucleation and growth rates, and thus increased particle size. At least in DMF solvent, the authors ascribed the true role of added formic acid modulator to small amounts of water contamination within the acid, as similar enhancement were achievable from direct addition of small amounts of water (which is required for the hydrolysis of the $ZrCl_4$ precursor).

Nonetheless, addition of formic acid was still seen to yield larger crystals (as evidenced by SEM), suggesting that the coordinating modulation of the formic acid also remains intact.

Adding a high modulator concentration can also induce defects, including vacancies, into the resulting MOF structure. Cliffe et al. demonstrated that addition of a formic acid modulator during the synthesis of **fcu** UiO-67(Hf) yielded a new layered structure with a lower ligand:metal ratio, dubbed **hcp** UiO-67.[66] Monitoring of the PXRD and SAXS signals showed that the **hcp** UiO-67 was formed via a three-stage process initially involving the formation of a noncrystalline inorganic aggregate followed by the subsequent crystallization of **fcu** UiO-67(Hf) and, eventually, **hcp** UiO-67(Hf). Comparison of the pair distribution functions (PDFs) from a variety of samples within the UiO-67 family showed that **fcu** UiO-67(Hf) is consistent with a "double cluster" formed by condensation of the hafnium oxide nodes to compensate for its ligand deficiency.

In many cases, direct information regarding the mode of action of a promoter is difficult to obtain; instead, the ultimate *effect* of the promoter on nucleation and growth is typically measured. A rare exception comes from a series of works by Huber and coworkers, who examined the role of a 4-decylbenzoic acid modulator in MOF-5 growth, providing unique insights into the *modus operandi* of a modulator species. Rather than x-ray approaches, they utilized time-resolved small angle neutron scattering (SANS) and static and dynamic light scattering.[132,133] The authors employed a zinc benzoate precursor compound that directly provides the pre-formed MOF SBUs and examined growth both in the presence and absence of the modulator.[132] Static light scattering showed that particle growth in the presence of the modulator was slowed significantly, particularly in the initial stages of growth, suggesting the influence of the modulator is primarily in the particle formation process; no significant impact on the final particle shape was observed. Later, many of the same authors probed the spatial localization of the modulator using SANS.[133] The authors isolated the scattering signal of the modulator via contrast matching using a mixture of deuterated and hydrogenated DMF solvents designed to match the scattering contrast of MOF-5. They found a focusing/narrowing of the particle size distribution, with larger particles disappearing while small particles continue to nucleate; this focusing was significantly accelerated in the presence of the modulator. Analysis of the contrast matched scattering signal strongly supported a model of a modulator monolayer shell surrounding the MOF-5 particle, possibly bound via the carboxylate group (see Fig. 7).The authors attributed the observed particle size narrowing to the formation of this shell, although a detailed mechanistic explanation for the focusing was not given.

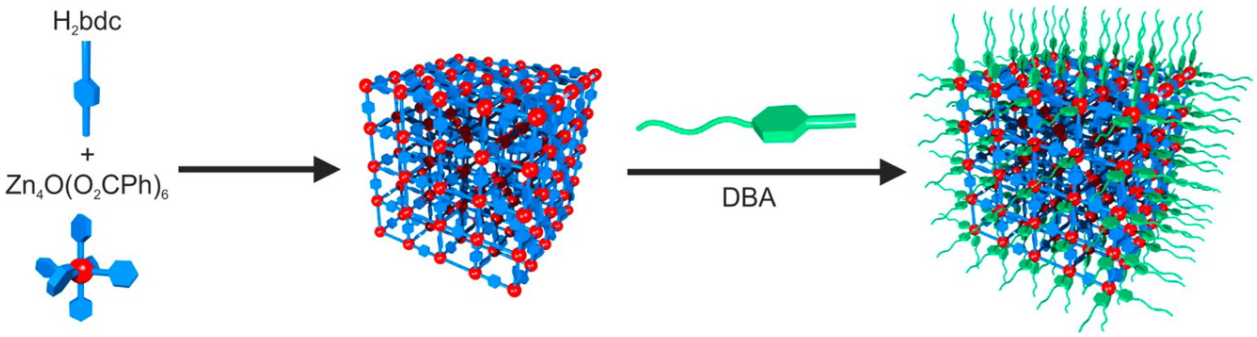

Figure 7: Concept of trapping MOF-5 nanocrystals by time-delayed addition of the coordination modulator DBA (4-Decylbenzoic acid) to the mixture of pre-SBU $[Zn_4O(C_6H_5COO)_6]$ and BDC (1,4-Benzene-dicarboxylic acid) at room temperature; the nanocrystal growth is controlled by the formation of a capping Shell of DBA modulators. Reproduced with permission from ref. 133. Copyright 2014 American Chemical Society.

A structure directing agent / modulator need not consist of a small molecule additive, but could instead include an inorganic template,[134] or even the solvent / co-solvent. Logar and coworkers identified such a solvent-directed synthesis in the cases of MIL-100(Fe) and MIL-45(Fe), probing the Fe K-edge during crystallization using XAS.[135] Depending on the nature of the solvent (H_2O vs. H_2O/acetone), synthesis yielded either MIL-100 (containing Fe(III)) or MIL-45 (Fe(II)), in both cases starting from an $FeCl_3$ precursor. The authors concluded that the acetone co-solvent plays an essential role in the synthesis of MIL-45 by acting as an in situ reducing agent, reducing Fe(III) to Fe(II) to yield the MIL-45 product; in the the absence of acetone, MIL-100 was observed. In this case, the structure directing influence is not via templating, but rather indirect, steering the synthesis toward the desired product through the in situ production of a necessary reagent.

4.4.6 Growth on a Substrate

The ability to grow MOFs onto substrates promises to enable a variety of exciting applications, including membranes (for separations), sensors, and catalysis.[136] As such, a number of groups have explored the growth of various MOFs on a variety of substrates, including those deposited on self-assembled monolayers (SAMs), and have often probed the growth of the resulting surface via XRD methods. For example, it has been often observed that the nature of the SAM functionalization can influence the dominant crystallographic orientation of the resulting MOF. To this end, Biemmi et al. examined the growth of HKUST-1 on an Au surface coated with a thiol-based SAM under a variety of functionalizations, monitoring growth

with time-resolved XRD.[137] Use of -COOH and -OH functionalized SAMs yielded films oriented in the [100] and [111] directions, respectively, whereas methyl functionalization led to less oriented growth. The authors speculated that this specificity may be due to the oriented attachment of growth units at the interface,[137,138] followed by subsequent oriented growth. Interestingly, growth on the methyl surface, while not highly oriented, was faster. In this case, attachment may be due to dispersive interactions between an organically-terminated crystal face and the alkyl SAM.

Several authors have also examined the oriented growth of ZIFs on variety of other substrates. Bux et al. used a combination of ex situ time-resolved XRD and SEM to probe the oriented growth of ZIF-8 membranes on α-alumina.[139] After initiating growth via deposition of seed ZIF-8 crystallites, they eventually observed the growth of a ZIF-8 layer that grew with a strong preference for the {100} plane parallel to the support. They found that this crystallographically-preferred orientation grew in with time / thickness from an initially random orientation, and explained their result in terms of an evolutionary model[140] whereby crystallites with high degrees of anisotropic growth (perpendicular to the surface) overgrow their neighbors and form the top, oriented, layer. An evolutionary model was also employed by Kida et al. to explain a similar transition from random to preferential growth of ZIF-8 on a glass substrate, monitoring growth via a combination of XRD, FTIR, and SEM.[141]

Finally, one study has shown how the substrate utilized for growth need not be crystalline. Centrone et al. monitored the growth of MIL-47 on polyacylonitrile (PAN) using a variety of techniques, including XRD and SEM.[136] The PAN substrate undergoes acid hydrolysis under reaction conditions to yield a carboxylic acid functionalized material — the same functionality as the MOF building block. This feature appears essential, as the MOF does not grow on related unfunctionalized surfaces. Time-resolved XRD measurements of the deposited MIL-47 showed evidence for three phases: undissolved reactants, a disordered MIL-47 precursor, and crystalline MIL-47, the latter appearing only at later synthesis times. The authors interpreted these results as evidence for crystalline MIL-47 growth at the expense of a disordered precursor consisting of the same building blocks but lacking long-range order.

5 AFM

5.1 Overview

Atomic force microscopy (AFM) is a powerful technique for investigating growing MOF surfaces and thin films. By scanning a mechanical tip across a sample surface, AFM provides a direct measurement of intermolecular forces at the atomic scale, generating a three-dimensional surface profile with characteristic nm spatial and μs or better temporal resolution. As a result, both in situ and ex situ AFM have frequently been applied to explore crystal growth (but not, as of yet, nucleation) for several ubiquitous MOF systems, including MOF-5, HKUST-1, and various ZIFs. Ex situ AFM experiments on crystal surfaces have been employed to study the influence of various reaction parameters, such as the metal-to-ligand ratio and (for thin films) the choice of substrate. More recently, in situ AFM techniques have also been developed, in turn enabling detailed analyses of step heights, surface termination effects, and relative growth rates for different crystal facets. Consequently, in situ AFM shows great promise as a direct, time-resolved approach to quantify growth rates, postulate and/or substantiate new growth mechanisms, and identify and characterize fundamental MOF growth units.

5.2 Mechanistic Analyses

5.2.1 Evidence for Classical Growth Mechanism(s)

Attfield and coworkers have performed a number of AFM studies to investigate ZIF crystal growth; consistent with classical models described in Section 2.2.1, they have found evidence for both "birth and spread" and spiral growth mechanisms at low supersaturation. Probing the solvothermal growth of ZIF-8 in DMF, in situ AFM revealed that both birth and spread and spiral growth occurred simultaneously on different regions of the (110) crystal face (see Fig. 8).[142] Later, Cubillas, Anderson, and Attfield used in situ AFM to monitor growth of two ZIFs with LTA topology, $[Zn(Im)_{2-x}(bIm)_x]$ and ZIF-76.[143] Their results indicated that crystal growth of ZIF-76 began via a birth and spread mechanism, with a relatively high nucleation rate. However, as the supersaturation level dropped and surface nucleation rates decreased, spiral growth was observed (see Fig. 2), a finding which is in line with classical theories of growth.

The same work by Cubillas et al. also provided important microscopic details regarding the mechanisms of ZIF growth. Using step height analyses, Attfield and coworkers found that

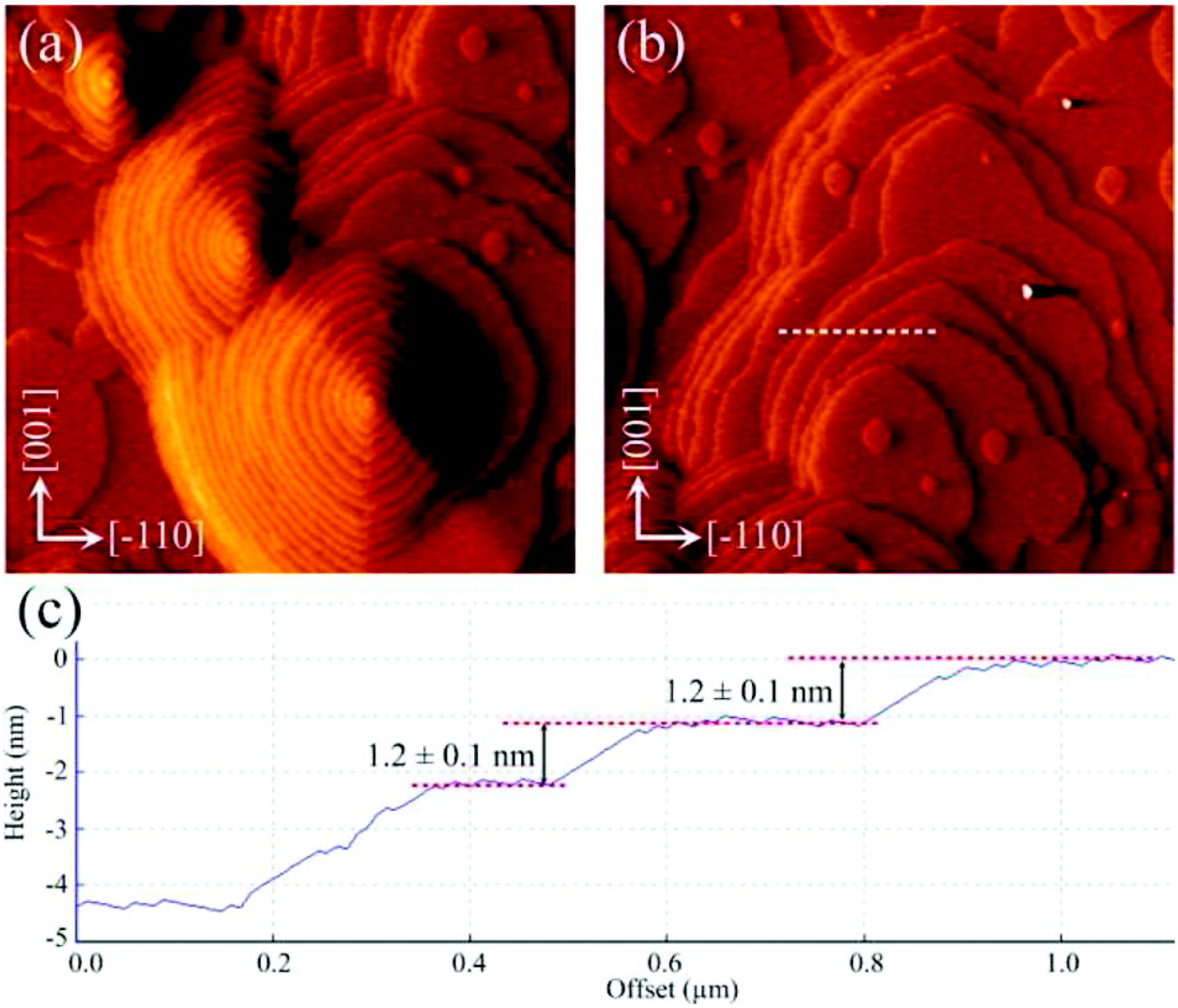

Figure 8: In situ AFM deflection images (4.0 x 4.0 μm^2) of the (110) face of ZIF-8 showing growth steps formed by (a) spiral growth mechanism and (b) "birth and spread" mechanism; (c) cross-sectional analyses of some growth steps revealing the 1.2 ± 0.1-nm step heights corresponding to the d_{110} crystal spacing of the material. Dashed white line in (b) indicates the line along which the cross-sectional analysis shown in (c) was performed. Reproduced with permission from ref. 142. Copyright 2011 American Chemical Society.

crystal growth proceeded via two-dimensional nucleation and further spreading of metastable sub-layers. Importantly, these sub-layers were temporarily bridged and stabilized by non-framework species before finally forming stable terraces; furthermore, this general mechanism was found to hold for several other MOF systems including HKUST-1[144,145] and MOF-5,[146] suggesting that such a mechanism could be widely applicable to a diverse set of nanoporous crystalline materials.

5.2.2 Characterization of Fundamental Growth Unit(s)

Due to the ability of AFM to resolve sub-nm step heights at the growing MOF crystal interface, several studies have employed in situ AFM to identify the fundamental growth unit(s) involved in MOF growth. In 2012, Cubillas et al. used in situ AFM to track the surface growth of MOF-5.[146] In an important insight, a time-resolved step height analysis revealed that simple monomeric units (Zn^{2+} ions and H_2bdc linkers), and *not* the full SBUs, were responsible for the growth of MOF-5, with non-framework species playing a crucial role in stabilizing partially formed layers. By varying the Zn/H_2bdc concentration ratio, the authors discovered that both the underlying atomistic-level growth mechanism and the resulting crystal morphology depended strongly on the relative metal/ligand concentrations, although the nature of the growth unit was unaltered. A subsequent study on MOF-5, this time via a "controlled SBU approach", used in situ AFM to discern whether or not the SBU [$Zn_4O(O_2CC_6H_5)_6$] remained intact during growth.[147] Critically, step height analysis showed no evidence for growth by full SBU units; instead, the SBUs were found to undergo at least partial dissociation prior to framework incorporation. Furthermore, and consistent with prior work, Zn^{2+} ions and H_2bdc linkers were both found to be important fundamental growth units. Despite these mechanistic similarities, the SBU-containing growth solution *was* found to influence the relative growth rates along different crystallographic directions, sometimes leading to faster nucleation when compared to simpler zinc salts. Consequently, although the MOF-5 SBUs were not fundamental growth units, partially-dissociated SBUs may fill this role, and the presence of SBUs clearly influenced the overall growth mechanism.

Similar in situ AFM analyses have also been conducted on HKUST-1,[144,148] ZIF-8,[142] and ZIF-76,[143] all of which implicate simple solvated metal ions and organic linkers (rather than larger complexes) as fundamental growth units. In each of these studies, the authors observed growth via successive metastable sublayer formation (often with metal ion-terminated sublayers showing the greatest stability), and frequently found that non-framework species were essential for stabilizing these sublayers. Given the diversity of topologies that have been

studied thus far, MOF growth via stabilized attachment of simple organic and/or inorganic monomeric unit may well be a fairly general phenomenon in MOF crystallization.

Nevertheless, a few contrasting studies do support the role of more complex, pre-assembled structures in growth. For example, an early in situ AFM study of a 1D Cu coordination polymer identified small oligomeric moieties (possibly polymeric chains) as plausible growth units.[149] More recently, an in situ study on the MOF CdIF-4 observed pre-assembled metal-ligand complexes as fundamental growth units, finding no evidence for stable attachment of simple organic linkers. These contrasting studies highlight the difficulties in drawing broad generalizations regarding the nature of fundamental MOF growth units.

5.2.3 Surface Growth Features: Termination and Defects

AFM has also been used to probe other aspects of growing MOF surfaces, including preferred surface termination(s) and growth defects. In the former case, analysis of AFM-measured step heights provides a method to deduce the surface termination of the MOF. In the case of HKUST-1, Attfield and coworkers measured characteristic growth step heights of ∼1.5 nm, corresponding to the d_{111} crystal spacing of the HKUST-1 structure,[144] thus suggesting a surface termination motif involving a layer of Cu-centered octahedra and trimesate groups (see Fig. 9). In addition, the measured step height distribution was inconsistent with the full dimeric SBU acting as the fundamental growth unit of HKUST-1, but rather suggested simpler (smaller) fragments. As for the case of ZIF-8, many of the same authors found characteristic growth steps heights of ∼1.2 nm, corresponding to the d_{110} crystal spacing.[142] Further height analysis of substep heights implied that the surface plane was formed by a layer of $[Zn(MeIm)_3]^-$, likely with solvent (rather than $MeIm^-$) acting as the terminating species. This surface termination motif further confirmed that units simpler than SBUs (likely monomeric species) can act as the fundamental growth units.

AFM can also provide important insight into MOF surface defects. Shoaee et al. found growth hillocks in their ex situ AFM study of HKUST-1 {111}, explaining them as dislocation growth spirals.[148] Many of these growth spirals were found to originate from screw dislocations, and their prevalence suggests that spiral growth may be dominant in late-stage HKUST-1 crystallization. The atomistic structure of these screw dislocations was analyzed in great detail by Walker and Slater using isotropic continuum elastic (ICE) theory,[150] whereby surface fracturing of the crystal, primarily along the <110> direction, was also observed and ascribed to post-synthetic treatment of the crystal. Based on bonding arguments, the authors hypothesized that these fractures most likely occur along the {100} and {200} planes,

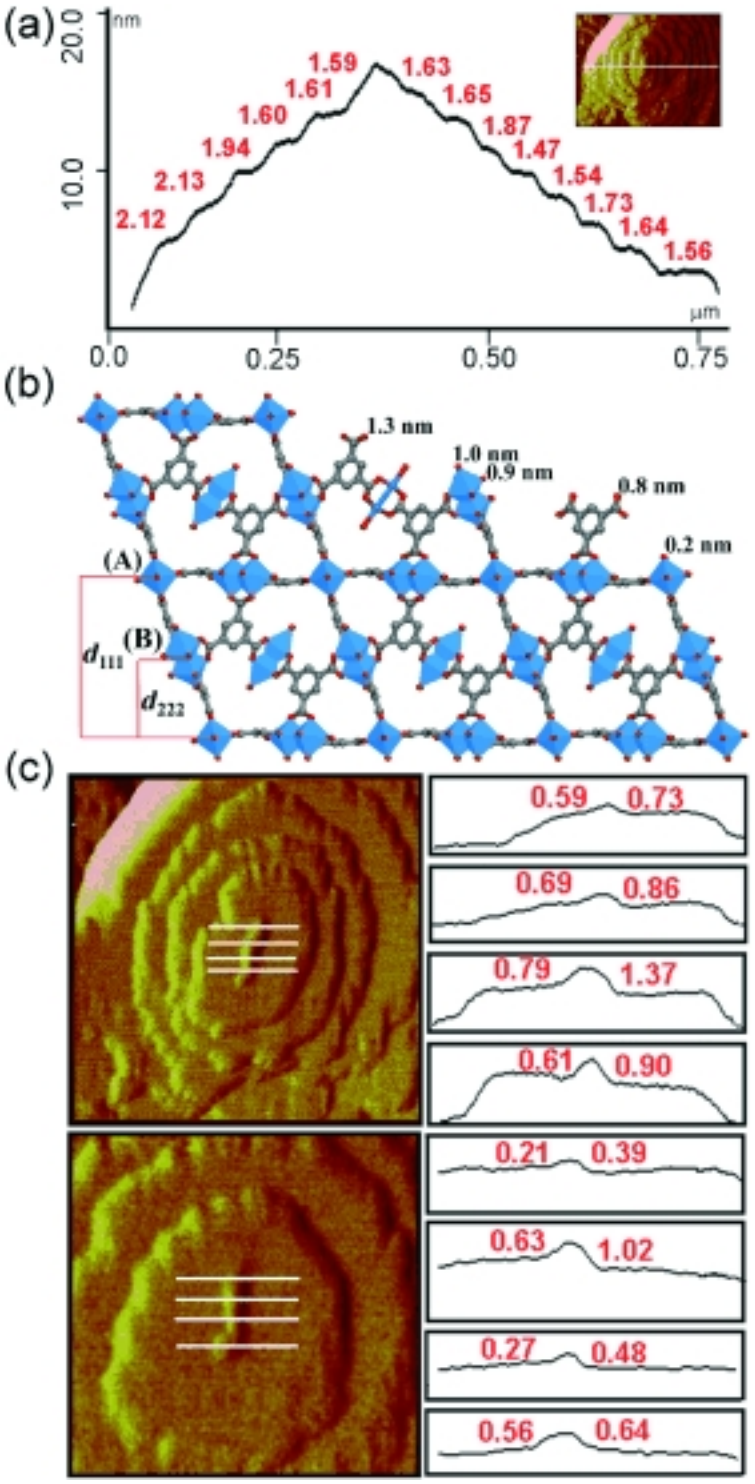

Figure 9: a) Cross-sectional analysis of a typical step train on the 111 face of HKUST-1; b) the structure of HKUST-1 viewed down a 110 direction highlighting possible d_{111} and d_{222} crystal spacings and the perpendicular height of the oxygen atoms of possible intermediate surface terminations above the copper species in the layer (A); c) cross-sectional analyses at various points along different nuclei on the top most layer of a growth hillock. All heights are quoted in nm. Reproduced from ref. 144 with permission from John Wiley and Sons.

thus avoiding breaking strong bonds.

5.3 Influence of Reaction Parameters

5.3.1 Influence of Solution Composition

As with SEM (discussed in Section 7), AFM allows for time-resolved studies of crystal morphology, thus enabling detailed molecular-level investigations into the influence of reaction parameters (e.g. solvent) on the resulting crystal growth. As an example, Cubillas et al. explored the effect of solution composition on the growth rate and resulting morphology of MOF-5 under low supersaturation.[146] With Zn/H_2bdc ratios greater than 1, the authors found growth along the <100> direction to be slower than <110>, yielding square terraces with steps parallel to <100>. Conversely, with $Zn/H_2bdc \sim 1$, growth along <110 > was slower, which instead lead to rhombus-shaped terraces with steps parallel to <110>. Subsequently, Cubillas et al. used in situ AFM to examine the epitaxial crystal growth of a mixed metal core(MOF-5)-shell(Co/Zn-MOF-5)-shell(MOF-5) crystals at room temperature and low supersaturation.[151] The authors found evidence that the addition of Co to the growth solution slowed or even (at high Co concentrations) halted the overall rate of surface growth as compared to Co-free conditions. Furthermore, the presence of Co altered the relative growth rates along the [110] and [100] directions, inducing crystal morphology changes. The authors explained these observations in terms Co-induced solution species that may inhibit growth at step edge or kink sites.

5.3.2 SURMOF Growth on Substrates

In addition to AFM studies on bulk MOF growth, many authors have performed AFM analyses of surface-attached metal-organic frameworks (SURMOFs), with a specific emphasis on HKUST-1 growth on functionalized substrates. Compared to growth in bulk solution, growth on substrates generally appears to yield crystalline products with lower defect concentrations. For example, Szymonski et al. employed AFM to study the (111) surface of HKUST-1 microcrystals grown on COOH-terminated SiO_2/Si(100) wafers in air and under ultra high vacuum (UHV) conditions.[152] Compared to prior AFM studies on bulk, solution-synthesized HKUST-1 crystals, they found that crystals grown on the substrate were free from screw dislocations and exhibited a homogeneous (111) termination. In contrast, previous studies on bulk HKUST-1 exhibited a high density of screw dislocations and chemical inhomogeneity, with both (111) and (222) terminations. Later, John et al. used in situ AFM

to investigate the growth processes of oriented HKUST-1 crystals grown on self-assembled monolayers (SAMs) on Au substrates.[145] In contrast to their prior work on bulk HKUST-1,[148] the SURMOF showed low-defect monolayer growth. This growth was 2D and appeared to nucleate at the same point on each surface layer. Real-time high-resolution AFM defect images and step height analysis supported a layer-by-layer growth mechanism of a 1.5 nm d_{111} step of HKUST-1 and anisotropic advancement of the triangular growth steps.

AFM can also be used to provide insights into the fundamental nature of the HKUST-1 SURMOF growth layers themselves. For instance, Munuera et al. utilized AFM to probe the layer-by-layer growth of HKUST-1 SURMOFs on functionalized self-assembled monolayers (SAMs).[153] According to the AFM images, the resulting oriented SURMOFs exhibited high homogeneity over areas on the scale of several square mm. Using a selective deposition method, the authors found that the number of growth layers was proportional to the number of immersion cycles and that each immersion cycle yielded a "half layer" with a thickness of 1.317 nm in the [100] direction, which was initiated by copper ions binding to carboxylate units on SAMs with subsequent coordinating BTC units to Cu ions.

More recently, Ohnsorg et al. used AFM to probe the layer-by-layer growth of HKUST-1 SURMOF via liquid-phase epitaxy.[154] Using scanning probe microscopy, the authors examined the first ten fundamental layers of HKUST-1 and found that the thin film first nucleated as small isolated nanocrystallites and then expanded in size as the deposition cycles increased, consistent with an island formation (i.e. Volmer–Weber) growth mechanism. The authors also explored the role of deposition temperature and substrate quality, finding that higher temperatures yielded smaller particles and higher / smoother substrate coverage, whereas substrate quality had minimal influence on film formation.

6 Other Probes of MOF Thin-film Growth

Beyond AFM, the nucleation and growth of MOF thin films has also be investigated by a variety of other experimental techniques, some of which are highlighted here.

6.1 Quartz Crystal Microbalance

Quartz crystal microbalances (QCMs) exploit the shift in the natural resonant frequency of a quartz crystal as a function of its mass. Under a number of simplifying assumptions, changes in this resonant frequency can also be related to the mass deposited onto a thin-film

coated quartz electrode, yielding a powerful approach for measuring sub-microgram mass changes in thin films.

Two separate studies have recently used QCM to monitor thin-film HKUST-1 growth. Stavila et al. used QCM to perform a quantitative kinetic analysis of HKUST-1 thin-film growth, recording rate constants for the deposition of each layer.[155] The QCM data indicated that the initial layer of $Cu_2(OAc)_4$ grew in via a zero activation energy sticking process with no significant rearrangements or bond-breaking reaction(s). By contrast, growth of subsequent layers [alternating ethanolic H_3btc and $Cu(OAc)_2$] proceeded in a temperature-dependent fashion with relatively low activation energies (14.7 - 21.7 kJ/mol, depending on the layer) and large negative activation entropies (-347.6 to -330.8 kJ/mol K), consistent with a concerted acetate/btc linker exchange (bond breaking and formation occurring simultaneously) and a tight transition state. Importantly, and regardless of the substrate, the global activation energies determined from Eyring-Polanyi analysis of the QCM data were approximately an order of magnitude lower than previously measured for bulk HKUST-1.[89]

A similar study by Nijem et al. used a combination of ex-situ XRD, SEM, and QCM-D (QCM with dissipation analysis) to probe the growth mechanism(s) of thin film HKUST-1 as a function of film thickness.[156] For thin films, the authors found that growth proceeded via rigid attachment of subunits in a layer-by-layer growth mechanism; however, as the film thickness increased (>40 layers), the authors instead observed a grain growth mechanism, non-rigid attachment of subunits (which was particularly pronounced for the $Cu(OAc)_2$ units), and a shift in crystallographic orientation of the supported layers. The authors attributed these effects to heterogeneous nucleation on the more energetically-favorable [200] surface, with non-rigidly attached $Cu(OAc)_2$ serving as a nucleation site.

6.2 SPR

As an alternative to QCM, surface plasmon resonance (SPR) is capable of measuring changes in film thicknesses, with nanometer sensitivity, by propagating electromagnetic waves across a material interface and correlating changes in the resonant frequencies to film thickness. Shekhah et al. employed SPR to monitor the thin-film growth of HKUST-1, finding that no HKUST-1 growth was observed when utilizing $Cu(NO_3)_2$ as the metal precursor under solvothermal conditions, whereas a $Cu(OAc)_2$ precursor produced regular growth cycles whose growth rate depended on surface orientation.[157] The authors ascribed these differences to the lack of solution-phase dimeric paddlewheel structures in the $Cu(NO_3)_2$ solution; in contrast, dimeric $Cu(OAc)_2$ structures are similar to the dimer paddlewheel SBU of HKUST-

1, and the authors hypothesized that the presence of such paddlewheel species in solution is important for HKUST-1 growth.

6.3 IRRAS

Infrared reflection adsorption spectroscopy (IRRAS), a surface-sensitive IR technique, has also been used in several recent studies to track the growth of SURMOFs. In conjunction with complementary surface X-ray diffraction (SXRD) studies, Zhuang et al. used IRRAS to study the temperature-dependent orientation of a Cu_2-paddlewheel MOF grown on two different SAM-functionalized Au surfaces, PPP1 (carboxylic acid terminated) and MTCA (Lewis base terminated).[158] While the composition of the SAM surface clearly affects the orientation of the growing crystal, the authors were additionally able to explain how the deposition temperature affects the resulting crystal orientation and morphology. In a subsequent study on an orthorhombic $[Cu_2(sdb)_2(bipy)]$ MOF, Yu et al. again used IRRAS and SXRD to determine how surface area minimization and Ostwald ripening could out compete templating effects in the oriented growth of the MOF with either PPP1 or MTCA functionalized surfaces.[159] As measured by IRRAS data taken after one deposition cycle, and in contrast with the Cu_2-paddlewheel results, both PPP1 and MTCA displayed the same orientational preference, indicating that the SAM surface chemistry did not play a large role in determining crystal orientation for the $[Cu_2(sdb)_2(bipy)]$ system. Instead, their results supported the important role of surface energy minimization and Ostwald ripening over templating effects (at least of less symmetric crystals) in MOF thin-film growth.

7 SEM/TEM

7.1 Overview

Scanning electron microscopy (SEM) and transmission electron microscopy (TEM) are spatially-localized imaging techniques which have been employed in a large number of time-resolved studies of MOF growth. Both SEM and TEM probe the interaction of a sample with an electron beam, monitoring either the scattered or transmitted electron, respectively. While SEM produces surface profile images of a comparatively large area for both bulk and thin film materials, TEM is limited to studies of thin films, but generates two dimensional projection images with higher resolution. TEM also requires the use of a higher energy beam compared to SEM; because MOF stability is known to be sensitive to this higher energy

beam, TEM studies of MOF materials are, at present, less common than SEM studies (see Wiktor et al.[160] for details). Nevertheless, recent advances[160] in TEM imaging techniques, including cryo-TEM,[161] can help limit beam damage effects, and these advances have begun to be employed in the study of MOF materials.[162]

Due to the need for near vacuum conditions, SEM/TEM cannot typically be utilized in situ under solution-phase conditions, thus imposing limits on the achievable time resolution for each technique. (Note, however, that newly-developed cryo and liquid-phase sample preparation techniques *do* allow for such in situ characterizations;[161,163] see Section 7.2.3 for an example.) Instead, SEM/TEM has almost invariably been used to provide detailed, ex situ, spatially-localized imaging information about MOF crystal growth in the size regime from tens of nm to microns. Numerous studies have utilized SEM/TEM to monitor particle size distributions and/or the morphological evolution of MOFs during growth, thus enabling (vida infra) a detailed understanding of both classical and non-classical crystal growth pathways as well as the influence of various reaction parameters.

Beyond imaging, SEM/TEM instruments can also be used as the basis of several sophisticated scattering and spectroscopy techniques. In combination with SEM/TEM images, electron diffraction[164] (ED) and high resolution TEM (HRTEM) can be utilized to characterize crystal structures (even for nanosized crystals, which cannot be analyzed by XRD), identify surface facets, and detect defects in MOF crystals.[160,165] Two other techniques, energy dispersive X-ray spectroscopy (EDX)[163] and electron energy loss spectroscopy (EELS), both provide quantitative, element-specific compositional information. EDX is primarily sensitive to the presence of heavy elements (i.e. metal species within the MOF), while EELS is usually more suitable for study of light elements.[160]

7.2 Mechanistic Analyses

7.2.1 Ostwald Ripening

Ostwald ripening has often been observed during the crystal growth of MOFs, and several studies have been devoted to investigations of ZIF-8 in particular.[30,64] In one such study, Cravillon et al. monitored the crystal morphologies observed during formate-modulated ZIF-8 crystal growth under solvothermal conditions using EDXRD (see Section 4.4.5) and SEM.[64] Importantly, SEM revealed that the homogeneity of the crystal particle morphologies strongly depended on stirring conditions, with more homogeneous morphologies observed under the unstirred conditions typically used in solvothermal ZIF-8 synthesis. Under

these static conditions, the authors initially found a mixture of large and small crystals, with the latter primarily adhered to the surface of the larger crystals, thus suggesting that heterogeneous nucleation on the surface of existing crystals occurred concurrently with crystal growth. Eventually, the smaller crystals were found to disappear via Ostwald ripening; meanwhile, the morphologies of the larger crystals evolved from cubic, to truncated cubic, to truncated rhombic dodecahedron, and eventually into an equilibrium rhombic dodecahedron morphology. A separate study of ZIF-8 formation, this time using room temperature TEM along with selected area electron diffraction (SAED), revealed a substantial increase in the characteristic particle size during synthesis (from 10 min to 24 hours), again consistent with Ostwald ripening effects (see Fig. 10).[30]

Ostwald ripening processes have also been observed in a variety of other ZIF systems. Ban et al. used SEM to monitor the evolution of ZIF-78 crystals under extended solvothermal synthesis.[166] Over a period of 6 – 48 hours, they observed an Ostwald ripening process involving a decrease in crystal defects, an increase in average crystal size, and evolution into well-defined hexagonal rods. Later work by Feng et al., who examined ZIF-67 via SEM, is in agreement with many of these conclusions, showing a growth in average particle size with time (consistent with Ostwald ripening) in conjunction with increased faceting and sharpening of edges and corners.[104] In a related study, Verma and coworkers used AFM and SEM to track the oriented growth of a cubic copper MOF in DMF on either a glass or silicon substrate.[167] Over a period of 30 days, both AFM and SEM images revealed not only the formation of cuboidal aggregates, but also a solution-phase Ostwald ripening process.

7.2.2 Elucidation of Non-classical Growth Pathways

Although classical models of crystal growth dictate that growth occurs from a nucleus via layer-by-layer deposition of the building units, non-classical growth mechanisms have also been observed in some MOF systems. Time-resolved SEM and/or TEM measurements have the potential to track the morphological evolution of MOFs during crystallization, thus facilitating the identification of various non-classical growth mechanisms — including, aggregation, reversed crystal growth and/or splitting growth.

Aggregation-Mediated Pathways Time-resolved SEM/TEM has been previously utilized to probe the time-dependent morphological evolution of MOF microstructures, providing direct insight into aggregation-mediated growth pathways. Such aggregation-mediated pathways can give rise to extraordinary crystal morphologies that strongly deviate from sim-

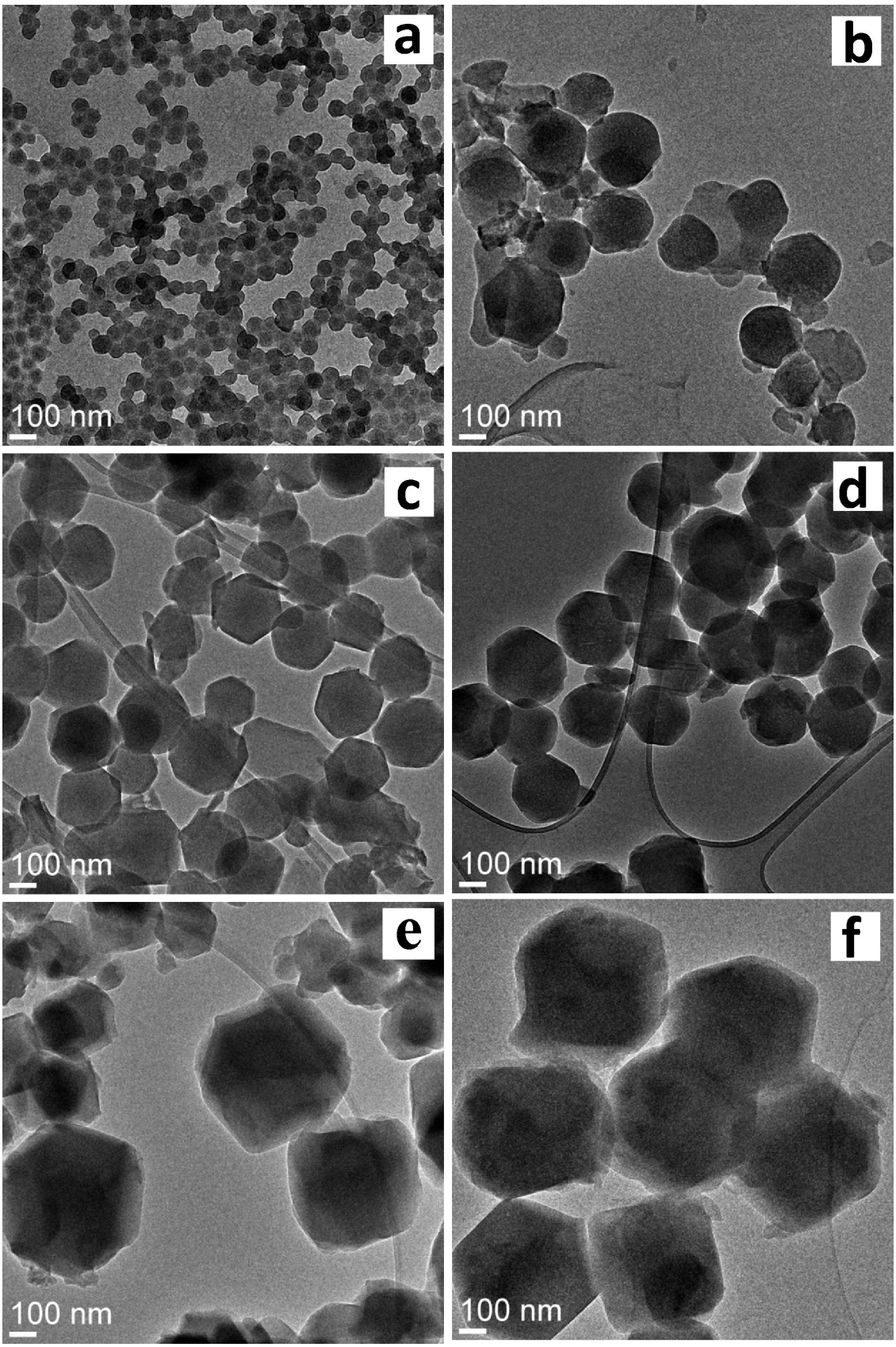

Figure 10: TEM images of ZIF-8 as a function of synthesis time: (a) 10 min; (b) 30 min; (c) 40 min; (d) 60 min; (e) 12 h; (f) 24 h. Reproduced with permission from ref. 30. Copyright 2010 American Chemical Society.

ple predictions based upon classical theories. In one example, Li and coworkers demonstrated the synthesis of novel hierarchical Zn-Hcptpy "microflowers" via a hydrothermal approach, with morphology controllable via the concentration of the triethylamine (TEA) base.[168] SEM was utilized to monitor the morphological evolution, probing the details of microflower formation and growth. Based on SEM analysis, it was proposed that this formation process started with coordination and nucleation of Zn^{2+} with Hcptpy, followed by aggregation and secondary nucleation to form cross-linked sheets and further self-assembly into hierarchical microflowers.

Beyond the formation of hierarchical structures, aggregation has been also observed in the formation of MOF-5. Zheng et al. utilized both SEM and HRTEM to characterize intermediate species identified during the crystallization of MOF-5 from DMF solution.[169] The authors proposed a novel formation mechanism for MOF-5 based on initial $Zn_5(OH)_8(NO_3)_2 \cdot 2\,H_2O$ nanoplate formation, aggregation to form larger microplates, microplates packing to form layered inorganic-organic composite, and eventual transformation into 3D crystalline MOF-5 (see Fig. 11). Aggregation of the resulting MOF-5 nanocrystallites yielded porous structures that eventually transitioned into cubic single crystals via surface recrystallization in a commonly-observed process known as 'reversed crystal growth' (vide infra).

Reversed Crystal Growth Reversed crystal growth is a non-classical growth phenomenon that was first discovered in zeolites by Zhou and co-workers in 2007.[170] In such reversed growth, crystal growth occurs via aggregation of nanocrystallites followed by surface recrystallization, with single crystal growth extending from surface to core in the opposite direction predicted via classical growth. Reversed crystal growth has also been observed in MOFs such as MOF-5. In this case, Greer et al. identified a complex pathway towards growth of a thermodynamically-stable cubic phase, beginning with the formation of MOF-5 nanoplatelets, and followed by aggregation to form larger polycrystalline "microcubes".[171] At later times, the authors found that nanoplatelets interconnected and grew to form an interpenetrated "house-of-cards" structure, and that growth over even longer timescales eventually led to a single crystal cubic shell that grew inward (toward the core) via Ostwald ripening. In a separate study, similar reversed growth was also observed for the Zn-based RHO ZIF using SEM, TEM and PXRD.[172] A detailed growth mechanism for the ZIF was proposed: At the early stage of growth process, spherical aggregates formed from disordered precursor materials. These aggregates joined to form porous pseudo-rhombic dodecahedral particles, followed by surface recrystallization leading to a single-crystal outer shell encasing

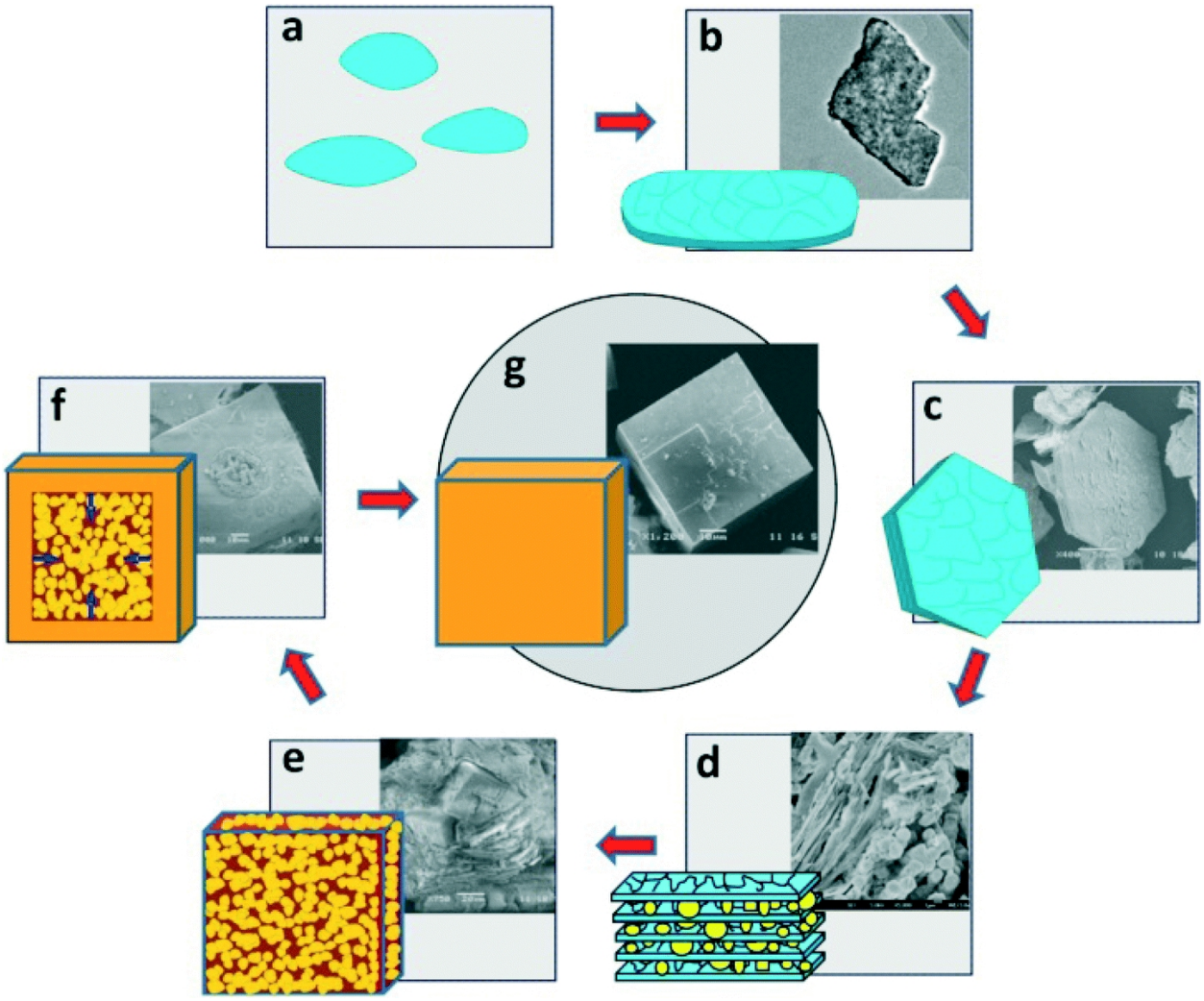

Figure 11: Schematic drawing of a proposed formation mechanism of MOF-5 cubes. (a) $Zn_5(OH)_8(NO_3)_2 \cdot {}_2H_2O$ nanoplatelets. (b) Large microplate consisting of nanoplatelets and 1,4-BDC molecules. (c) Inorganicorganic composite layered particles with packing of the $Zn_5(OH)_8(NO_3)_2 \cdot {}_2H_2O$ microplates along the [100] zone axis. (d) Multiple nucleation of MOF-5 and development of nanocrystallites inside the microplates. (e) Aggregation of MOF-5 nanocrystallites into porous cubic particles in the layered particles. (f) Surface re-crystallisation of the cubic particles into single crystalline shells. (g) Extension of re-crystallisation from the surface to the core, leading to true single crystals. Reproduced from ref. 169 with permission of The Royal Society of Chemistry.

a porous core. Finally, a single crystal was formed by extending crystallization from surface to core.

Splitting Crystal Growth Splitting crystal growth, defined as the splitting / fracture of a crystal at growing faces to yield sheaf-like structures, has been invoked to explain sheaf-like morphologies exhibited by some naturally-occurring crystals. Such crystal splitting is generally believed to be associated with fast crystal growth and is dependent on solution supersaturation.[173] Using SEM and TEM, Zhang and coworkers observed splitting crystal growth in the formation of various La-containing MOF nanocrystals.[174,175] In particular, hierarchical flower-like superstructures, consisting of well aligned nanowires, were discovered in the crystallization of Eu(1,3,5-BTC)$_6$.[174] (Notably, these hierarchically-structured motifs bore similarity to those previously observed in inorganic materials, such as $LnVO_4$ and Bi_2S_3, whose morphologies have also been attributed to splitting crystal growth.[173,176]) The hierarchical structures in Eu(1,3,5-BTC)$_6$ were presumed to originate from 'fractal' splitting of the MOF during the early stages of the reaction. In addition, the extent of splitting was seen to decrease with concentration and temperature, likely because those factors increased the number of nuclei and thus slowed the growth process, in turn decreasing the degree of splitting. Subsequently, many of the same authors also confirmed the presence of split growth in the crystallization of another La-containing MOF, Ce(1,3,5-BTC)$_6$.[175] Depending on stirring conditions and heating method, well-organized sheaf-like structures were observed by SEM at very early growth stages, followed by evolution into a much denser "straw-sheaflike" structure as a consequence of splitting growth.

Self-templated Formation Mechanism As shown above, observations of complex or hierarchical nano-/micro-structures can often indicate the presence of non-classical growth pathways. A fascinating example of this can be found in the growth of hollow MOF microparticles (hollow-Zn-BTC), which Lee et al. observed using SEM and TEM.[177] The author's imaging studies demonstrated a "self-templating" mechanism for crystal growth, initiated by the formation of solid microspheres. This solid formation was subsequently followed by templated secondary-growth along the outer surface of the microspheres; simultaneously, the initial spherical particles dissolved, ultimately resulting in hollow nanoparticles. In contrast to the initial solid microspheres (which were poorly crystalline and nonporous), the final hollow nanoparticles were found to be highly crystalline.

7.2.3 TEM Studies of ZIF Growth

Recently, advances such as liquid cell TEM (LCTEM) have been utilized to facilitate powerful in situ probes of ZIF nucleation and growth. Patterson et al. used in situ LCTEM to monitor the growth and dynamics of ZIF-8 at high magnification and in real time.[163] From analysis of their movies of ZIF-8 growth, they concluded that the formation of ZIF-8 particles does not occur via aggregation, but rather through the growth of smaller subunits in solution; these results are consistent with the conclusions of the prior SAXS/WAXS studies of Cravillon et al.[31] The authors note that nucleation can also be limited by local depletion of reactants in solution, yielding surface limited growth.

In a separate study, and with the assistance of a direct-detection electron counting camera, local structural features of MOFs — which cannot be solved by diffraction-based techniques — were probed by Han and coworkers using high-resolution TEM (HRTEM).[165] The authors were able to obtain ZIF-8 structural information with spatial resolution of individual Zn atomic columns and organic linkers at an ultralow electron beam dose. They observed 'armchair'-type rather than 'zigzag'-type termination for the (110) surfaces and coherent interfacial structures between assembled ZIF-8 crystals. Additionally, their observations showed that the self-assembly of ZIF-8 crystals generated larger interfacial cavities compared to bulk, thus enhancing the diffusion of guest molecules.

In addition, Carreon and coworkers have used selected-area electron diffraction (SAED) to probe the local crystallinity of ZIF-8.[30,178?] SAED showed well-defined patterns confirming ZIF crystallinity even at short synthesis times when grown at room temperature in methanol.[30] At early synthesis time, the ZIF phase was found to coexist with a secondary ZnO phase exhibiting a nanoneedle morphology, whose identity was confirmed via SEAD and EDS.[?]

7.3 Influence of Reaction Parameters

7.3.1 Influence of Heating Methods

SEM studies of MOF crystal growth demonstrate how different heating methods can influence the resulting particle size distribution. As an example, the morphological evolution of the imidazolate framework Potsdam (IFP) series of MOFs was monitored via SEM by Behrens et al.[179] Under microwave synthesis conditions, the authors found that the resulting crystallites transform from an initially spherical "nucleation" phase into hexagonal particles after ∼40 minutes of reaction. In that case, the particle size distribution was rather narrow and did

not evolve strongly with time, suggesting that the particles' size remains relatively constant even as their morphology evolves. In contrast, conventional electric heating yielded a broader particle size distribution with a larger average size, consistent with a lower nucleation rate. Similar results were obtained by Albuquerque et al. in the case of MOF-74(Ni), where TEM showed that microwave heating yielded smaller grains as compared to those without microwave exposure, likely due to higher nucleation rates under microwave conditions.[124] In a separate study, Masoomi and Morsali used SEM to show how the applied power of alternative microwave / ultrasonic heating can also have an important influence on morphologies, and demonstrated that increased ultrasonic power yielded more uniform plate-like morphologies of the Cd-based TMU-9 MOF.[180]

7.3.2 Electrochemical Synthesis

SEM has also been utilized to detect intermediates and unravel the pathways involved in the electrochemical synthesis of MOFs.[181–183] The electrochemical growth of HKUST-1 was examined by Schafer et al. with a combination of SEM and Raman.[181] A key question in this case was the role of oxygen species in the synthesis when using a Cu electrode as the copper source. HKUST-1 was found to grow only when using Cu_2O (but not CuO), which can be generated either by O_2 (in the absence of an applied potential) or via electrochemical oxidation. Subsequent direct electrochemical oxidation of the solid Cu_2O to yield CuBTC (HKUST-1) was proposed to occur at the solution-cuprite interface in the presence of the linker, consistent with the tight attachment of the resulting crystals to the electrode as seen in SEM. Their results support the conclusion that nucleation of HKUST-1 under electrochemical conditions occurs at the electrode surface rather than in solution and thus differs fundamentally from the expected solvothermal mechanism.

As a follow-up study, Campagnol et al. used SEM and QCM to address an open question regarding late-stage electrochemical HKUST-1 growth. Namely, does late-stage growth occur at the Cu_2O-CuBTC-electrolyte interface, or via solution-based process involving attachment of Cu^{2+} ions? The authors proposed a model for the electrochemical anodic growth of HKUST-1 that involves four phases: nucleation initiated at the electrode surface by release of Cu^{2+} into the solution; island growth of crystals on the surface caused by nucleation adjacent to existing crystals; intergrowth to form a compact layer; and finally detachment due to stress and undercutting of MOF crystals. A key insight from this work is that late-stage electrochemical growth of the MOF indeed occurs at the MOF-solution interface, specifically after dissolution of the metal cation at the metal-MOF interface and migration

of the nascent metal cations to the MOF-solution interface.

7.3.3 Unconventional Techniques for ZIF Growth

The combination of novel reactor or reaction schemes and SEM/TEM imaging have allowed additional insights into ZIF growth. In conjunction with solvo-jet techniques, Choi et al. used SEM to examine the evolution of ZIF-8 particles.[184] By varying the flow rate through the tubular reactor, the nucleation and growth times were varied and the influence on the resulting crystallites was examined via SEM. Slower flow rates (and thus longer residence times) yielded larger and more uniform particles sizes, consistent with longer growth periods. Faster flow yielded irregular particles, whereas slower flow yielded rhombic dodecahedral crystals. SEM and TEM were also used to examine the morphological evolution of particles as they passed through the reactor. Early stages of the reaction showed aggregation of very small particles, without a well-defined shape. These later evolved into truncated rhombic dodecahedral nanoparticles and eventually larger rhombic dodecahedra or rhobicuboctahedra with sharp edges. The authors concluded that crystal growth and facet development occurred in the vapor jet region of the reactor.

In a separate study, Avci et al. used SEM to monitor the morphological evolution of ZIF-8 and ZIF-67 crystals under post-synthetic anisotropic wet-chemical etching.[185] The authors utilized a weak acid (xylenol orange) that protonated the 2-methylimidizole linkers, breaking the metal-linker bond, and coordinating / sequestering the resulting metal cations. The evolution of the ZIF crystallites was monitored with SEM, showing preferential etching of crystal facets exposing high densities of metal-ligand bonds and surfaces of higher dimensionality (i.e. edges over vertices), with the latter phenomenon exploited to generate hollow ZIF microboxes.

7.3.4 Influence of Crystallization Promoters / Modulators

As with XRD, SEM/TEM has also been extensively utilized to explore the role of modulators on MOF crystallization. These SEM/TEM studies offer distinct but complementary insight compared to XRD, with SEM/TEM primarily focused on the influence of the modulator on the the size/morphology of the resulting crystal rather than on quantifying crystal nucleation and/or growth rates.

Coordination modulation is frequently invoked to describe the mode of action for MOF crystallization modulators, with competitive association potentially tuning crystal morphologies and/or size distributions. For example, Kitagawa and coworkers examined the influence

of a monocarboxylic acid modulator on microwave-assisted HKUST-1 synthesis, characterizing the resulting particle sizes and morphology via TEM.[186] They found that addition of dodecanoic acid strongly influenced particle morphology, yielding cubic particles at high modulator concentrations vs. gel-like morphologies in the absence of the modulator. Increasing modulator concentrations led to systematically larger crystals, supporting a role for the additive as a coordination modulator that complexes with the Cu^{2+} cations, thereby decreasing the supersaturation of the precursors and the nucleation rate.

Through selective coordination modulation, modulators can also serve as capping agents to inhibit growth of selected crystal facets, thus yielding anisotropic MOF growth. Using an acetic acid modulator, Tsuruoka et al. performed a time-dependent TEM studies of anisotropic $[Cu_2(ndc)_2(dabco)n\ ]$ nanocrystals formation.[187] Based on their TEM images and ED pattern, the authors related crystal morphologies with their structures and proposed a formation mechanism whereby initial nanoparticle growth was followed by aggregation to yield nanocubes. Further nanocube growth was tuned by selective coordination modulation to the (100) surfaces, yielding preferential growth of nanorods in the [001] direction. Later, Pham et al. demonstrated that the addition of modulators (acetic acid and pyridine) with different functionalities could selectively cap facets of the growing MOF crystals, thus leading to nanocrystals with different desired morphologies.[188]

Surfactants can also act as modulators to induce anisotropic growth via adsorption / desorption on various MOF facets. Time-resolved ex-situ experiments SEM were performed by Yuan et al. to monitor the formation process of Zn-BDC MOF nanorods via a surfactant-assisted approach.[189] An added surfactant, CTAB, was found to act as both a stabilizer and a dispersant, thus controlling both the size and morphology of the resulting MOF. Investigations on the morphological evolution with reaction time using SEM revealed evolution from small primary nanosheets to the final rod-like shape in the presence of CTAB, in contrast to irregular microcrystalline particles in its absence. More recently, Li et al. used SEM to examine the influence of a poly(vinylpyrrolidone) (PVP) surfactant on the morphology of IRMOF-3.[190] By monitoring the time-evolution of the synthesized structures under various reaction conditions, the authors proposed that the observed morphological transitions were due to selective adsorption of PVP onto specific crystal facets.

Beyond coordination modulation, deprotonation modulation can be utilized to influence acid/base equilibria and the protonation state of the organic linker. To this end, Li and coworkers demonstrated the synthesis of novel hierarchical Zn-Hcptpy microflowers via a hydrothermal approach using a triethylamine (TEA) modulator.[168] By altering the con-

centration of TEA (and thus system pH), the authors obtained different morphologies and particle sizes of Zn-Hcptpy product, with morphology evolving with increasing pH from fiber-like, to microfibers, to flower-like to irregular cubic.

Through deprotonation modulation, solvent or solvent mixtures can also play a significant role in altering MOF growth and the resulting crystal morphology. Jian et al. examined ZIF-8 growth in aqueous (rather than organic) solvents, using a variety of Zn sources.[191] SEM showed that the initial crystallites formed were approximately spherical with bumpy surfaces. Via Ostwald ripening, larger particles were eventually formed and reached their equilibrium dodecahedron shape. Notably, interesting differences were also observed compared to ZIF synthesis in organic solvent, likely due to the high pKa of Hmim in water. In particular, the authors suggested that excess Hmim linker may, in this case, serve as a base in the deprotonation of nascent $Zn(Hmim)_n^{2+}$ clusters.

Similar solvent-induced deprotonation modulation has also been observed in other MOF systems. By varying the water ratio in a DMF/water solvent system, a series of NH_2-MIL-53(Al) crystals with various sizes and morphologies were solvothermally synthesized by Guo and coworkers.[192] SEM showed that the crystals initially emerged as spherical aggregates, which then evolved to single crystals and finally in size with various observed morphologies (e.g. cube-like, ellipsoidal and rhomboid crystals). Moreover, the authors examined the influence of water on the nucleation and crystal growth process. Small amounts of water were found to trigger the deprotonation of the organic linker, whereas excess water was observed to inhibit deprotonation; consequently, deprotonation modulation was deemed responsible for altering the nucleation rate and crystal morphology. Asha et al. reached very similar conclusions regarding the importance and modulating role of trace water in a Cd-based MOF.[193] In this case, SEM images revealed that the product morphology evolved from rod-like, to block-type, to plate-like crystalline materials as a function of increasing water content in the DMF/water solvent.

Modulators can sometimes play a dual role in both coordination and deprotonation modulation. Using SEM and XRD, the effects of three different modulators (sodium formate, sodium acetate and triethylamine) on HKUST-1 nucleation and growth were examined by Wang et al..[194] In the case of sodium formate, the authors proposed a bifunctional role for the formate modulator, with higher pH increasing the deprotonation of the organic linkers, increasing nucleation rate and subsequently decreasing crystal sizes. The resulting nanocrystals were then stabilized by the formate "capping" agent, preventing further growth. Very similar conclusions about the bifunctionality of a sodium acetate modulator were reached in

a related study on the crystallization of a lanthanide [Dy(BTC)(H_2O)] MOF, using SEM and TEM to monitor the crystal growth.[195] In both cases, the authors emphasize that nanometer-size particles are achievable only via pH adjustment (to enhance nucleation) and a capping agent (to hinder growth).

The particular influence of a modulator may depend on the nature of the metal source, as demonstrated by Xin et al. in the synthesis of HKUST-1.[196] Via SEM and TEM, the authors observed that the influence of the modulator depended on the nature of the copper source, either $Cu(NO_3)_2$ or $Cu(OAc)_2$; crucially, the latter species directly provides the binuclear copper NBUs necessary for the rapid nucleation of HKUST-1. The modulators (TEA or sodium acetate) were observed to play opposite roles: in the case of $Cu(NO_3)_2$, the deprotonation modulation favored nucleation, generating smaller particle sizes. In contrast, with $Cu(OAc)_2$ (which already rapidly nucleates) as a copper source, high modulator concentrations yielded slower reaction rates, thus yielding larger (sub-micron) particles.

Alterations in a modulator's metal binding affinity, acidity, etc. can also influence the resulting MOF crystal morphology. Using organic solvents as capping agents, Liu et al. concluded that variations in a solvent's metal coordinating ability resulted in different modulation effects in the growth of a Co-based MOF.[197] Solvents with weak metal binding (EtOH, THF) could induce anisotropic growth via facet-selective adsorption; solvents with stronger metal affinity, by contrast, could even alter the resulting crystalline phase. Time-resolved SEM studies showed that these solvent-induced changes were evident at the very early stages of crystal growth, even prior to significant crystal growth. In a separate study, Liu et al. compared the influence of acetate and glycerol modulators on the growth of Fe-based MOFs via SEM, with the modulators showing profoundly different modes of action.[198] Introduction of acetate into the growth mixture generated smaller, rod-like particles, as compared to faceted octahedra. In this case, the additive increases solution pH and acted primarily as a deprotonation modulator, with other bases yielding similar changes. By contrast, addition of glycerol improved particle monodispersity and yielded bipyramdial hexagons. This influence was attributed to suppression of Ostwald ripening via decreased diffusion.

8 Optical Microscopy

Optical microscopy is a less well-utilized technique in studying MOF synthesis, in part due to its lower spatial resolution as compared to electron microscopy (typically sub-micrometer vs. sub-nanometer).[199] Nevertheless, owing to the fact that optical microscopy is spatially-

resolved, relatively cheap, and nondestructive, it can be a powerful method for imaging three-dimensional crystal morphologies.[200] In practice, optical microscopy often serves as a complementary technique to XRD, SEM and/or TEM in the study of inhomogeneous nucleation and growth.

Briefly, optical microscopy has been employed in three principle ways in prior time-resolved studies of MOF nucleation and grow. First, it has been used in several studies to quantify rates of heterogeneous nucleation.[201–204] Second, optical microscopy has been utilized as a complementary technique to detect crystal sizes and morphologies.[146,203,205] Notably, the study by Conato and Jacobson combined both approaches to quantify, via image analysis, the kinetics of crystal growth for SAM-supported MOF-5.

Third, and in a unique twist, *nonlinear* optical microscopy has been utilized in studies of MOFs to observe spatially-localized inhomogeneities in the final crystal products. Specifically, in the previously-discussed interpenetration study of MUF-9 (see Section 4),[122] nonlinear second harmonic generation (SHG) microscopy was utilized as a sensitive probe for interpenetration, owing to the difference in point group symmetry between non-centrosymmetric, non-interpenetrated α-MUF-9 and centrosymmetric, interpenetrated β-MUF-9. Unlike XRD, which is a spatially-averaged technique, the SHG microscopy was able to reveal how both homogeneous and inhomogeneous sub-lattice interpenetration could be observed as a function of synthesis conditions.

9 Light Scattering

9.1 Overview

Light scattering (LS) techniques, including dynamic light scattering (DLS) and static light scattering (SLS), offer an in situ probe of particle size distributions (within the nanometer regime upward), thus offering a relatively unique window into the early stages of MOF nucleation and growth. By measuring the autocorrelation of scattered laser light, DLS yields an estimate of particle diffusion, which (via the Stokes-Einstein relation) can be related to a particles hydrodynamic radius. In contrast, SLS measures scattered intensity as a function of angle, yielding information about particle size (radius of gyration, R_g) and apparent molecular weight (M_w). The connection between the R_g and M_w can yield further insight into particle geometry, for example spherical vs. rod-like particles. Time-resolved SLS (TR-SLS), in particular, is capable of probing the evolution of MOF nucleation and growth with high temporal resolution. Nevertheless, a major limitation of LS is the need for homogeneous

sample solutions, which in practice can necessitate using reagent concentrations more dilute than those employed in traditional MOF synthesis. Because LS is hindered by increasing solution turbidity and the resulting multiple scattering events, local microscopy methods (e.g. SEM/TEM) are often utilized in conjunction with LS to provide complementary data regarding late stages of MOF growth.[206,207]

9.2 Mechanistic Analyses

9.2.1 Elucidation of Nucleation and Growth Mechanism(s)

The time-dependent size and mass information obtainable from in situ light scattering can provide crucial insights into the initial stages of MOF nucleation and growth. Such approaches have been applied several times in the past, including to various ZIFs. Cravillion et al. used TR-SLS to investigate the early stages of the room temperature synthesis of nanocrystalline ZIF-8 in methanol.[208] They observed rapid formation of ∼50 nm particles within the first minutes of mixing, with the authors attributing further subsequent growth in particle size and mass to likely agglomeration / aggregation of the 'primary' nanocrystals. Later, examining a similar ZIF-8 synthesis, many of the same authors found evidence for continuous relatively slow nucleation and fast crystal growth, processes which were not well separated.[206] Moreover, based on the correlation between R_g and M_w derived from TR-SLS and complementary ex situ SEM results, the authors concluded that growth occurs via a combination of particle aggregation (early stages) and monomer addition (later stages) of particle growth.

Exploring related ZIF systems, Huber and coworkers combined time-resolved static and dynamic light scattering techniques to investigate the crystal growth of a dense zinc imidazolate framework with zni topology (ZIF-zni).[207] They found that crystallization followed a two-stage mechanism, where metastable ∼120 nm primary particles were initially formed and then subsequently acted as "monomers" in an aggregation / addition process to form larger secondary particles — very similar to results for ZIF-8.

Later, Huber and coworkers combined in situ TR-SLS/DLS and TR-SAXS/WAXS experiments to follow ZIF-71 nanocrystal growth.[106] The authors proposed a detailed mechanism for the crystallization of ZIF-71 (see Fig. 12), which involved initial formation of amorphous clusters and subsequent growth via "coagulation" / aggregation, further evolution to amorphous particles via monomer addition (with the nature of these monomers potentially ranging from small clusters to isolated metal ions or linkers), and finally crystalline domain growth

via particle reorganization. In all cases, these ZIF-related studies highlight the importance of non-classical growth mechanisms (particularly aggregation), at least in the early stages of ZIF growth. Their strongly similar conclusions also suggest the possibility that the general pathways governing ZIF nucleation and growth may be relatively universal, independent of ZIF topology.

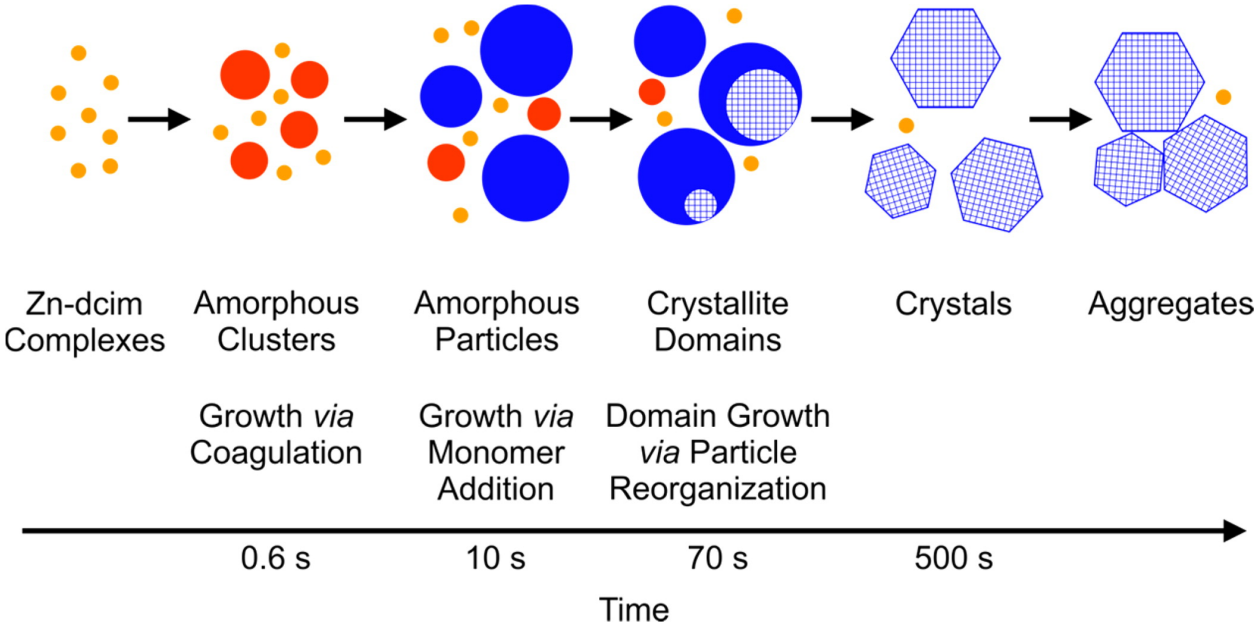

Figure 12: A simplistic scheme outlining the proposed steps and intermediates in the formation of ZIF-71 in 1-propanolic solution containing $Zn(NO_3)_2 \cdot 6H_2O$ as the metal salt and Hdcim as the linker. The times given correspond to the in situ experiments with the composition Zn^{2+}/Hdcim/1-PrOH = 1:4:2000. Reproduced with permission from ref. 106. Copyright 2016 American Chemical Society.

Still, the above conclusions on ZIFs are certainly not universal across MOFs. Using TLS, Hermes et al. investigated the homogeneous nucleation and crystal growth of MOF-5 in diethylformamide (DEF).[209] Their results show that MOF-5 crystallization proceeded with rapid nucleation well-separated from subsequent slow growth, with (interestingly) the high-symmetry cubic shaped MOF-5 crystallites present even at very early stages of growth. In contrast, TL-SLS studies on HKUST-1 tell a very different story.[210,211] In particular, Zacher et al. used TR-SLS to monitor the growth of HKUST-1, finding (in that case) that nucleation was slow and strongly overlapped with growth.[210]

9.3 Influence of Reaction Parameters

9.3.1 Influence of Modulators

TR-SLS can also provide unique insight into the influence of modulators — both deprotonation and coordination — during MOF formation. Cravillion et al. reported that, using an excess of the bridging bidentate ligand and an auxiliary monodentate ligand (carboxylate, N-heterocycle, or alkylamine), they could tune the size of ZIF-8 nanocrystals and microcrystals between ∼10nm to 1μm.[206] During nucleation and growth, the monodentate ligands were found to act as a competitive binding agent in metal-linker coordination equilibria, and as a base in deprotonation equilibria. The authors emphasized the strong influence of the basic modulating agent in decreasing the nucleation rate of ZIF particles in solution, thus yielding larger particle sizes. In a separate study, Hermes et al. explored the effect of adding a p-perfluoromethylbenzenecarboxylate (pfmbc) surfactant capping agent during MOF-5 synthesis.[209] Their TR-SLS data shows that the pfmbc additive causes particle sizes to stabilize between 100-150 nm in size, depending on the additive concentration. They hypothesized that pfmbc competes with the bdc linker in the coordination of $[Zn_4O]^{6+}$ units, perhaps even etching the growing MOF crystallite.

10 NMR

10.1 Ex Situ Studies

In contrast to many of the aforementioned techniques, which typically probe the growing solid-phase MOF, with Nuclear Magnetic Resonance (NMR) spectroscopy it is possible to study pre-crystalline intermediates, the developing crystal, and even the mother liquid itself. Using standard NMR techniques, a variety of ex situ studies have been carried out to characterize important solution-phase pre-crystalline intermediates. A 2010 study by Kumar et al. used CP-MAS ^{13}C NMR to distinguish between various possible ligand binding modes in prototypical zinc(II) acetate coordination compounds. The authors also demonstrated (via ^{1}H and ^{13}C NMR) that the observed species were prone to low-energy "carboxylate shift" reactions in solution.[212] A follow-up study on Cd(II) coordination compounds allowed for a direct comparison between metals,[213] and showed that Cd(II) salts exhibited a greater tendency to polymerize as compared to the corresponding Zn(II) salts, with the latter instead favoring discrete complex formation. The authors attributed this difference in reactivity to the greater ionic radius of cadmium, which allows for higher coordination numbers in

Cd(II) compounds, Furthermore, plausible formation mechanisms for all compounds could be obtained on the basis of Ramanan and Whittingham's point zero charge (pzc) model (see Section 2.1). In a separate study, Zakaria et al. used time-course ^{1}H NMR to reveal the effect of a trisodium citrate chelating agent on the formation of 2D cyano-bridged Cu-Pt coordination polymers.[214] The authors found that Cu^{2+} cations were stabilized by citrate anions and slowly released into solution to form the final CP via a controlled growth process, thus producing size-controlled single-crystal final products.

In addition to probing pre-crystalline intermediates, ex situ NMR studies have also been used to study various mechanistic processes that can occur concurrently with nucleation and growth, including reactant diffusion and linker exchange and/or incorporation. For instance, Hirai et al. took advantage of bi-directional diffusion to synthesize a novel Zn-based MOF, and utilized ^{1}H NMR to analyze the composition of both the growing crystal (via digestion) and the mother liquid as a function of time.[205] Based on the NMR experiments, a plausible dissolution-recrystallization mechanism was proposed to account for formation of the overall product morphology. NMR has also been used to carry out time-resolved studies of competitive linker incorporation in mixed-ligand MOFs. For a series of $[Zn_4O(bdc)_{3-x}(bdc{-}X)_x]$, MOFs, where X = Br or I, Burrows et al. used crystal digestion and ex situ ^{1}H NMR to quantify the incorporation of the halogenated linkers (bdc-X) into the growing MOF structure, and observed that the relative linker incorporation rates were well-correlated with the relative crystal growth rates of the various linkers ($[Zn_4O(bdc)_3]$ >$[Zn_4O(bdc{-}Br)_3]$ ∼ $[Zn_4O(bdc{-}I)_3]$) for the homoleptic MOFs.[215] Importantly, the authors argued that the composition of these (and possibly other) mixed-linker MOFs are not uniform; instead, the MOF core is enriched with the fastest-growing linker, while the outside of the MOF crystal would exhibit a higher percent incorporation of slower-growing linker(s) due to the relative enrichment of these linkers in the mother liquid late in the reaction.

10.2 In Situ Studies

A limitation of many of the aforementioned NMR studies is that, in the absence of specialized equipment, these experiments must be performed near ambient temperatures and pressures, as opposed to typical solvothermal conditions. As with XRD studies of MOF crystallization, special reactor tubes that can withstand high temperature, pressure, and corrosion are required for in situ analysis of solvo- or hydrothermal reactions. Such reaction vessels were developed and calibrated in 2000 by Taulelle and co-workers,[216,217] and have been recently utilized for in situ NMR characterization of MOFs. Note that these advances in in situ NMR

characterization of MOFs were recently reviewed in Férey et al.[37].

Because ^{27}Al is a relatively high-sensitivity nucleus with 100% natural abundance, many in situ NMR studies have focused on the synthesis of Al-based MOFs, where both ^{1}H and ^{27}Al NMR can be used to probe the formation process. A 2012 study by Haouas et al. used this approach to probe the types of species present in solution during the syntheses of MIL-96, MIL-100, and MIL-110.[218] On the basis of the observed time-resolved chemical shifts, the authors assigned coordination environments to each species present in the mother liquid (see Fig. 13b). In conjunction with time-resolved ex situ powder XRD and SEM studies, which were used to correlate the appearance/disappearance of each solution species with the timescale for growth of various solid intermediates and products, the authors concluded that the availability of the benzenetricarboxylate (btc) linker (which was controlled by the slow hydrolysis of Me_3btc) played an important role in determining the final product, and that both the btc/Al ratio and the rate of btc dissolution were important parameters in selecting for one MOF phase over another (see Fig. 13a). Furthermore, the authors observed that dimeric $Al_2{-}(btc)_1$ was present in all syntheses studied; whereas this species was present throughout the synthesis of MIL-110, for MIL-96 and MIL-100, $Al_2{-}(btc)_1$ was only observed at early stages of the reaction, with the disappearance of this species leading to growth of a new $Al_2{-}(btc)_2$ building unit. Based on these data, the authors proposed $Al_2{-}(btc)_1$ as a common intermediate in all Al-based MIL syntheses, with the Al/btc ratio and rate of btc dissolution determining whether or not the $Al_2{-}(btc)_1$ unit was retained in the final product.

In another study of the MIL series, Goesten et al. used in situ ^{1}H and ^{27}Al NMR to elucidate the role of N,N-dimethylformamide (DMF) in promoting NH_2-MIL-101(Al) formation.[219] From earlier XRD experiments,[98] it was determined that either NH_2-MIL-101(Al) or NH_2-MIL-53(Al) could form from a common NH_2-MOF-235(Al) intermediate, and that solvent effects (DMF vs. H_2O) played a critical role in determining the final product. Building on this work, Goesten et al. showed that ^{1}H NMR peaks assigned to H$-$Cl$\cdots$DMF grew as a function of time, and were concurrent with a downfield-shift and broadening of the ^{1}H NMR signal for water.[219] These observations led the authors to conclude that DMF serves as a molecular promoter for a water dissociation reaction ($Cl^- + H_2O + DMF \longrightarrow OH^- + H{-}Cl\cdots DMF$) that transforms water-coordinated NH_2-MOF-235(Al) into hydroxy-coordinated NH_2-MIL-101(Al).

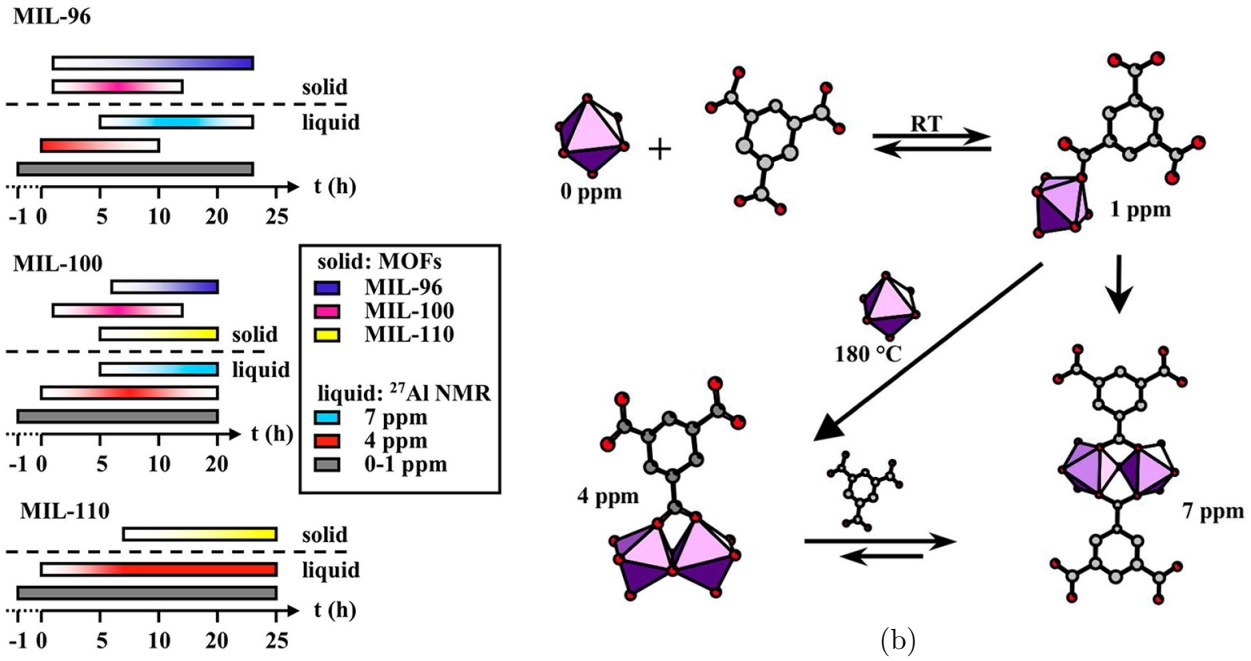

Figure 13: (a) Comparison between NMR observation in solution and the nature of the solid product along the synthesis course of MIL-96, MIL-100, and MIL-110 according to the in situ NMR and ex situ XRD and SEM studies. (b) The primary Al-btc complexes formed during the early stages of MIL-96, MIL-100, and MIL-110 syntheses. Part a and b are reproduced with permission from ref. 218. Copyright 2012 American Chemical Society.

11 Mass Spectrometry

11.1 Overview

Mass spectrometry (MS) is capable of identifying the stoichiometry and crystallization behavior of MOF pre-nucleation species. As with NMR spectroscopy, MS has thus far primarily been used to probe the mother liquid, and often serves as a powerful complement to ex situ solid-phase-sensitive techniques such as XRD and AFM. As with any ex situ characterization technique, there remains a danger that solution-phase species may be lost or chemically-altered during the measurement process. This danger is especially notable in mass spectrometry, where both ionization and fragmentation processes can lead to significant differences (both in terms of concentration and species identity) between the species present in the mother liquid and those recorded by the spectrometer.[220,221] Soft-ionization techniques, such as electrospray ionization (ESI) or its cold-temperature analog, cryospray ionization (CSI), can minimize difficulties with ionization and fragmentation, thus reducing discrepancies between the in situ and ex situ results.[222,223] Consequently, several studies have used ESI-MS or CSI-MS in order to gain novel insight into MOF nucleation and growth processes.

11.2 Identification of NBUs and Nucleation Mechanisms

Because it serves as a direct and sensitive probe of the mother liquid, MS is particularly well-suited for identifying MOF nucleation building units (NBUs), allowing for the proposal and critical evaluation of putative MOF nucleation mechanisms. Consequently, many MS studies on MOF systems have focused on identifying and characterizing stable solution-phase species during the nucleation process. Rood et al. performed one of the earliest such studies, in which ESI-MS was used to identify stable intermediates during the nucleation a homochiral Mg-camphoric acid (H_2cam) based MOF.[224] From the ESI-MS and product MS/MS experiments, the authors implicated a soluble, 3-fold paddlewheel structure ($[Mg_2(Hcam)_3]^+$) as the predominant NBU in the self-assembly process. Similarly, Bai et al. used ESI-MS to show that pre-synthesized pentanuclear NBU clusters of the form $[M_5(btz)_6(NO_3)_4(H_2O)_4]$ (btz=benzotriazolate; M=Co, Ni) retained their structure during the formation of a three-dimensional diamond network.[225]

A separate study by Lim et al. showed how ESI-MS could be used in a time-resolved manner to identify NBUs during the formation of ZIF-8.[226] The authors identified a large

number of zinc-imidazolate complexes, many of which had been postulated earlier by Cravillon et al.; $[Zn(Him)_2(NO_3)]^+$, for example, was consistently detected with high intensity, leading the authors to propose this species as the most basic unit in ZIF formation. Interestingly, a second tetranuclear zinc species, $[Zn_4(Im)_5(HIm)_5(NO_3)_4]^-$, was observed to grow in as a function of time and subsequently deplete around the time of first particle formation, suggesting (although not proving) that this complex plays a fundamental role in ZIF-8 nucleation.

In a seminal study using CSI-MS, Seeber et al. directly observed the intermediates involved in the nucleation of two topologically-distinct copper-based supramolecular MOFs.[227] Based on the CSI-MS results, several key structural components (see Fig. 14), ranging from simple monometallic units to higher-nuclearity (up to seven copper atom) aggregation units, were observed for the two MOFs. Importantly, none of the complex and high nuclearity species that were present in the CSI-MS spectra were observed by ESI-MS (a harder ionization technique), nor could these species be observed by CSI-MS under reaction conditions that did not closely resemble actual crystallization conditions. These observations highlight the high sensitivity and utility of CSI-MS in detecting non-covalently bound pre-nucleation species.

MS is not restricted to studying nucleation, and we note one example in which MS experiments have also been used as a complementary probe of the mother liquid during MOF *growth*. In particular, Wagia et al. used a combination of ESI-MS and AFM to show that Cd(eIm) (HeIm=2-ethylimidazole) units attach to the growing CdIF-4 surface, with ESI-MS providing direct evidence for the presence of Cd(eIm) units in solution.[228]

12 Absorption and Raman Spectroscopies

In select cases, and depending on the chemical composition of the system of study, various absorption or Raman spectroscopies can be employed to monitor MOF nucleation and growth. For example, certain classes of MOFs contain intermediates and/or final products that exhibit strong electronic transitions that can be probed in situ during MOF growth. Using a MOF formed from cobalt(II) nitrate and 4,4-bipyridine (bpy) precursors, Petersen et al. demonstrated how resonance Raman (RR) spectroscopy could be used to detect and monitor metal-ligand interactions in solution during crystal growth.[229] Exploiting the enhanced signal-to-noise of RR and the $\pi \rightarrow \pi^*$ electronic transition of bpy allowed the authors to detect the presence of soluble Co(II)-bpy complexes at low (mM) reagent concentrations.

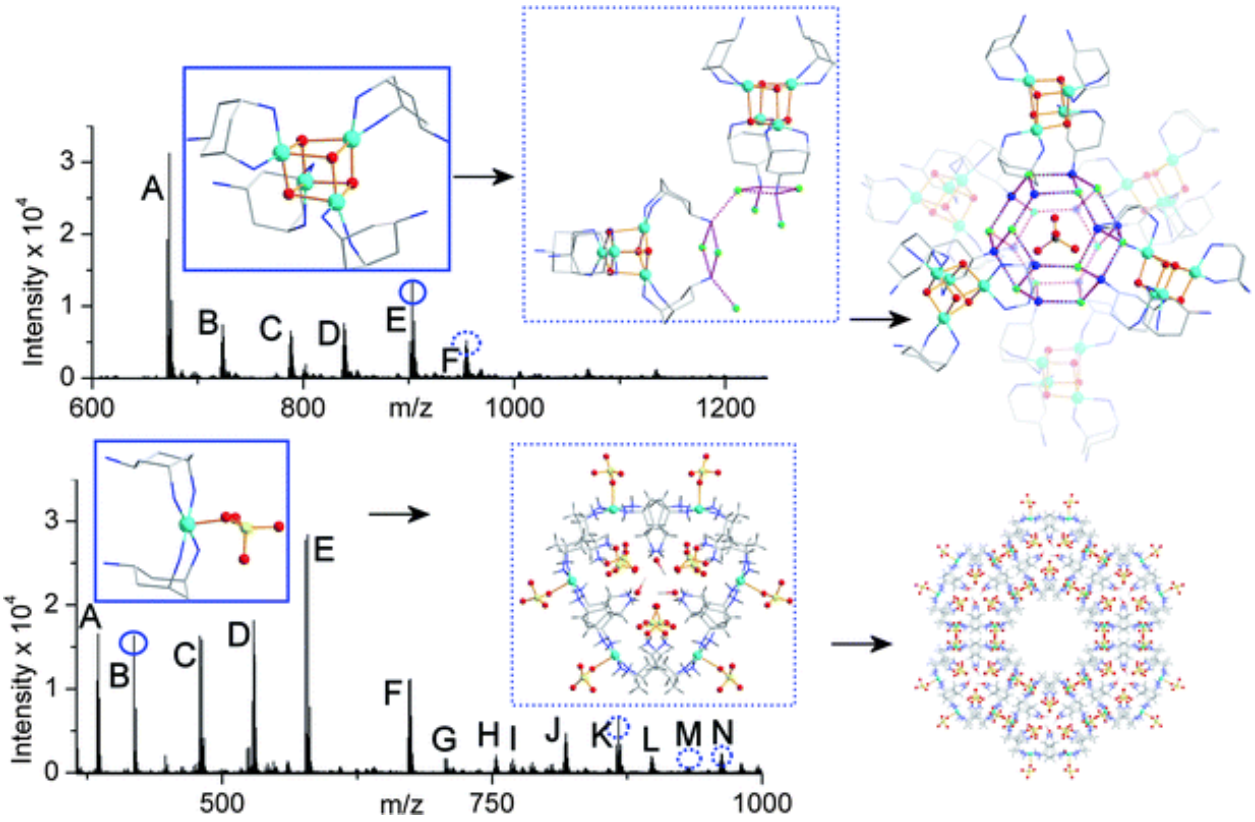

Figure 14: CSI-MS of the reaction solutions of compounds 1 ($[Cu_4O_4(trans{-}tachH)_4F_4]\cdot 8\,CH_3OH\cdot 20H_2O$, top) and 2 ($\{[Cu(trans{-}tachH)_2(SO_4)]SO_4\}\cdot MeOH\cdot 4H_2O$, bottom) before crystallization with segments of the crystal structures of compounds determined after crystallization. The species in the blue boxes (top $\{Cu_4\}$; bottom $\{Cu_1\}$) are directly observed in the spectra (round circles) and the species in the dotted blue boxes (top $\{Cu_8 + Cu_1\}$; bottom $\{Cu_6\}$) are observed as more complex derivatives (dotted circles). Carbon atoms are shown in light grey, copper in sky blue, nitrogen in dark blue, oxygen in red, fluoride in green, sulfur in yellow. Hydrogen atoms are omitted for clarity. Reproduced from ref. 227 with permission of The Royal Society of Chemistry.

Based on this RR data, the authors posited the involvement of soluble Co^{2+}-bpy complexes as solution-phase intermediates in the growth of the MOF crystal. Although neither RR nor UV/Vis could conclusively determine the nature of these Co^{2+}-bpy species, the RR suggested that more than one such species was likely present in solution and that some bpy may be coordinated to two metal cations. Finally, by recognizing that high concentrations of Co^{2+}-bpy species were required for crystal formation, the authors were able to rationally design a new fast and energetically-efficient direct mixing route to form the 2D MOF.

Raman spectroscopies have also been used to monitor the mechanochemical synthesis of MOFs and coordination polymers. Ma et al. used ex situ Raman to probe the mechanochemical synthesis of ZIF-6, probing reaction progress by repeated sampling of the reaction mixture over time, with kinetics determined via the amount of unreacted imidazole linker.[230] They found second order reaction kinetics, with a rate proportional to the remaining reactants and a rate constant highly sensitive to the grinding frequency. The authors thus concluded that the rate is dictated by the frequency of "reactive encounters". Real-time in situ Raman monitoring has also been used in the case of Cd-based coordination polymers, probing the growth of stretching modes involving Cd.[231] In that case, depending on the linker:metal ratio, either 3D or 1D coordination polymers were observed.

Lee et al. used a combination of UV/Vis adsorption spectroscopy and inductively coupled plasma atomic emission spectroscopy (ICP-AES) to quantitatively measure metal exchange rates in the formation of zinc-copper (ZnTPO–CuHTPO) and terbium-copper (TbTPO–CuHTPO) based MOFs, both of which were formed from a common copper MOF (CuHTPO) precursor.[232] Ex situ ICP-AES was used to determine relative metal concentrations in each MOF as a function of time, with complementary UV/Vis work confirming that Cu^{2+} ions were indeed released into solution. Tb^{3+} exchange was observed to occur more quickly (and to a greater extent) than Zn^{2+} exchange, which the authors attributed to the greater charge of the Tb^{3+} cation.

In a similar vein, Yang and coworkers utilized ICP to monitor the post-synthetic modification, via metal substitution, of ZIF-108.[233] Upon exposure to solutions of alternative metal cations, including Co^{2+} and Cu^{2+}, a fraction of the original Zn^{2+} cations were replaced, ultimately yielding a mixed-metal MOF. Monitoring the kinetics of this transformation via ICP showed a steady increase in hetero-cation concentration with time, with Co^{2+} exhibiting a faster replacement rate compared to Cu^{2+}. Interestingly, the authors demonstrated that the transformations were neither single crystal-single crystal nor dissolution-recrystallization, but rather occurred via a low energy pathway involving heterogeneous nucleation on the

existing parent structure, accompanied by its dissolution.

13 Computational Studies

As a complement to in situ or time-resolved experimental studies, computational studies can offer unique insight into MOF nucleation and growth processes. Such studies are challenging, since both nucleation and growth processes require bridging substantial time- and length-scale gaps (thus incurring significant computational expense), and because it is generally difficult to model the required metal-ligand bond formation and cleavage reactions. As a consequence, most early computational studies of MOF formation have instead focused on elucidating the thermodynamic factors that govern synthesis selectivity. As highlighted below, however, several recent studies have been able to critically evaluate proposed reaction pathways and, in a few instances, directly simulate aspects of MOF nucleation and/or growth.

A particular advantage of computational MOF studies is the ability to provide atomic-level information on reaction mechanisms and energetics, and this feature has been especially utilized in the study of MOF systems where varying synthetic conditions lead to distinct MOF products. Several such computational studies have thus examined NH_2-MOF-235(Al), a MOF which has been shown (depending on reaction conditions) to transform either to NH_2-MIL-101(Al) or NH_2-MIL-53(Al). Goesten et al. used density functional theory (DFT) to determine that, while NH_2-MIL-53(Al) was thermodynamically favored in DMF and H_2O solvents as compared to NH_2-MIL-101(Al), the relative energy difference between the two MOFs was smaller in DMF.[219] Their result supports the hypothesis that DMF (relative to water) stabilizes both the NH_2-MOF-235(Al) intermediate and the kinetically-favored NH_2-MIL-101(Al) product, allowing the reaction to proceed under kinetic control in DMF.

Yang and Clark also analyzed solvation effects in the MIL series by using a combination of DFT and molecular mechanics (MM) calculations.[234] Those authors studied the role of DMF/H_2O in the synthesis of NH_2-MOF-235(Al), which is the common intermediate observed in both NH_2-MIL-101(Al) and NH_2-MIL-53(Al) syntheses. Utilizing a cluster model of NH_2-MOF-235(Al) and a continuum solvation model, the authors' DFT calculations demonstrated that both DMF and H_2O solvent exchange was facile for the NH_2-MOF-235(Al) system but, by contrast, H_2O/linker exchange was comparatively more favorable than DMF/linker exchange. The authors also used molecular dynamics simulations to study the dynamics of solvent organization around NH_2-MOF-235(Al), concluding that DMF preferentially solvates NH_2-MOF-235(Al) in H_2O/DMF mixtures, and that (more generally)

other hydrophobic cosolvents also form distinct solvation shells around the MOF cluster. Their results highlight the importance of solvation effects in MOF crystallization via the creation of favorable solvation environments that may favor one product topology over another.

MOF surface termination effects, a key aspect of MOF growth, have also been explored using computational methods. Using a first-principles, DFT-derived force field developed specifically for the HKUST-1 system,[235] Amirjalayer et al. calculated surface energies for various plausible surface terminations of the MOF.[236] Although their calculations largely omitted the influence of solvent, the authors determined that the most stable surface terminations for HKUST-1 were a reconstructed [111] surface, followed by a low acetate density [001] surface, in accord with experimental observations. Notably, surface free energies were significantly endergonic, primarily due to entropic contributions; this, along with DFT calculations on small model copper complexes, suggests that HKUST-1 formation is primarily an entropically-driven process.

Several recent computational studies have also more directly explored the kinetics of MOF nucleation and growth.[90,98] Cantu et al. used DFT calculations to determine the energetics and mechanistic pathways for SBU formation in the ubiquitous MIL-101(Cr) system.[237] Starting from hydrated chromium(III) ions, $[Cr(H_2O)_6]^{3+}$, and partially deprotonated terephthalate linkers, the authors calculated energetics for all plausible intermediates and transition states in the stepwise formation of the final SBU, taking into account both spin and solvation effects. Based on these results, the authors proposed a low-energy pathway leading to SBU formation (see Fig. 15), and determined that the highest energy barriers within this pathway occurred during the formation of bridged di- and tri-chromium metal clusters. Finally, the authors utilized a simple transition state theory (TST)-based kinetic model to estimate the formation rate and activation energy of SBU formation, and found qualitative agreement between their model and experimentally-determined values.

Other authors have utilized a variety of approaches to simulate large-scale MOF *growth*, as opposed to the initial stages of MOF nucleation. Yoneya et al. used molecular dynamics simulations in conjunction with a coarse-grained (continuum) solvent to simulate the self-assembly of a 2D Pd(II)(4,4-bpy)$_2$ MOF.[238] By changing the far-field relative dielectric constant, which indirectly controls the metal-ligand binding energy, the authors demonstrated that the appearance of regular MOF growth was highly sensitive to the metal-ligand binding strength. Similar simulation on a Ru(II) MOF yielded only disordered, non-regular networks, possibly rationalizing the lack of experimentally-synthesizable Ru(II)(4,4-bpy)$_2$

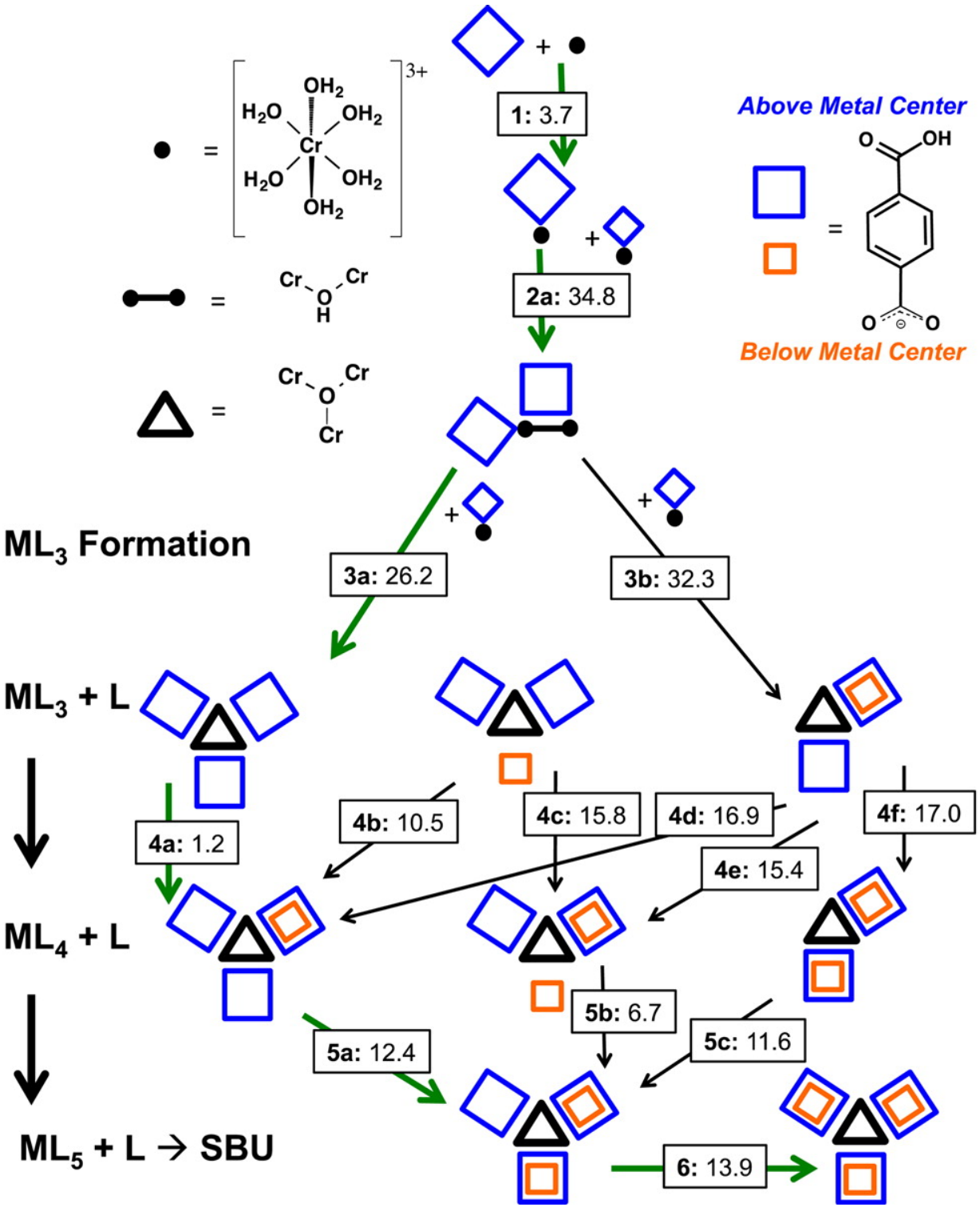

Figure 15: Reaction series that form the SBU of MIL-101. Reaction numbers in bold, energy barriers in kilocalories/mole. Not all water molecules shown explicitly for clarity. Least energy path in bold arrows. All Cr atoms are Cr(III). Reproduced with permission from ref. 237. Copyright 2014 American Chemical Society.

compounds. Once again, modification of the metal-ligand parameters enabled formation of a regular 3D MOF network. Overall, their results support a range of metal-ligand binding energies that lead to successful MOF formation, outside of which metal-ligand coordination is either too strong or too weak to lead to yield lattice formation.

Umemura et al. used coarse-grained Monte Carlo (MC) simulations to model the resulting crystal morphologies of HKUST-1 grown in both the presence and absence of a modulator.[239] By treating the modulator as a perturbation to the interaction energies of attachment for each HKUST-1 growth unit, the authors found that the simulated HKUST-1 formed octahedron, truncated octahedron, cuboctahedron, and finally cubic morphologies with increasing modulator concentration, in agreement with both field emission SEM experiments and Bravais, Friedel, Donnay, and Harker theory. Their results thus provide insight into the underlying mechanism for crystal morphology control via coordination modulation and growth-site blocking.

Very recently, Anderson et al. demonstrated a more general coarse-grained approach to simulate crystal growth using kinetic Monte Carlo.[240] The authors employed their methodology to model the growth of a wide variety of materials, including both zeolites and MOFs. Due to the cage-like structures of zeolites and MOFs, the authors simplified the problem by treating these cages as coarse-grained units of growth, and simulated growth by computing the energetics of condensation and dissolution of polyhedral units at individual surface sites, including common defects (e.g. screw dislocations). In the case of HKUST-1, both the crystal habit and surface terrace topology obtained from simulation matched well with experiments, though the simulation predicted a different lattice direction for the screw dislocation. This coarse-grained approach seems extremely promising in addressing the challenging length- and time-scale gaps that often plague computational modeling of crystal growth.

14 Conclusions

In pursuit of a better understanding of the mechanisms underlying MOF nucleation and growth, the past decade has seen significant progress towards noninvasive, real-time measurements of MOF formation across the experimentally-relevant range of time-scales, length-scales, and phase regimes. For clarity, the various scattering, microscopy, spectroscopy, and simulation techniques discussed in this Review — along with the general types of information that have historically been obtained from each individual technique — are summarized in Fig. 16. Generally speaking, scattering methods (XRD, SAXS/WAXS, DLS/SLS, and

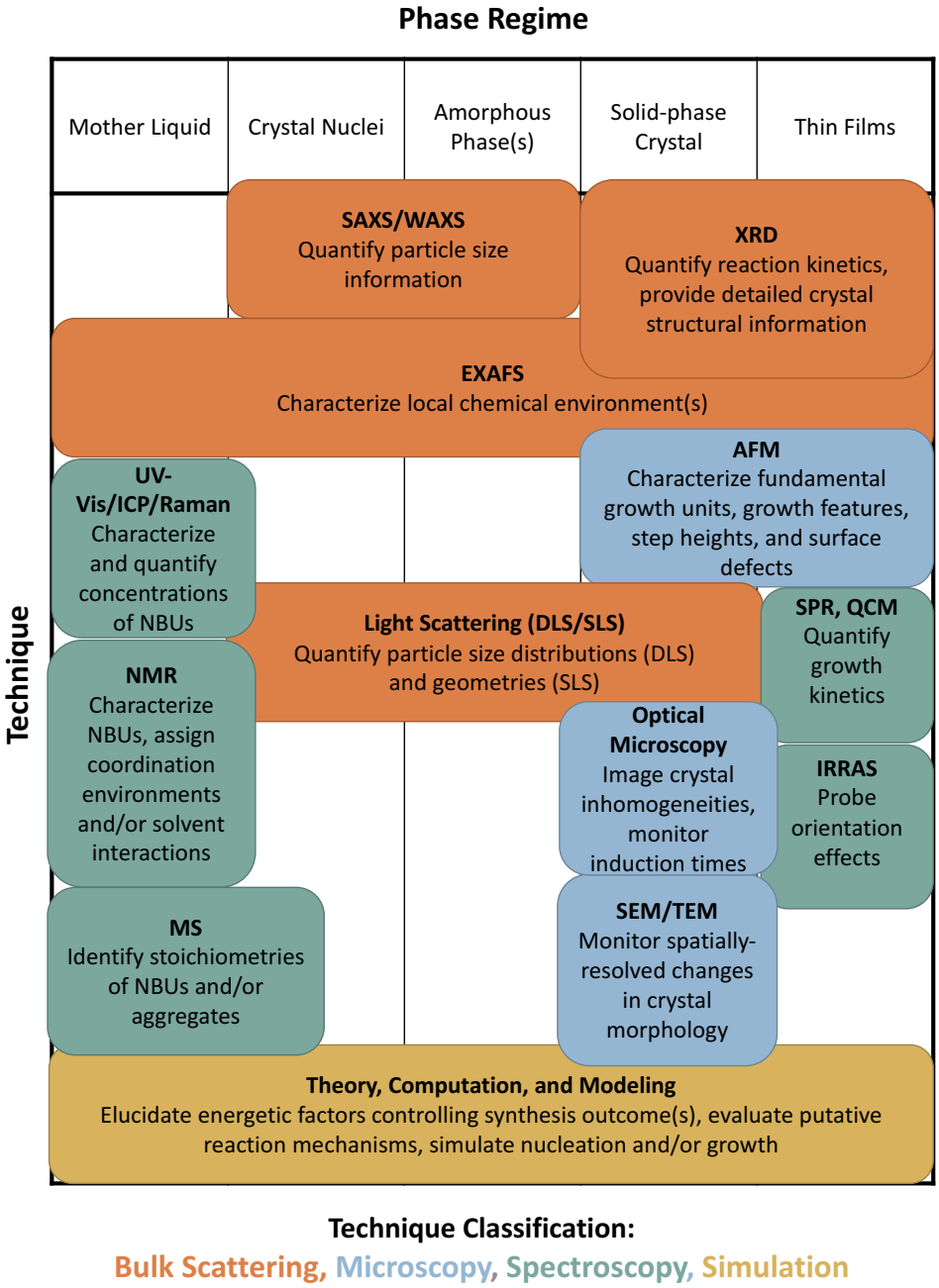

Figure 16: Summary of the major experimental and computational techniques used for time-resolved, in situ, and/or mechanistic studies of MOF nucleation and growth. Each technique has been grouped into one of four categories: bulk scattering methods (orange), microscopy (blue), spectroscopy (green), and simulation (gold). A brief description of each technique is provided, which lists the phase regime(s) to which the technique is sensitive, along with what type(s) of information can be gained from the technique.

EXAFS) have provided spatially-averaged structural information in several disparate phase regimes, and are particularly relevant for time-resolved study of particle size distributions, crystal structural parameters, and (in some cases) local chemical environments. Spatially-localized microscopy techniques (AFM, SEM, TEM, and optical microscopy) have nicely complemented the above bulk scattering methods, and have enabled both imaging of MOF materials along with the characterization of crystal morphologies, surface defects, fundamental growth units, and other growth features. Though less commonly employed, at present, spectroscopic methods (NMR, MS, UV-Vis, ICP, Raman) have contributed vital (and often unique) insight into the structures and stoichiometries of complexes within the MOF mother liquid. Additionally, select spectroscopies (SPR, QCM, IRRAS) have also been employed in the characterization of MOF thin films in order to quantify growth kinetics and probe orientation effects. Lastly, a variety of theory, computation, and modeling methods have offered a complementary approach towards probing all phase regimes of MOF nucleation and growth, with particular utility towards exploring thermodynamic preferences between competing reaction products, assessing putative reaction mechanisms, and directly simulating nucleation/growth dynamics. Thus, it is clear that no single technique is capable of fully exploring all aspects of MOF crystallization. Rather, the entire host of scattering, microscopy, spectroscopy, and simulation techniques have been and will be required to thoroughly investigate and understand the underlying mechanism(s) of MOF formation.

So, what conclusions can be drawn from the totality of direct, in situ, and/or time-resolved studies of MOF nucleation and growth? Unfortunately, universal conclusions are difficult to draw due the tremendous chemical and structural diversity of MOFs — the very fact that makes them such an interesting target of study. On the other hand, we can identify several mechanistic trends and motifs regarding MOF nucleation and growth, many of which may hold for one or more classes of MOF materials. Rather than attempting to conclude with any universal insight into MOF synthesis, and so as to avoid oversimplification, we instead offer a scope of the important mechanisms that have been frequently observed in these studies of MOF nucleation and/or growth, paying special attention to mechanisms that apply to several classes of MOFs or which can be influenced by varying one or more reaction parameters.

MOF nucleation mechanisms: Due to their ability to probe the mother liquid and/or small nucleated particles, DLS, EXAFS, SAXS, NMR, and MS have proved particularly useful in distinguishing between putative MOF nucleation mechanisms, many of which were

outlined in Section 2.1. From these studies, it is clear that, when they can be identified, MOF nucleation building units (NBUs) are highly system-specific. Many studies have implicated discrete NBUs as intermediates in a classical picture of MOF nucleation, though the extent to which these NBUs resemble the SBUs of the final product(s) vary by system.[111,218,224–227,237] Complete SBUs as NBUs are certainly possible actors, particularly in controlled SBU approaches,[111,147,157,225] however a wide range of other NBUs (partial SBUs, higher-nuclearity aggregations of complete SBUs, or even species dissimilar to the final SBUs) have also been observed.[218,224,226,227,237]

In addition to studies that largely support classical NBU hypotheses, other work suggests a more non-classical picture of nucleation. Of particular note are several light-scattering and/or SAXS/WAXS studies[31,106,206,207] that support the possibility of amorphous clusters, rather than crystalline nuclei, as the initial structures in MOF formation. Nano-aggregation mechanisms have also been observed via NMR[218] and MS,[227] further complicating the simple classical picture of nucleation presented above.

MOF growth mechanisms: Insofar as growth is concerned, a frequent topic of study is the nature of the MOF growth units. AFM analyses of surface steps heights have provided insight into the nature of these MOF growth units and the possible role of non-framework species in crystal growth,[142,144–146] and (as might be expected) frequently show steps heights that are commensurate with crystal lattice plane spacings. Thanks to data obtained via other complementary approaches, there is now also evidence for several MOFs that grow via classical monomer addition mechanisms (as opposed to aggregation-based growth, discussed below), with relatively small growth units that range from simple solvated metal ions and organic ligands to more complex partial or full SBUs.[15,111,142–144,146,147,153,228] Note that, in general, such growth units may differ from the NBUs discussed above.

Late-stage growth in MOFs can be monitored via time-resolved AFM or SEM. AFM studies on a variety of MOF systems suggest that growth frequently proceeds via classical "birth and spread" and/or "spiral growth" mechanisms, at least at lower supersaturations and late-stage growth.[142–144] In a complementary fashion, SEM and other microscopy studies provide some general insight into the larger morphological evolution of MOFs during synthesis. They generally show significant structural evolution of the growing MOF into its final (presumably thermodynamically stable) faceting, often accompanied by sharpening of the facet edges and corners with time.[104] SEM also indicates significant evolution of the MOF particle size distribution, which is generally consistent with the loss of small particles via

Ostwald ripening.[30,64,166,167]

Depending on the system and chosen reaction parameters, non-classical growth mechanisms have also been frequently observed in MOF formation. In contrast to the picture of small growth unit attachment presented above, several notable light-scattering studies have provided a picture of ZIF growth based on the aggregation, addition, and/or coalescence of amorphous, nanometer-scale 'primary particles'.[31,106,206,207] Aggregation mechanisms have also been observed via SEM[168–172] and for systems beyond ZIFs,[169–171] possibly suggesting a broader role for aggregation in MOF formation.

Many MOF studies have evidenced another major feature of non-classical growth: crystallization via the formation of sequential intermediates, consistent with Ostwalds Rule of Stages.[62,90,107] Amorphous-to-crystalline transitions,[30,31,106,206,207] dissolution-recrystallization,[52,54,55,115] and solid-phase transformations[53,135] have all been observed in one or more studies. A particularly notable example of Ostwalds Rule of Stages is the cases of NH_2–MIL–53(Al) / NH_2–MIL–101(Al), both of which are formed from the same precursors via a common MOF-235 intermediate phase.[97,98,113] In a number of other cases, crystallization has been shown to proceed via a building up of intermediates of increasing dimensionality, from complexes, to chains, layers, and eventually 3D crystalline solids.[82,112,116–118,149]

Influence of reaction parameters: Broadly speaking, a key challenge in MOF synthesis is to predict the structure that will be generated from a given combination of reagents. Due to the high temperatures involved in solvothermal synthesis, it has often been presupposed that such syntheses often yield the most thermodynamically stable product structure, rather than a kinetic one.[87,112] (Note that this tendency toward thermodynamic control would lie in contrast to that of zeolite systems, whose stronger Si-O or Al-O bonds are more resistant to cleavage as compared to the weaker linkages found in hybrid systems and are are thus more prone to kinetic trapping).[7] Nonetheless, the literature in this Review provides numerous examples of how certain reaction parameters — particularly reaction time, heating method, and the choice of starting reagents, modulating agents, and solvent(s) — can allow the creative and determined scientist to isolate a diverse array of structures from a similar set of starting materials.

In particular, the realization that MOFs may crystallize via intermediate or precursor structures[52–54,62,98] allows for the possibility of adjusting reaction times to isolate these intermediates prior to their transition into the thermodynamically favored (but potentially undesired) product. Additionally, a great diversity of studies highlight the importance of

heating methods, with microwave or ultrasound approaches modifying crystallization mechanisms and generally enhancing nucleation / growth rates — despite the lack of a definitive microscopic explanation for these enhancements.[79,83,85,87–89,93,95,124,179,180] In terms of MOF chemical composition, a large number of studies also indicate that cations with higher lability yield higher nucleation / growth rate constants as compared to more inert cations, while similar trends in terms of linker length or functionalization are far less clear.[12,85,87,88,94]

Numerous time-resolved and in situ studies now provide both empirical evidence and mechanistic insight towards understanding the influence of modulating agents and/or solvent in MOF crystallization.[97,113,186,187,192–196] In the case of modulating agents, various studies have supported both coordination and/or protonation state modulation.[64,105,110,132,133] As for solvent selection, recent experimental and computational studies are now beginning to provide more detailed microscopic explanations for empirically-observed strong solvent effects,[103,135,219,234] including the possibility of real time monitoring of changes in cation coordination spheres during MOF synthesis as the reaction progresses.[103] Exciting advances such as these suggest that selection of MOF reaction parameters may in the future be increasingly guided by non-empirical insight, based in part on these and other similar detailed observations of MOF nucleation and growth.

15 Outlook and Future Directions

Despite significant progress in the field of MOF synthesis, much work remains to be accomplished. Though by no means exhaustive, here we outline some remaining open questions and possible avenues for future fruitful investigations regarding MOF nucleation and growth. In some cases, these questions may be accessible via using existing experimental and/or computational techniques (or synergistic combinations thereof), however others may require advances in instrumentation[160] and/or computational methods.

Nucleation and early-growth studies: Relative to studies of late-stage growth, which can be investigated using a variety of techniques, experimental studies (especially ones which provide molecular-level insight) of nucleation and early-stage growth are extremely challenging due to the required spatial and temporal resolution.[15] As such, there remains, in many cases, a general dearth of information regarding the structure(s) that predominate during this crucial regime. It is likely that a combination of instrumental techniques (utilized separately or in tandem), perhaps in conjunction with corresponding computational studies, will

be necessary to provide a complete picture of the early stages of MOF synthesis.[15]

Multi-phase investigations: The vast majority of direct, in situ, or time-resolved studies to date have focused primary on one phase of the MOF (e.g. mother liquid or solid), leaving many questions unanswered as to how these different phases interact and equilibrate during the course of the synthesis. For example, it is currently difficult to know which, if any, of the pre-formed building units discovered within the mother liquid actually contribute to either early- or late-stage crystal growth. The use of several methods in tandem, while simultaneously probing multiple phases, may yield significant new insights into MOF nucleation and growth.[14]

Investigations of non-classical nucleation and growth mechanisms: The role of various non-classical nucleation and growth mechanisms in MOF crystallization also appears ripe for future study, especially given the growing evidence of their influence.[11] In particular, the role of amorphous nuclei and/or intermediates is a question of particular relevance. While these amorphous structures are inaccessible via XRD methods, they remain attractive targets for other powerful approaches such as SAXS/WAXS, TLS, and/or recently developed in situ NMR methods.[241]

Large-scale studies of MOF nucleation and growth: Although it is now clear that there is no simple universal theory of MOF crystallization, it remains plausible that within *particular* classes of MOFs important general trends for nucleation and growth may hold. Unfortunately, most existing MOF studies investigate only one system (or, in rare cases, a handful of related systems). Coupled with the vast array of synthetic conditions and data analysis approaches, this heterogeneity makes it complicated to cleanly compare and contrast features of MOF crystallization between systems. So as to facilitate mechanistic comparisons within and between different classes of MOF materials and elucidate any general trends in MOF crystallization, large-scale and/or systematic investigations of MOF nucleation and growth mechanisms will be required, with an emphasis on investigations which cover a wide array of MOF classes and topologies.

Acknowledgement

This work was partially supported by the National Science Foundation Graduate Research Fellowship (MVV) under Grant No. DGE-1256259 and by Chemical Sciences, Geosciences

and Biosciences Division, Office of Basic Energy Sciences, Office of Science, U.S. Department of Energy, under award DE-SC0014059. J.R.S is a Camille Dreyfus Teacher-Scholar

References

(1) Furukawa, H.; Cordova, K. E.; O'Keeffe, M.; Yaghi, O. M. The Chemistry and Applications of Metal-Organic Frameworks. *Science* **2013**, *341*.

(2) Gangu, K. K.; Maddila, S.; Mukkamala, S. B.; Jonnalagadda, S. B. A Review on Contemporary Metal-Organic Framework Materials. *Inorganica Chimica Acta* **2016**, *446*, 61 – 74.

(3) Silva, P.; Vilela, S. M. F.; Tome, J. P. C.; Almeida Paz, F. A. Multifunctional Metal–Organic Frameworks: From Academia to Industrial Applications. *Chem. Soc. Rev.* **2015**, *44*, 6774–6803.

(4) James, S. L. Metal–Organic Frameworks. *Chem. Soc. Rev.* **2003**, *32*, 276.

(5) Férey, G. Hybrid Porous Solids: Past , Present , Future. *Chem. Soc. Rev.* **2008**, *37*, 191–214.

(6) Seoane, B.; Castellanos, S.; Dikhtiarenko, A.; Kapteijn, F.; Gascon, J. Multi-scale Crystal Engineering of Metal Organic Frameworks. *Coord. Chem. Rev.* **2016**, *307*, 147–187.

(7) Cheetham, A. K.; Rao, C. N. R.; Feller, R. K. Structural Diversity and Chemical Trends in Hybrid Inorganic-organic Framework Materials. *Chem. Commun.* **2006**, 4780–4795.

(8) Rowsell, J. L. C.; Yaghi, O. M. Metal–Organic Frameworks: A New Class of Porous Materials. *Microporous Mesoporous Mater.* **2004**, *73*, 3–14.

(9) Stock, N.; Biswas, S. Synthesis of Metal-Organic Frameworks (MOFs): Routes to Various MOF Topologies, Morphologies, and Composites. *Chem. Rev.* **2012**, *112*, 933–969.

(10) Sun, Y.; Zhou, H.-C. Recent Progress in the Synthesis of Metal–Organic Frameworks. *Sci. Technol. Adv. Mater.* **2015**, *16*, 054202.

(11) Rimer, J. D.; Tsapatsis, M. Nucleation of Open Framework Materials: Navigating the Voids. *MRS Bull.* **2016**, *41*, 393–398.

(12) Wu, Y.; Henke, S.; Kieslich, G.; Schwedler, I.; Yang, M.; Fraser, D. A. X.; O'Hare, D. Time-Resolved In Situ X-ray Diffraction Reveals Metal-Dependent Metal-Organic Framework Formation. *Angew. Chem. Int. Ed.* **2016**, *55*, 14081–14084.

(13) Rubio-Martinez, M.; Batten, M. P.; Polyzos, A.; Carey, K.-C.; Mardel, J. I.; Lim, K.-S.; Hill, M. R. Versatile, High Quality and Scalable Continuous Flow Production of Metal-Organic Frameworks. *Sci. Rep.* **2014**, *4*, 5443.

(14) Morris, R. E. How Does Your MOF Grow? *ChemPhysChem* **2009**, *10*, 327–329.

(15) Attfield, M. P.; Cubillas, P. Crystal Growth of Nanoporous Metal Organic Frameworks. *Dalt. Trans.* **2012**, *41*, 3869–3878.

(16) De Yoreo, J. J.; Gilbert, P. U. P. A.; Sommerdijk, N. A. J. M.; Penn, R. L.; Whitelam, S.; Joester, D.; Zhang, H.; Rimer, J. D.; Navrotsky, A.; Banfield, J. F.; Wallace, A. F.; Michel, F. M.; Meldrum, F. C.; Cölfen, H.; Dove, P. M. Crystallization by Particle Attachment in Synthetic, Biogenic, and Geologic Environments. *Science* **2015**, *349*, aaa6760.

(17) Walton, R. I.; Millange, F. *The Chemistry of Metal-Organic Frameworks*; Wiley-VCH Verlag GmbH & Co. KGaA, 2016; pp 729–764.

(18) Sosso, G. C.; Chen, J.; Cox, S. J.; Fitzner, M.; Pedevilla, P.; Zen, A.; Michaelides, A. Crystal Nucleation in Liquids: Open Questions and Future Challenges in Molecular Dynamics Simulations. *Chem. Rev.* **2016**, *116*, 7078–7116.

(19) Karthika, S.; Radhakrishnan, T. K.; Kalaichelvi, P. A Review of Classical and Nonclassical Nucleation Theories. *Cryst. Growth Des.* **2016**, *16*, 6663–6681.

(20) Randolph, A. D.; Larson, M. A. *Theory of Particulate Processes (Second Edition)*; Elsevier, 1988; pp 109–134.

(21) Erdemir, D.; Lee, A. Y.; Myerson, A. S. Nucleation of Crystals From Solution: Classical and Two-Step Models. *Acc. Chem. Res.* **2009**, *42*, 621–629.

(22) Thompson, R. W. *Verified Syntheses of Zeolitic Materials*; 2001; pp 21–23.

(23) Cubillas, P.; Anderson, M. W. *Zeolites and Catalysis*; Wiley-VCH Verlag GmbH & Co. KGaA, 2010; pp 1–55.

(24) Furukawa, S.; Reboul, J.; Diring, S.; Sumida, K.; Kitagawa, S. Structuring of Metal-Organic Frameworks at the Mesoscopic/macroscopic Scale. *Chem. Soc. Rev.* **2014**, *43*, 5700–5734.

(25) Eddaoudi, M.; Sava, D. F.; Eubank, J. F.; Adil, K.; Guillerm, V. Zeolite-like Metal–Organic Frameworks (ZMOFs): Design , Synthesis , and Properties. *Chem. Soc. Rev.* **2015**, *44*, 228–249.

(26) Aerts, A.; Kirschhock, C. E. A.; Martens, J. A. Methods for In Situ Spectroscopic Probing of the Synthesis of a Zeolite. *Chem. Soc. Rev.* **2010**, *39*, 4626–4642.

(27) Cundy, C. S.; Cox, P. A. The Hydrothermal Synthesis of Zeolites: Precursors, Intermediates and Reaction Mechanism. *Micropor. Mesopor. Mater.* **2005**, *82*, 1–78.

(28) Férey, G. Building Units Design and Scale Chemistry. *J. Solid State Chem.* **2000**, *152*, 37–48.

(29) Taulelle, F. Crystallogenesis of Microporous Metallophosphates. *Curr. Opin. Solid State Mater. Sci.* **2001**, *5*, 397–405.

(30) Venna, S. R.; Jasinski, J. B.; Carreon, M. A. Structural Evolution of Zeolitic Imidazolate Framework-8. *J. Am. Chem. Soc.* **2010**, *132*, 18030–18033.

(31) Cravillon, J.; Schröder, C. A.; Nayuk, R.; Gummel, J.; Huber, K.; Wiebcke, M. Fast Nucleation and Growth of ZIF-8 Nanocrystals Monitored by Time-Resolved In Situ Small-Angle and Wide-Angle X-Ray Scattering. *Angew. Chem. Int. Ed.* **2011**, *50*, 8067–8071.

(32) Ramanan, A.; Whittingham, M. S. How Molecules Turn Into Solids: the Case of Self-Assembled Metal-Organic Frameworks. *Cryst. Growth Des.* **2006**, *6*, 2419–2421.

(33) Singh, M.; Kumar, D.; Thomas, J.; Ramanan, A. Crystallization of Copper(ii) Sulfate Based Minerals and MOF from Solution: Chemical Insights into the Supramolecular Interactions. *J. Chem. Sci.* **2010**, *122*, 757–769.

(34) Brunet, P.; Simard, M.; Wuest, J. D. Molecular Tectonics. Porous Hydrogen-Bonded Networks With Unprecedented Structural Integrity. *J. Am. Chem. Soc.* **1997**, *119*, 2737–2738.

(35) Desiraju, G. R. Supramolecular Synthons in Crystal Engineering — A New Organic Synthesis. *Angew. Chem. Int. Ed. Engl.* **1995**, *34*, 2311–2327.

(36) Hosseini, M. W. Molecular Tectonics: From Simple Tectons to Complex Molecular Networks. *Acc. Chem. Res.* **2005**, *38*, 313–323.

(37) Férey, G.; Haouas, M.; Loiseau, T.; Taulelle, F. Nanoporous Solids: How Do They Form? An In Situ Approach. *Chem. Mater.* **2014**, *26*, 299–309.

(38) Wulff, G. Zur Frage Der Geschwindigkeit Des Wachstums Und Der Aufl Ösung Der Krystallfl Ächen. *Z. Kristallogr. Mineral.* **1901**, *34*, 449–530.

(39) Voorhees, P. W. The Theory of Ostwald Ripening. *J. Stat. Phys.* **1985**, *38*, 231–252.

(40) Flügel, E. A.; Ranft, A.; Haase, F.; Lotsch, B. V. Synthetic Routes Toward MOF Nanomorphologies. *J. Mater. Chem.* **2012**, *22*, 10119.

(41) Khan, N. A.; Jhung, S. H. Synthesis of Metal-Organic Frameworks (MOFs) With Microwave or Ultrasound: Rapid Reaction, Phase-selectivity, and Size Reduction. *Coord. Chem. Rev.* **2015**, *285*, 11–23.

(42) Kirkpatrick, R. J. Crystal Growth from the Melt : A Review. *Am. Miner.* **1975**, *60*, 798–814.

(43) Burton, W. K.; Cabrera, N.; Frank, F. C. The Growth of Crystals and the Equilibrium Structure of Their Surfaces. *Philos. Trans. R. Soc. London A Math. Phys. Eng. Sci.* **1951**, *243*, 299–358.

(44) Lovette, M. A.; Browning, A. R.; Griffin, D. W.; Sizemore, J. P.; Snyder, R. C.; Doherty, M. F. Crystal Shape Engineering. *Ind. Eng. Chem. Res.* **2008**, *47*, 9812–9833.

(45) Cölfen, H.; Mann, S. Higher-Order Organization by Mesoscale Self-Assembly and Transformation of Hybrid Nanostructures. *Angew. Chem. Int. Ed.* **2003**, *42*, 2350–2365.

(46) Zhang, J.-P.; Huang, X.-C.; Chen, X.-M. Supramolecular Isomerism in Coordination Polymers. *Chem. Soc. Rev.* **2009**, *38*, 2385–2396.

(47) Ostwald, W. Studies on the Formation and Transformation of Solid Compounds: Report I. Supersaturation and Practicing Cooling. *Z. Phys. Ch.* **1897**, *22*, 289–330.

(48) Van Santen, R. A. The Ostwald Step Rule. *J. Phys. Chem* **1984**, *88*, 5768–5769.

(49) Patel, A. R.; Venkateswara Rao, A. Crystal Growth in Gel Media. *Bull. Mater. Sci.* **1982**, *4*, 527–548.

(50) Burnett, B. J.; Choe, W. Sequential Self-assembly in Metal–Organic Frameworks. *Dalt. Trans.* **2012**, *41*, 3889–3894.

(51) Kole, G. K.; Vittal, J. J. Solid-state Reactivity and Structural Transformations Involving Coordination Polymers. *Chem. Soc. Rev.* **2013**, *42*, 1755–1775.

(52) Millange, F.; Medina, M. I.; Guillou, N.; Férey, G.; Golden, K. M.; Walton, R. I. Time-Resolved In Situ Diffraction Study of the Solvothermal Crystallization of Some Prototypical Metal–Organic Frameworks. *Angew. Chem. Int. Ed.* **2010**, *49*, 763–766.

(53) Wu, Y.; Moorhouse, S. J.; O'Hare, D. Time-Resolved In Situ Diffraction Reveals a Solid-State Rearrangement During Solvothermal MOF Synthesis. *Chem. Mater.* **2015**, *27*, 7236–7239.

(54) Yeung, H. H.-M.; Wu, Y.; Henke, S.; Cheetham, A. K.; O'Hare, D.; Walton, R. I. In Situ Observation of Successive Crystallizations and Metastable Intermediates in the Formation of Metal–Organic Frameworks. *Angew. Chem. Int. Ed.* **2016**, *55*, 2012–2016.

(55) Schweinefuß, M. E.; Baburin, I. A.; Schröder, C. A.; Näther, C.; Leoni, S.; Wiebcke, M. Indium Imidazolate Frameworks With Differently Distorted ReO_3-Type Structures: Syntheses, Structures, Phase Transitions, and Crystallization Studies. *Cryst. Growth Des.* **2014**, *14*, 4664–4673.

(56) Rao, C. N. R.; Natarajan, S.; Choudhury, A.; Neeraj, S.; Ayi, A. A. Aufbau Principle of Complex Open-Framework Structures of Metal Phosphates With Different Dimensionalities. *Acc. Chem. Res.* **2001**, *34*, 80–87.

(57) Murugavel, R.; Walawalkar, M. G.; Dan, M.; Roesky, H. W.; Rao, C. N. R. Transformations of Molecules and Secondary Building Units to Materials: A Bottom-Up Approach. *Acc. Chem. Res.* **2004**, *37*, 763–774.

(58) Oliver, S.; Kuperman, A.; Ozin, G. A. A New Model for Aluminophosphate Formation: Transformation of a Linear Chain Aluminophosphate to Chain, Layer, and Framework Structures. *Angew. Chem. Int. Ed.* **1998**, *37*, 46–62.

(59) Pienack, N.; Bensch, W. In-Situ Monitoring of the Formation of Crystalline Solids. *Angew. Chem. Int. Ed.* **2011**, *50*, 2014–2034.

(60) Jensen, K. M. Ø.; Tyrsted, C.; Bremholm, M.; Iversen, B. B. In Situ Studies of Solvothermal Synthesis of Energy Materials. *ChemSusChem* **2014**, *7*, 1594–1611.

(61) Wu, Y.; Breeze, M. I.; O'Hare, D.; Walton, R. I. High Energy X-rays for Following Metal–Organic Framework Formation: Identifying Intermediates in Interpenetrated MOF-5 Crystallisation. *Microporous Mesoporous Mater.* **2017**, *254*, 178–183.

(62) McKinstry, C.; Cussen, E. J.; Fletcher, A. J.; Patwardhan, S. V.; Sefcik, J. Effect of Synthesis Conditions on Formation Pathways of Metal Organic Framework (MOF-5) Crystals. *Cryst. Growth Des.* **2013**, *13*, 5481–5486.

(63) Ragon, F. et al. Acid-functionalized UiO-66(Zr) MOFs and Their Evolution After Intra-framework Cross-linking: Structural Features and Sorption Properties. *J. Mater. Chem. A* **2015**, *3*, 3294–3309.

(64) Cravillon, J.; Schröder, C. A.; Bux, H.; Rothkirch, A.; Caro, J.; Wiebcke, M. Formate Modulated Solvothermal Synthesis of ZIF-8 Investigated Using Time-resolved In Situ X-ray Diffraction and Scanning Electron Microscopy. *CrystEngComm* **2012**, *14*, 492–498.

(65) Ahnfeldt, T.; Stock, N. Synthesis of Isoreticular CAU-1 Compounds: Effects of Linker and Heating Methods on the Kinetics of the Synthesis. *CrystEngComm* **2012**, *14*, 505–511.

(66) Cliffe, M. J.; Castillo-Martínez, E.; Wu, Y.; Lee, J.; Forse, A. C.; Firth, F. C.; Moghadam, P. Z.; Fairen-Jimenez, D.; Gaultois, M. W.; Hill, J. A.; Magdysyuk, O. V.; Slater, B.; Goodwin, A. L.; Grey, C. P. Metal-Organic Nanosheets Formed Via Defect-Mediated Transformation of a Hafnium Metal-Organic Framework. *J. Am. Chem. Soc.* **2017**, *139*, 5397–5404.

(67) Shoemaker, D. P.; Chung, D. Y.; Mitchell, J. F.; Bray, T. H.; Soderholm, L.; Chupas, P. J.; Kanatzidis, M. G. Understanding Fluxes as Media for Directed Synthesis: In Situ Local Structure of Molten Potassium Polysulfides. *J. Am. Chem. Soc.* **2012**, *134*, 9456–9463.

(68) Tyrsted, C.; Lock, N.; Jensen, K. M.; Christensen, M.; Bøjesen, E. D.; Emerich, H.; Vaughan, G.; Billinge, S. J.; Iversen, B. B. Evolution of Atomic Structure During Nanoparticle Formation. *IUCrJ* **2014**, *1*, 165–171.

(69) Norby, P. In-Situ XRD as a Tool to Understanding Zeolite Crystallization. *Curr. Opin. Colloid Interface Sci.* **2006**, *11*, 118–125.

(70) Feyand, M.; Näther, C.; Rothkirch, A.; Stock, N. Systematic and In Situ Energy Dispersive X-ray Diffraction Investigations on the Formation of Lanthanide Phosphonatobutanesulfonates: $Ln(O_3P\text{-}C_4H_8\text{-}SO_3)(H_2O)$ (Ln LaGd). *Inorg. Chem.* **2010**, *49*, 11158–11163.

(71) Feyand, M.; Hübner, A.; Rothkirch, A.; Wragg, D. S.; Stock, N. Copper Phosphonatoethanesulfonates: Temperature Dependent In Situ Energy Dispersive X-ray Diffraction Study and Influence of the Ph on the Crystal Structures. *Inorg. Chem.* **2012**, *51*, 12540–12547.

(72) Schmidt, C.; Stock, N. High-Throughput and In Situ Energy Dispersive X-ray Diffraction Investigation on the Formation of the New Metal Organogermanate $Cu(OOCC_2H_4Ge)_2O_3$. *Cryst. Growth Des.* **2011**, *11*, 5682–5687.

(73) Kojima, T.; Choi, W.; Kawano, M. Single-crystal Growth of Coordination Networks Via the Gas Phase and Dependence of Iodine Encapsulation on the Crystal Size. *Chem. Commun.* **2014**, *50*, 13793–13796.

(74) Avrami, M. Kinetics of Phase Change. I General Theory. *J. Chem. Phys.* **1939**, *7*, 1103–1112.

(75) Avrami, M. Kinetics of Phase Change. II Transformation–Time Relations for Random Distribution of Nuclei. *J. Chem. Phys.* **1940**, *8*, 212–224.

(76) Avrami, M. Granulation, Phase Change, and Microstructure Kinetics of Phase Change. III. *J. Chem. Phys.* **1941**, *9*, 177–184.

(77) Finney, E. E.; Finke, R. G. Nanocluster Nucleation and Growth Kinetic and Mechanistic Studies: A Review Emphasizing Transition-metal Nanoclusters. *J. Colloid Interface Sci.* **2008**, *317*, 351–374.

(78) Hancock, J. D.; Sharp, J. H. Method of Comparing Solid-State Kinetic Data and Its Application to the Decomposition of Kaolinite, Brucite, and $BaCO_3$. *J. Am. Ceram. Soc.* **1972**, *55*, 74–77.

(79) Seoane, B.; Zamaro, J. M.; Tellez, C.; Coronas, J. Sonocrystallization of Zeolitic Imidazolate Frameworks (ZIF-7 , ZIF-8 , ZIF-11 and ZIF-20)). *CrystEngComm* **2012**, *14*, 3103–3107.

(80) Khawam, A.; Flanagan, D. R. Solid-state kinetic models: Basics and mathematical fundamentals. *J. Phys. Chem. B* **2006**, *110*, 17315–17328.

(81) Finney, E. E.; Finke, R. G. Is There a Minimal Chemical Mechanism Underlying Classical Avrami-erofe'ev Treatments of Phase-transformation Kinetic Data. *Chem. Mater.* **2009**, *21*, 4692–4705.

(82) Kondo, A.; Nakagawa, T.; Kajiro, H.; Chinen, A.; Hattori, Y.; Okino, F.; Ohba, T.; Kaneko, K.; Kanoh, H. Dynamic Changes in Dimensional Structures of Co-Complex Crystals. *Inorg. Chem.* **2010**, *49*, 9247–9252.

(83) Ahnfeldt, T.; Moellmer, J.; Guillerm, V.; Staudt, R.; Serre, C.; Stock, N. High-Throughput and Time-Resolved Energy-Dispersive X-Ray Diffraction (EDXRD) Study of the Formation of CAU-1-$(OH)_2$: Microwave and Conventional Heating. *Chem. - A Eur. J.* **2011**, *17*, 6462–6468.

(84) Niekiel, F.; Ackermann, M.; Guerrier, P.; Rothkirch, A.; Stock, N. Aluminum-1,4-cyclohexanedicarboxylates: High-Throughput and Temperature-Dependent In Situ EDXRD Studies. *Inorg. Chem.* **2013**, *52*, 8699–8705.

(85) Khan, N. A.; Haque, M. M.; Jhung, S. H. Accelerated Syntheses of Porous Isostructural Lanthanide–Benzenetricarboxylates (Ln–BTC) Under Ultrasound at Room Temperature. *Eur. J. Inorg. Chem.* **2010**, *2010*, 4975–4981.

(86) Moorhouse, S. J.; Wu, Y.; OHare, D. An In Situ Study of Resin-assisted Solvothermal Metal–Organic Framework Synthesis. *J. Solid State Chem.* **2016**, *236*, 209–214.

(87) Haque, E.; Jhung, S. H. Synthesis of Isostructural Metal–organic Frameworks, CPO-27s, With Ultrasound, Microwave, and Conventional Heating: Effect of Synthesis Methods and Metal Ions. *Chem. Eng. J.* **2011**, *173*, 866–872.

(88) El Osta, R.; Feyand, M.; Stock, N.; Millange, F.; Walton, R. I. Crystallisation Kinetics of Metal Organic Frameworks From In Situ Time-Resolved X-ray Diffraction. *Powder Diffr.* **2013**, *28*, S256–S275.

(89) Khan, N. A.; Haque, E.; Jhung, S. H. Rapid Syntheses of a Metal–Organic Framework Material $Cu_3(BTC)_2(H_2O)_3$ Under Microwave: a Quantitative Analysis of Accelerated Syntheses. *Phys. Chem. Chem. Phys.* **2010**, *12*, 2625–2631.

(90) Millange, F. et al. A Time-resolved Diffraction Study of a Window of Stability in the Synthesis of a Copper Carboxylate Metal–Organic Framework. *CrystEngComm* **2011**, *13*, 103–108.

(91) El Osta, R.; Frigoli, M.; Marrot, J.; Medina, M. E.; Walton, R. I.; Millange, F. Synthesis, Structure, and Crystallization Study of a Layered Lithium Thiophene-Dicarboxylate. *Cryst. Growth Des.* **2012**, *12*, 1531–1537.

(92) Chevreau, H.; Permyakova, A.; Nouar, F.; Fabry, P.; Livage, C.; Ragon, F.; Garcia-Marquez, A.; Devic, T.; Steunou, N.; Serre, C.; Horcajada, P. Synthesis of the Biocompatible and Highly Stable MIL-127(Fe): From Large Scale Synthesis to Particle Size Control. *CrystEngComm* **2016**, *18*, 4094–4101.

(93) Haque, E.; Khan, N. A.; Kim, C. M.; Jhung, S. H. Syntheses of Metal–Organic Frameworks and Aluminophosphates Under Microwave Heating: Quantitative Analysis of Accelerations. *Cryst. Growth Des.* **2011**, *11*, 4413–4421.

(94) Haque, E.; Jeong, J. H.; Jhung, S. H. Synthesis of Isostructural Porous Metal-benzenedicarboxylates: Effect of Metal Ions on the Kinetics of Synthesis. *CrystEngComm* **2010**, *12*, 2749–2754.

(95) Haque, E.; Khan, N. A.; Park, J. H.; Jhung, S. H. Synthesis of a Metal–Organic Framework Material, Iron Terephthalate, by Ultrasound, Microwave, and Conventional Electric Heating: A Kinetic Study. *Chem. Eur. J.* **2010**, *16*, 1046–1052.

(96) Reinsch, H.; Stock, N. Formation and Characterisation of Mn-MIL-10. *CrystEngComm* **2013**, *15*, 544–550.

(97) Juan-Alcañiz, J.; Goesten, M.; Martinez-Joaristi, A.; Stavitski, E.; Petukhov, A. V.; Gascon, J.; Kapteijn, F.; Juan-Alcaniz, J.; Goesten, M.; Martinez-Joaristi, A.; Stavitski, E.; Petukhov, A. V.; Gascon, J.; Kapteijn, F. Live Encapsulation of a Keggin Polyanion in NH2-MIL-101(Al) Observed by In Situ Time Resolved X-ray Scattering. *Chem. Commun.* **2011**, *47*, 8578–8580.

(98) Stavitski, E.; Goesten, M.; Juan-Alcañiz, J.; Martinez-Joaristi, A.; Serra-Crespo, P.; Petukhov, A. V.; Gascon, J.; Kapteijn, F. Kinetic Control of Metal–Organic Framework Crystallization Investigated by Time-Resolved In Situ X-Ray Scattering. *Angew. Chem. Int. Ed.* **2011**, *50*, 9624–9628.

(99) Ragon, F.; Chevreau, H.; Devic, T.; Serre, C.; Horcajada, P. Impact of the Nature of the Organic Spacer on the Crystallization Kinetics of UiO-66(Zr)-Type MOFs. *Chem. Eur. J.* **2015**, *21*, 7135–7143.

(100) Ragon, F.; Horcajada, P.; Chevreau, H.; Hwang, Y. K.; Lee, U.-H.; Miller, S. R.; Devic, T.; Chang, J.-S.; Serre, C. In Situ Energy-Dispersive X-ray Diffraction for the Synthesis Optimization and Scale-up of the Porous Zirconium Terephthalate UiO-66. *Inorg. Chem.* **2014**, *53*, 2491–2500.

(101) Schoenecker, P. M.; Belancik, G. A.; Grabicka, B. E.; Walton, K. S. Kinetics Study and Crystallization Process Design for Scale-up of UiO-66-NH2 Synthesis. *AICHE J.* **2013**, *59*, 1255–1262.

(102) Breeze, M. I. et al. Structural Variety in Ytterbium Dicarboxylate Frameworks and In Situ Study Diffraction of Their Solvothermal Crystallisation. *CrystEngComm* **2017**, *19*, 2424–2433.

(103) Wu, Y.; Breeze, M. I.; Clarkson, G. J.; Millange, F.; O'Hare, D.; Walton, R. I. Exchange of Coordinated Solvent During Crystallization of a Metal-Organic Framework Observed by In Situ High-Energy X-ray Diffraction. *Angew. Chemie - Int. Ed.* **2016**, *55*, 4992–4996.

(104) Feng, X.; Carreon, M. A. Kinetics of Transformation on ZIF-67 Crystals. *J. Cryst. Growth* **2015**, *418*, 158–162.

(105) Goesten, M.; Stavitski, E.; Pidko, E. A.; Gücüyener, C.; Boshuizen, B.; Ehrlich, S. N.; Hensen, E. J. M.; Kapteijn, F.; Gascon, J. The Molecular Pathway to ZIF-7 Microrods Revealed by In Situ Time-Resolved Small- and Wide-Angle X-Ray Scattering, Quick-Scanning Extended X-Ray Absorption Spectroscopy, and DFT Calculations. *Chem. Eur. J.* **2013**, *19*, 7809–7816.

(106) Saha, S.; Springer, S.; Schweinefuß, M. E.; Pontoni, D.; Wiebcke, M.; Huber, K. Insight Into Fast Nucleation and Growth of Zeolitic Imidazolate Framework-71 by In Situ Time-Resolved Light and X-ray Scattering Experiments. *Cryst. Growth Des.* **2016**, *16*, 2002–2010.

(107) Friščić, T.; Halasz, I.; Beldon, P. J.; Belenguer, A. M.; Adams, F.; Kimber, S. a. J.; Honkimäki, V.; Dinnebier, R. E. Real-time and In Situ Monitoring of Mechanochemical Milling Reactions. *Nat. Chem.* **2013**, *5*, 66–73.

(108) Moh, P. Y.; Brenda, M.; Anderson, M. W.; Attfield, M. P. Crystallisation of Solvothermally Synthesised ZIF-8 Investigated at the Bulk , Single Crystal and Surface Level. *CrystEngComm* **2013**, *15*, 9672–9678.

(109) Zhu, M.; Venna, S. R.; Jasinski, J. B.; Carreon, M. A. Room-temperature Synthesis of ZIF-8: The Coexistence of ZnO Nanoneedles. *Chem. of Mater.* **2011**, *23*, 3590–3592.

(110) Zahn, G.; Zerner, P.; Lippke, J.; Kempf, F. L.; Lilienthal, S.; Schröder, C. A.; Schneider, A. M.; Behrens, P. Insight Into the Mechanism of Modulated Syntheses: In Situ Synchrotron Diffraction Studies on the Formation of Zr-fumarate MOF. *CrystEngComm* **2014**, *16*, 9198–9207.

(111) Surblé, S.; Millange, F.; Serre, C.; Férey, G.; Walton, R. I. An EXAFS Study of the Formation of a Nanoporous Metal–Organic Framework: Evidence for the Retention of Secondary Building Units During Synthesis. *Chem. Commun.* **2006**, 1518–1520.

(112) Mahata, P.; Prabu, M.; Natarajan, S. Role of Temperature and Time in the Formation of Infinite MOM Linkages and Isolated Clusters in MOFs: A Few Illustrative Examples. *Inorg. Chem.* **2008**, *47*, 8451–8463.

(113) Goesten, M. G.; Stavitski, E.; Juan-Alcañiz, J.; Martinez-Joaristi, A.; Petukhov, A. V.; Kapteijn, F.; Gascon, J. Small-angle X-ray Scattering Documents the Growth of Metal–Organic Frameworks. *Catal. Today* **2013**, *205*, 120–127.

(114) Kim, H.; Das, S.; Kim, M. G.; Dybtsev, D. N.; Kim, Y.; Kim, K. Synthesis of Phase-Pure Interpenetrated MOF-5 and Its Gas Sorption Properties. *Inorganic Chemistry* **2011**, *50*, 3691–3696, PMID: 21413727.

(115) Schröder, C. A.; Baburin, I. A.; van Wüllen, L.; Wiebcke, M.; Leoni, S. Subtle Polymorphism of Zinc Imidazolate Frameworks: Temperature-dependent Ground States in the Energy Landscape Revealed by Experiment and Theory. *CrystEngComm* **2013**, *15*, 4036–4040.

(116) Dan, M.; Rao, C. N. R. A Building-Up Process in Open-Framework Metal Carboxylates That Involves a Progressive Increase in Dimensionality. *Angew. Chem. Int. Ed.* **2006**, *45*, 281–285.

(117) Thirumurugan, A.; Rao, C. N. R. 1,2-, 1,3- and 1,4-Benzenedicarboxylates of Cd and Zn of Different Dimensionalities: Process of Formation of the Three-dimensional Structure. *J. Mater. Chem.* **2005**, *15*, 3852–3858.

(118) Mahata, P.; Sundaresan, A.; Natarajan, S. The Role of Temperature on the Structure and Dimensionality of MOFs: an Illustrative Study of the Formation of Manganese Oxy-bis(benzoate) Structures. *Chem. Commun.* **2007**, 4471–4473.

(119) Feng, X.; Wu, T.; Carreon, M. A. Synthesis of ZIF-67 and ZIF-8 Crystals Using DMSO (Dimethyl Sulfoxide) as Solvent and Kinetic Transformation Studies. *J. Cryst. Growth* **2016**, *455*, 152–156.

(120) Goesten, M. G.; de Lange, M. F.; Olivos-Suarez, A. I.; Bavykina, A. V.; Serra-Crespo, P.; Krywka, C.; Bickelhaupt, F. M.; Kapteijn, F.; Gascon, J. Evidence for a Chemical Clock in Oscillatory Formation of UiO-66. *Nat. Commun.* **2016**, *7*, 11832.

(121) Fukushima, T.; Horike, S.; Kobayashi, H.; Tsujimoto, M.; Isoda, S.; Foo, M. L.; Kubota, Y.; Takata, M.; Kitagawa, S. Modular Design of Domain Assembly in Porous Coordination Polymer Crystals Via Reactivity-Directed Crystallization Process. *J. Am. Chem. Soc.* **2012**, *134*, 13341–13347.

(122) Ferguson, A.; Liu, L.; Tapperwijn, S. J.; Perl, D.; Coudert, F.-X.; Van Cleuvenbergen, S.; Verbiest, T.; van der Veen, M. A.; Telfer, S. G. Controlled Partial Interpenetration in Metal–Organic Frameworks. *Nat. Chem.* **2016**, *8*, 250–257.

(123) Conner, W. C.; Tompsett, G.; Lee, K. H.; Yngvesson, K. S. Microwave Synthesis of Zeolites: 1. Reactor Engineering. *J. Phys. Chem. B* **2004**, *108*, 13913–13920.

(124) Albuquerque, G. H.; Fitzmorris, R. C.; Ahmadi, M.; Wannenmacher, N.; Thallapally, P. K.; McGrail, B. P.; Herman, G. S. Gas-liquid Segmented Flow Microwave-assisted Synthesis of MOF-74(Ni) Under Moderate Pressures. *CrystEngComm* **2015**, *17*, 5502–5510.

(125) Užarević, K.; Halasz, I.; Friščić, T. Real-Time and In Situ Monitoring of Mechanochemical Reactions: A New Playground for All Chemists. *J. Phys. Chem. Lett.* **2015**, *6*, 4129–4140.

(126) Katsenis, A. D.; Puškarić, A.; Štrukil, V.; Mottillo, C.; Julien, P. A.; Užarević, K.; Pham, M.-H.; Do, T.-O.; Kimber, S. A. J.; Lazić, P.; Magdysyuk, O.; Dinnebier, R. E.; Halasz, I.; Friščić, T. In Situ X-ray Diffraction Monitoring of a Mechanochemical Reaction Reveals a Unique Topology Metal–Organic Framework. *Nat. Commun.* **2015**, *6*, 6662.

(127) Halasz, I.; Kimber, S. A. J.; Beldon, P. J.; Belenguer, A. M.; Adams, F.; Honkimäki, V.; Nightingale, R. C.; Dinnebier, R. E.; Friščić, T. In Situ and Real-time Monitoring of Mechanochemical Milling Reactions Using Synchrotron X-ray Diffraction. *Nat. Protoc.* **2013**, *8*, 1718–1729.

(128) Julien, P. A.; Užarević, K.; Katsenis, A. D.; Kimber, S. A. J.; Wang, T.; Farha, O. K.; Zhang, Y.; Casaban, J.; Germann, L. S.; Etter, M.; Dinnebier, R. E.; James, S. L.; Halasz, I.; Friščić, T. In Situ Monitoring and Mechanism of the Mechanochemical Formation of a Microporous MOF-74 Framework. *J. Am. Chem. Soc.* **2016**, *138*, 2929–2932.

(129) Stolar, T.; Batzdorf, L.; Lukin, S.; Žilić, D.; Motillo, C.; Friščić, T.; Emmerling, F.; Halasz, I.; Užarević, K. In Situ Monitoring of the Mechanosynthesis of the Archetypal Metal-Organic Framework HKUST-1: Effect of Liquid Additives on the Milling Reactivity. *Inorg. Chem.* **2017**, *56*, 6599–6608.

(130) Užarević, K.; Štrukil, V.; Mottillo, C.; Julien, P. A.; Puškarić, A.; Friščić, T.; Halasz, I. Exploring the Effect of Temperature on a Mechanochemical Reaction by In Situ Synchrotron Powder X-ray Diffraction. *Cryst. Growth Des.* **2016**, *16*, 2342–2347.

(131) Ban, Y.; Peng, Y.; Zhang, Y.; Jin, H.; Jiao, W.; Guo, A.; Wang, P.; Li, Y.; Yang, W. Dual-ligand Zeolitic Imidazolate Framework Crystals and Oriented Films Derived From Metastable Mono-ligand ZIF-108. *Micropor. Mesopor. Mater.* **2016**, *219*, 190–198.

(132) Nayuk, R.; Zacher, D.; Schweins, R.; Wiktor, C.; Fischer, R. A.; van Tendeloo, G.; Huber, K. Modulated Formation of MOF-5 Nanoparticles-A SANS Analysis. *J. Phys. Chem. C* **2012**, *116*, 6127–6135.

(133) Zacher, D.; Nayuk, R.; Schweins, R.; Fischer, R. A.; Huber, K. Monitoring the Coordination Modulator Shell at MOF Nanocrystals. *Cryst. Growth Des.* **2014**, *14*, 4859–4863.

(134) Liu, S.; Zhang, Y.; Meng, Y.; Gao, F.; Jiao, S.; Ke, Y. Fast Syntheses of MOFs Using Nanosized Zeolite Crystal Seeds In Situ Generated From Microsized Zeolites. *Cryst. Growth Des.* **2013**, *13*, 2697–2702.

(135) Birsa Čelič, T.; Rangus, M.; Lázár, K.; Kaučič, V.; Zabukovec Logar, N. Spectroscopic Evidence for the Structure Directing Role of the Solvent in the Synthesis of Two Iron Carboxylates. *Angew. Chem.* **2012**, *124*, 12658–12662.

(136) Centrone, A.; Yang, Y.; Speakman, S.; Bromberg, L.; Rutledge, G. C.; Hatton, T. A. Growth of Metal-Organic Frameworks on Polymer Surfaces. *J. Am. Chem. Soc.* **2010**, *132*, 15687–15691.

(137) Biemmi, E.; Scherb, C.; Bein, T. Oriented Growth of the Metal Organic Framework $Cu_3(BTC)_2(H_2O)_3 \cdot xH_2O$ Tunable With Functionalized Self-assembled Monolayers. *J. Am. Chem. Soc.* **2007**, *129*, 8054–8055.

(138) Hashimoto, M.; Okajima, S.; Kondo, T.; Hara, K.; Chun, W.-J. Thin Film Structures of Metal-Organic Framework $[Cu_3(BTC)_2(H_2O)_3]$n on $TiO_2(110)$. *Electrochemistry* **2014**, *82*, 335–337.

(139) Bux, H.; Feldhoff, A.; Cravillon, J.; Wiebcke, M.; Li, Y.-S.; Caro, J. Oriented Zeolitic Imidazolate Framework-8 Membrane With Sharp H_2/C_3H_8 Molecular Sieve Separation. *Chem. Mater.* **2011**, *23*, 2262–2269.

(140) van der DRIFT, A. Evolutionary Selection, a Principle Governing Growth Orientation in Vapour-Deposited Layers. *Philips Res. Repts.* **1967**, *22*, 267–288.

(141) Kida, K.; Fujita, K.; Shimada, T.; Tanaka, S.; Miyake, Y. Layer-by-layer Aqueous Rapid Synthesis of ZIF-8 Films on a Reactive Surface. *Dalt. Trans.* **2013**, *42*, 11128–11135.

(142) Moh, P. Y.; Cubillas, P.; Anderson, M. W.; Attfield, M. P. Revelation of the Molecular Assembly of the Nanoporous Metal Organic Framework ZIF-8. *J. Am. Chem. Soc.* **2011**, *133*, 13304–13307.

(143) Cubillas, P.; Anderson, M. W.; Attfield, M. P. Materials Discovery and Crystal Growth of Zeolite A Type Zeolitic-Imidazolate Frameworks Revealed by Atomic Force Microscopy. *Chem. Eur. J.* **2013**, *19*, 8236–8243.

(144) Shoaee, M.; Anderson, M. W.; Attfield, M. P. Crystal Growth of the Nanoporous Metal-Organic Framework HKUST-1 Revealed by In Situ Atomic Force Microscopy. *Angew. Chem. Int. Ed.* **2008**, *47*, 8525–8528.

(145) John, N. S.; Scherb, C.; Shöâeè, M.; Anderson, M. W.; Attfield, M. P.; Bein, T. Single Layer Growth of Sub-micron Metal–Organic Framework Crystals Observed by In Situ Atomic Force Microscopy. *Chem. Commun.* **2009**, *2*, 6294–6296.

(146) Cubillas, P.; Anderson, M. W.; Attfield, M. P. Crystal Growth Mechanisms and Morphological Control of the Prototypical Metal-Organic Framework MOF-5 Revealed by Atomic Force Microscopy. *Chem. Eur. J.* **2012**, *18*, 15406–15415.

(147) Cubillas, P.; Etherington, K.; Anderson, M. W.; Attfield, M. P. Crystal Growth of MOF-5 Using Secondary Building Units Studied by In Situ Atomic Force Microscopy. *CrystEngComm* **2014**, *16*, 9834–9841.

(148) Shöâeè, M.; Agger, J. R.; Anderson, M. W.; Attfield, M. P. Crystal Form, Defects and Growth of the Metal Organic Framework HKUST-1 Revealed by Atomic Force Microscopy. *CrystEngComm* **2008**, *10*, 646–648.

(149) Moret, M.; Rizzato, S. Crystallization Behavior of Coordination Polymers. 2. Surface Micro-Morphology and Growth Mechanisms of $[Cu(bpp)_3Cl_2 \cdot 2H_2O]$ by In Situ Atomic Force Microscopy. *Cryst. Growth Des.* **2009**, *9*, 5035–5042.

(150) Walker, A. M.; Slater, B. Comment Upon the Screw Dislocation Structure on HKUST-1 { 111 } Surfaces. *CrystEngComm* **2008**, *10*, 790–791.

(151) Cubillas, P.; Anderson, M. W.; Attfield, M. P. Influence of Isomorphous Substituting Cobalt Ions on the Crystal Growth of the MOF-5 Framework Determined by Atomic Force Microscopy of Growing Core-shell Crystals. *Cryst. Growth Des.* **2013**, *13*, 4526–4532.

(152) Szelagowska-Kunstman, K.; Cyganik, P.; Goryl, M.; Zacher, D.; Puterova, Z.; Fischer, R. A.; Szymonski, M. Surface Structure of Metal-Organic Framework Grown on Self-Assembled Monolayers Revealed by High-Resolution Atomic Force Microscopy. *J. Am. Chem. Soc.* **2008**, *130*, 14446–14447.

(153) Munuera, C.; Shekhah, O.; Wang, H.; Wöll, C.; Ocal, C. The Controlled Growth of Oriented Metal–Organic Frameworks on Functionalized Surfaces as Followed by Scanning Force Microscopy. *Phys. Chem. Chem. Phys.* **2008**, *10*, 7257–7261.

(154) Ohnsorg, M. L.; Beaudoin, C. K.; Anderson, M. E. Fundamentals of MOF Thin Film Growth Via Liquid-Phase Epitaxy: Investigating the Initiation of Deposition and the Influence of Temperature. *Langmuir* **2015**, *31*, 6114–6121.

(155) Stavila, V.; Volponi, J.; Katzenmeyer, A. M.; Dixon, M. C.; Allendorf, M. D. Kinetics and Mechanism of Metal–Organic Framework Thin Film Growth: Systematic Investigation of HKUST-1 Deposition on QCM Electrodes. *Chem. Sci.* **2012**, *3*, 1531–1540.

(156) Nijem, N.; Fürsich, K.; Kelly, S. T.; Swain, C.; Leone, S. R.; Gilles, M. K. HKUST-1 Thin Film Layer-by-Layer Liquid Phase Epitaxial Growth: Film Properties and Stability Dependence on Layer Number. *Cryst. Growth Des.* **2015**, *15*, 2948–2957.

(157) Shekhah, O.; Wang, H.; Zacher, D.; Fischer, R. A.; Wöll, C. Growth Mechanism of Metal–Organic Frameworks: Insights Into the Nucleation by Employing a Step-by-step Route. *Angew. Chem. Int. Ed.* **2009**, *48*, 5038–5041.

(158) Zhuang, J.-L.; Kind, M.; Grytz, C. M.; Farr, F.; Diefenbach, M.; Tussupbayev, S.; Holthausen, M. C.; Terfort, A. Insight Into the Oriented Growth of Surface-Attached Metal-Organic Frameworks: Surface Functionality, Deposition Temperature, and First Layer Order. *J. Am. Chem. Soc.* **2015**, *137*, 8237–8243.

(159) Yu, X.-J.; Zhuang, J.-L.; Scherr, J.; Abu-Husein, T.; Terfort, A. Minimization of Surface Energies and Ripening Outcompete Template Effects in the Surface Growth of Metal-Organic Frameworks. *Angew. Chem. Int. Ed.* **2016**, *55*, 8348–8352.

(160) Wiktor, C.; Meledina, M.; Turner, S.; Lebedev, O. I.; Fischer, R. A. Transmission Electron Microscopy on Metal–Organic Frameworks – a Review. *J. Mater. Chem. A* **2017**, *5*, 14969–14989.

(161) De Yoreo, J. J.; N. A. J. M., S. Investigating Materials Formation With Liquid-phase and Cryogenic TEM. *Nat. Rev. Mater.* **2016**, *1*, 16035.

(162) Wiktor, C.; Turner, S.; Zacher, D.; Fischer, R. A.; Tendeloo, G. V. Imaging of Intact MOF-5 Nanocrystals by Advanced TEM at Liquid Nitrogen Temperature. *Microporous Mesoporous Mater.* **2012**, *162*, 131–135.

(163) Patterson, J. P.; Abellan, P.; Denny, M. S.; Park, C.; Browning, N. D.; Cohen, S. M.; Evans, J. E.; Gianneschi, N. C. Observing the Growth of Metal-Organic Frameworks by In Situ Liquid Cell Transmission Electron Microscopy. *J. Am. Chem. Soc.* **2015**, *137*, 7322–7328.

(164) Nielsen, M. H.; Aloni, S.; De Yoreo, J. J. In Situ TEM Imaging of CaCO3 Nucleation Reveals Coexistence of Direct and Indirect Pathways. *Science* **2014**, *345*, 1158–1162.

(165) Zhu, Y.; Ciston, J.; Zheng, B.; Miao, X.; Czarnik, C.; Pan, Y.; Sougrat, R.; Lai, Z.; Hsiung, C.-E.; Yao, K.; Pinnau, I.; Pan, M.; Han, Y. Unravelling Surface and Interfacial Structures of a Metal–organic Framework by Transmission Electron Microscopy. *Nat. Mater.* **2017**, *16*, 532–536.

(166) Ban, Y.; Li, Y.; Liu, X.; Peng, Y.; Yang, W. Solvothermal Synthesis of Mixed-ligand Metal–Organic Framework ZIF-78 With Controllable Size and Morphology. *Micropor. Mesopor. Mater.* **2013**, *173*, 29–36.

(167) Venkatesh, V.; Pachfule, P.; Banerjee, R.; Verma, S. Evolution of an Adenine-Copper Cluster to a Highly Porous Cuboidal Framework: Solution-Phase Ripening and Gas-Adsorption Properties. *Chem. Eur. J.* **2014**, *20*, 12262–12268.

(168) Xiao, B.; Zhao, X.; Huang, C.; Li, Y. Facile Synthesis of Hierarchical Metal–Organic Microsheet-assembled Microflowers. *Mater. Lett.* **2015**, *152*, 139–141.

(169) Zheng, C. M.; Greer, H. F.; Chianga, C. Y.; Zhou, W. Z. Microstructural Study of the Formation Mechanism of Metal–Organic Framework MOF-5. *CrystEngComm* **2014**, *16*, 1064–1070.

(170) Chen, X.; Qiao, M.; Xie, S.; Fan, K.; Zhou, W.; He, H. Self-Construction of Core-Shell and Hollow Zeolite Analcime Icositetrahedra: A Reversed Crystal Growth Process Via Oriented Aggregation of Nanocrystallites and Recrystallization From Surface to Core. *J. Am. Chem. Soc.* **2007**, *129*, 13305–13312.

(171) Greer, H. F.; Liu, Y.; Greenaway, A.; Wright, P. A.; Zhou, W. Synthesis and Formation Mechanism of Textured MOF-5. *Cryst. Growth Des.* **2016**, *16*, 2104–2111.

(172) Self, K.; Telfer, M.; Greer, H. F.; Zhou, W. Reversed Crystal Growth of RHO Zeolitic Imidazolate Framework (ZIF). *Chem. Eur. J.* **2015**, *21*, 19090–19095.

(173) Tang, J.; Alivisatos, A. P. Crystal Splitting in the Growth of Bi_2S_3. *Nano Lett.* **2006**, *6*, 2701–2706.

(174) Liu, K.; You, H.; Zheng, Y.; Jia, G.; Zhang, L.; Huang, Y.; Yang, M.; Song, Y.; Zhang, H. Facile Shape-controlled Synthesis of Luminescent Europium Benzene-1,3,5-tricarboxylate Architectures at Room Temperature. *CrystEngComm* **2009**, *11*, 2622–2628.

(175) Liu, K.; You, H.; Jia, G.; Zheng, Y.; Huang, Y.; Song, Y.; Yang, M.; Zhang, L.; Zhang, H. Hierarchically Nanostructured Coordination Polymer: Facile and Rapid Fabrication and Tunable Morphologies. *Cryst. Growth Des.* **2010**, *10*, 790–797.

(176) Deng, H.; Liu, C.; Yang, S.; Xiao, S.; Zhou, Z.-K.; Wang, Q.-Q. Additive-mediated Splitting of Lanthanide Orthovanadate Nanocrystals in Water: Morphological Evolution From Rods to Sheaves and to Spherulites. *Cryst. Growth Des.* **2008**, *8*, 4432–4439.

(177) Lee, I.; Choi, S.; Lee, H. J.; Oh, M. Hollow Metal-Organic Framework Microparticles Assembled Via a Self-Templated Formation Mechanism. *Cryst. Growth Des.* **2015**, *15*, 5169–5173.

(178) Zhu, M.; Jasinski, J. B.; Carreon, M. A. Growth of Zeolitic Imidazolate Framework-8 Crystals From the SolidLiquid Interface. *J. of Mater. Chem.* **2012**, *22*, 7684.

(179) Behrens, K.; Mondal, S. S.; Nöske, R.; Baburin, I. A.; Leoni, S.; Günter, C.; Weber, J.; Holdt, H.-J. Microwave-Assisted Synthesis of Defects Metal-Imidazolate-Amide-Imidate Frameworks and Improved CO_2 Capture. *Inorg. Chem.* **2015**, *54*, 10073–10080.

(180) Masoomi, M. Y.; Morsali, A. Sonochemical Synthesis of Nanoplates of Two Cd(II) Based Metal–Organic Frameworks and Their Applications as Precursors for Preparation of Nano-materials. *Ultrason. Sonochem.* **2016**, *28*, 240–249.

(181) Schäfer, P.; van der Veen, M. A.; Domke, K. F. Unraveling a Two-step Oxidation Mechanism in Electrochemical Cu-MOF Synthesis. *Chem. Commun.* **2016**, *52*, 4722–4725.

(182) Van Assche, T. R.; Campagnol, N.; Muselle, T.; Terryn, H.; Fransaer, J.; Denayer, J. F. On Controlling the Anodic Electrochemical Film Deposition of HKUST-1 Metal–organic Frameworks. *Micropor. Mesopor. Mater.* **2016**, *224*, 302–310.

(183) Campagnol, N.; Van Assche, T.; Stappers, L.; Dincă, M.; Denayer, J. F. M.; Binnemans, K.; De Vos, D. E.; Fransaer, J. On the Electrochemical Deposition of Metal-Organic Frameworks. *J. Mater. Chem. A* **2016**, *4*, 3914–3925.

(184) Choi, H.-S.; Lee, S.-J.; Bae, Y.-S.; Choung, S.-J.; Im, S. H.; Kim, J. Scalable Continuous Solvo-jet Process for ZIF-8 Nanoparticles. *Chem. Eng. J.* **2015**, *266*, 56–63.

(185) Avci, C.; Ariñez-Soriano, J.; Carné-Sánchez, A.; Guillerm, V.; Carbonell, C.; Imaz, I.; Maspoch, D. Post-Synthetic Anisotropic Wet-Chemical Etching of Colloidal Sodalite ZIF Crystals. *Angew. Chem. Int. Ed.* **2015**, *54*, 14417–14421.

(186) Diring, S.; Furukawa, S.; Takashima, Y.; Tsuruoka, T.; Kitagawa, S. Controlled Multiscale Synthesis of Porous Coordination Polymer in Nano/micro Regimes. *Chem. Mater.* **2010**, *22*, 4531–4538.

(187) Tsuruoka, T.; Furukawa, S.; Takashima, Y.; Yoshida, K.; Isoda, S.; Kitagawa, S. Nanoporous Nanorods Fabricated by Coordination Modulation and Oriented Attachment Growth. *Angew. Chem. Int. Ed.* **2009**, *48*, 4739–4743.

(188) Pham, M.-H.; Vuong, G.-T.; Fontaine, F.-G.; Do, T.-O. Rational Synthesis of Metal–Organic Framework Nanocubes and Nanosheets Using Selective Modulators and Their Morphology-Dependent Gas-Sorption Properties. *Cryst. Growth Des.* **2012**, *12*, 3091–3095.

(189) Yuan, Y.; Wang, W.; Qiu, L.; Peng, F.; Jiang, X.; Xie, A.; Shen, Y.; Tian, X.; Zhang, L. Surfactant-assisted Facile Synthesis of Fluorescent Zinc Benzenedicarboxylate Metal–Organic Framework Nanorods With Enhanced Nitrobenzene Explosives Detection. *Mater. Chem. Phys.* **2011**, *131*, 358–361.

(190) Li, D.; Wang, H.; Zhang, X.; Sun, H.; Dai, X.; Yang, Y.; Ran, L.; Li, X.; Ma, X.; Gao, D. Morphology Design of IRMOF-3 Crystal by Coordination Modulation. *Cryst. Growth Des.* **2014**, *14*, 5856–5864.

(191) Jian, M.; Liu, B.; Liu, R.; Qu, J.; Wang, H.; Zhang, X. Water-based Synthesis of Zeolitic Imidazolate Framework-8 With High Morphology Level at Room Temperature. *RSC Adv.* **2015**, *5*, 48433–48441.

(192) Cheng, X.; Zhang, A.; Hou, K.; Liu, M.; Wang, Y.; Song, C.; Zhang, G.; Guo, X. Size- and Morphology-controlled NH_2-MIL-53(Al) Prepared in DMF–water Mixed Solvents. *Dalton Trans.* **2013**, *42*, 13698–13705.

(193) Asha, K. S.; Kavyasree, P. R.; George, A.; Mandal, S. The Role of Solvents in Framework Dimensionality and Their Effect on Band Gap Energy. *Dalton Trans.* **2015**, *44*, 1009–1016.

(194) Wang, F.; Guo, H.; Chai, Y.; Li, Y.; Liu, C. The Controlled Regulation of Morphology and Size of HKUST-1 by "Coordination Modulation Method". *Micropor. Mesopor. Mater.* **2013**, *173*, 181–188.

(195) Guo, H.; Zhu, Y.; Wang, S.; Su, S.; Zhou, L.; Zhang, H. Combining Coordination Modulation With Acid-Base Adjustment for the Control Over Size of Metal-Organic Frameworks. *Chem. Mater.* **2012**, *24*, 444–450.

(196) Xin, C.; Zhan, H.; Huang, X.; Li, H.; Zhao, N.; Xiao, F.; Wei, W.; Sun, Y. Effect of Various Alkaline Agents on the Size and Morphology of Nano-sized HKUST-1 for CO_2 Adsorption. *RSC Adv.* **2015**, *5*, 27901–27911.

(197) Liu, K.; Shen, Z.-R.; Li, Y.; Han, S.-D.; Hu, T.-L.; Zhang, D.-S.; Bu, X.-H.; Ruan, W.-J. Solvent Induced Rapid Modulation of Micro/nano Structures of Metal Carboxylates Coordination Polymers: Mechanism and Morphology Dependent Magnetism. *Sci. Rep.* **2014**, *4*, 6023.

(198) Liu, Y.; Gao, P.; Huang, C.; Li, Y. Shape- and Size-dependent Catalysis Activities of Iron-terephthalic Acid Metal–Organic Frameworks. *Sci. China Chem.* **2015**, *58*, 1553–1560.

(199) Centonze, V.; Pawley, J. B. Tutorial on Practical Confocal Microscopy and Use of the Confocal Test Specimen. *Handb. Biol. Confocal Microsc. Third Ed.* **2006**, 627–649.

(200) Bonilla, G.; Tsapatsis, M.; Vlachos, D. G.; Xomeritakis, G. Fluorescence Confocal Optical Microscopy Imaging of the Grain Boundary Structure of Zeolite MFI Membranes Made by Secondary (seeded) Growth. *J. Memb. Sci.* **2001**, *182*, 103–109.

(201) Falcaro, P. et al. A New Method to Position and Functionalize Metal–Organic Framework Crystals. *Nat. Commun.* **2011**, *2*, 237.

(202) Zanchetta, E.; Malfatti, L.; Ricco, R.; Styles, M. J.; Lisi, F.; Coghlan, C. J.; Doonan, C. J.; Hill, A. J.; Brusatin, G.; Falcaro, P. ZnO as an Efficient Nucleating Agent for Rapid, Room Temperature Synthesis and Patterning of Zn-Based Metal-Organic Frameworks. *Chem. Matter.* **2015**, *27*, 690–699.

(203) Conato, M. T.; Jacobson, A. J. Control of Nucleation and Crystal Growth Kinetics of MOF-5 on Functionalized Gold Surfaces. *Micropor. Mesopor. Mater.* **2013**, *175*, 107–115.

(204) Kulkarni, S. A.; Kadam, S. S.; Meekes, H.; Stankiewicz, A. I.; ter Horst, J. H. Crystal Nucleation Kinetics From Induction Times and Metastable Zone Widths. *Cryst. Growth Des.* **2013**, *13*, 2435–2440.

(205) Hirai, K.; Reboul, J.; Morone, N.; Heuser, J. E.; Furukawa, S.; Kitagawa, S. Diffusion-coupled Molecular Assembly: Structuring of Coordination Polymers Across Multiple Length Scales. *J. Am. Chem. Soc.* **2014**, *136*, 14966–14973.

(206) Cravillon, J.; Nayuk, R.; Springer, S.; Feldhoff, A.; Huber, K.; Wiebcke, M. Controlling Zeolitic Imidazolate Framework Nano- and Microcrystal Formation: Insight Into Crystal Growth by Time-Resolved In Situ Static Light Scattering. *Chem. Mater.* **2011**, *23*, 2130–2141.

(207) Hikov, T.; Schröder, C. A.; Cravillon, J.; Wiebcke, M.; Huber, K. In Situ Static and Dynamic Light Scattering and Scanning Electron Microscopy Study on the Crystallization of the Dense Zinc Imidazolate Framework ZIF-zni. *Phys. Chem. Chem. Phys.* **2012**, *14*, 511–521.

(208) Cravillon, J.; Münzer, S.; Lohmeier, S.-J.; Feldhoff, A.; Huber, K.; Wiebcke, M. Rapid Room-Temperature Synthesis and Characterization of Nanocrystals of a Prototypical Zeolitic Imidazolate Framework. *Chem. Mater.* **2009**, *21*, 1410–1412.

(209) Hermes, S.; Witte, T.; Hikov, T.; Zacher, D.; Bahnmüller, S.; Langstein, G.; Huber, K.; Fischer, R. A.; Bahnmueller, S.; Langstein, G.; Huber, K.; Fischer, R. A. Trapping Metal–Organic Framework Nanocrystals: An In-situ Time-resolved Light Scattering Study on the Crystal Growth of MOF-5 in Solution. *J. Am. Chem. Soc.* **2007**, *129*, 5324–5325.

(210) Zacher, D.; Liu, J.; Huber, K.; Fischer, R. A. Nanocrystals of $[Cu_3(btc)_2]$ (HKUST-1): a Combined Time-resolved Light Scattering and Scanning Electron Microscopy Study. *Chem. Commun.* **2009**, 1031–1033.

(211) Majano, G.; Pérez-Ramírez, J. Room Temperature Synthesis and Size Control of HKUST-1. *Helv. Chim. Acta* **2012**, *95*, 2278–2286.

(212) Kumar, U.; Thomas, J.; Thirupathi, N. Factors Dictating the Nuclearity/Aggregation and Acetate Coordination Modes of Lutidine-Coordinated Zinc(II) Acetate Complexes. *Inorg. Chem.* **2010**, *49*, 62–72.

(213) Saxena, P.; Thirupathi, N. Reactions of $Cd(OAc)_2 \cdot 2H_2O$ With Variously Substituted Pyridines. Efforts to Unravel the Factors That Determine Structure/nuclearity of the Products. *Polyhedron* **2015**, *98*, 238–250.

(214) Zakaria, M. B.; Hu, M.; Tsujimoto, Y.; Sakka, Y.; Suzuki, N.; Kamachi, Y.; Imura, M.; Ishihara, S.; Ariga, K.; Yamauchi, Y. Controlled Crystallization of Cyano-Bridged Cu-Pt Coordination Polymers With Two-Dimensional Morphology. *Chem. Asian J.* **2014**, *9*, 1511–1514.

(215) Burrows, A. D.; Fisher, L. C.; Richardson, C.; Rigby, S. P. Selective Incorporation of Functional Dicarboxylates Into Zinc Metal–Organic Frameworks. *Chem. Commun.* **2011**, *47*, 3380–3382.

(216) Taulelle, F.; Haouas, M.; Gerardin, C. NMR of Microporous Compounds: From In Situ Reactions to Solid Paving. **1999**, *158*, 299–311.

(217) Gerardin, C.; Haouas, M.; Lorentz, C.; Taulelle, F. NMR Quantification in Hydrothermal In Situ Syntheses. *Magn. Reson. Chem.* **2000**, *38*, 429–435.

(218) Haouas, M.; Volkringer, C.; Loiseau, T.; Férey, G.; Taulelle, F. In Situ NMR, Ex Situ XRD and SEM Study of the Hydrothermal Crystallization of Nanoporous Aluminum Trimesates MIL-96, MIL-100, and MIL-110. *Chem. Mater.* **2012**, *24*, 2462–2471.

(219) Goesten, M. G.; Magusin, P. C. M. M.; Pidko, E. A.; Mezari, B.; Hensen, E. J.; Kapteijn, F.; Gascon, J. Molecular Promoting of Aluminium Metal–Organic Framework Topology MIL-101 by N,N-dimethylformamide. *Inorg. Chem.* **2014**, *53*, 882–887.

(220) Glish, G. L.; Vachet, R. W. The Basics of Mass Spectrometry in the Twenty-first Century. *Nat. Rev. Drug Discov.* **2003**, *2*, 140–150.

(221) El-Aneed, A.; Cohen, A.; Banoub, J. Mass Spectrometry, Review of the Basics: Electrospray, MALDI, and Commonly Used Mass Analyzers. *Appl. Spectrosc. Rev.* **2009**, *44*, 210–230.

(222) Fenn, J. B.; Mann, M.; Meng, C. K.; Wong, S. F.; Whitehouse, C. M. Electrospray Ionization for Mass Spectrometry of Large Biomolecules. *Science* **1989**, *246*, 64–71.

(223) Yamaguchi, K. Cold-Spray Ionization Mass Spectrometry: Applications in Structural Coordination Chemistry. *Mass Spectrom.* **2013**, *2*, S0012.

(224) Rood, J. A.; Boggess, W. C.; Noll, B. C.; Henderson, K. W. Assembly of a Homochiral, Body-Centered Cubic Network Composed of Vertex-Shared Mg_{12} Cages: Use of Electrospray Ionization Mass Spectrometry to Monitor Metal Carboxylate Nucleation. *J. Am. Chem. Soc.* **2007**, *129*, 13675–13682.

(225) Bai, Y. L.; Tao, J.; Huang, R. B.; Zheng, L. S. The Designed Assembly of Augmented Diamond Networks From Predetermined Pentanuclear Tetrahedral Units. *Angew. Chem. Int. Ed.* **2008**, *47*, 5344–5347.

(226) Lim, I. H.; Schrader, W.; Schüth, F. Insights Into the Molecular Assembly of Zeolitic Imidazolate Frameworks by ESI-MS. *Chem. Mater.* **2015**, *27*, 3088–3095.

(227) Seeber, G.; Cooper, G. J. T.; Newton, G. N.; Rosnes, M. H.; Long, D.-L.; Kariuki, B. M.; Kögerler, P.; Cronin, L. Following the Self Assembly of Supramolecular MOFs Using X-ray Crystallography and Cryospray Mass Spectrometry. *Chem. Sci.* **2010**, *1*, 62–67.

(228) Wagia, R.; Strashnov, I.; Anderson, M. W.; Attfield, M. P. Determination of the Preassembled Nucleating Units That Are Critical for the Crystal Growth of the Metal-Organic Framework CdIF-4. *Angew. Chem. Int. Ed.* **2016**, *55*, 9075–9079.

(229) Petersen, T. D.; Balakrishnan, G.; Weeks, C. L. MOF Crystal Growth: UV Resonance Raman Investigation of Metal-ligand Binding in Solution and Accelerated Crystal Growth Methods. *Dalt. Trans.* **2015**, *44*, 12824–12831.

(230) Ma, X.; Yuan, W.; Bell, S. E. J.; James, S. L. Better Understanding of Mechanochemical Reactions: Raman Monitoring Reveals Surprisingly Simple 'Pseudo-fluid' Model for a Ball Milling Reaction. *Chem. Commun.* **2014**, *50*, 1585.

(231) Gracin, D.; Štrukil, V.; Friščic, T.; Halasz, I.; Užarevic, K. Laboratory Real-time and In Situ Monitoring of Mechanochemical Milling Reactions by Raman Spectroscopy. *Angew. Chemie - Int. Ed.* **2014**, *53*, 6193–6197.

(232) Lee, W. R.; Ryu, D. W.; Phang, W. J.; Park, J. H.; Hong, C. S. Charge Effect of Foreign Metal Ions and the Crystal Growth Process in Hybridized Metal–Organic Frameworks. *Chem. Commun.* **2012**, *48*, 10847–10849.

(233) Ban, Y.; Li, Y.; Peng, Y.; Jin, H.; Jiao, W.; Liu, X.; Yang, W. Metal-Substituted Zeolitic Imidazolate Framework ZIF-108: Gas-Sorption and Membrane-Separation Properties. *Chem. Eur. J.* **2014**, *20*, 11402–11409.

(234) Yang, X.; Clark, A. E. Preferential Solvation of Metastable Phases Relevant to Topological Control Within the Synthesis of Metal–Organic Frameworks. *Inorg. Chem.* **2014**, *53*, 8930–8940.

(235) Tafipolsky, M.; Amirjalayer, S.; Schmid, R. First-principles-derived Force Field for Copper Paddle-wheel-based Metal–Organic Frameworks. *J. Phys. Chem. C* **2010**, *114*, 14402–14409.

(236) Amirjalayer, S.; Tafipolsky, M.; Schmid, R. Surface Termination of the Metal-Organic Framework HKUST-1: A Theoretical Investigation. *J. Phys. Chem. Lett.* **2014**, *5*, 3206–3210.

(237) Cantu, D. C.; McGrail, B. P.; Glezakou, V.-A. Formation Mechanism of the Secondary Building Unit in a Chromium Terephthalate Metal-Organic Framework. *Chem. Mater.* **2014**, *26*, 6401–6409.

(238) Yoneya, M.; Tsuzuki, S.; Aoyagi, M. Simulation of Metal–Organic Framework Self-assembly. *Phys. Chem. Chem. Phys.* **2015**, *17*, 8649–8652.

(239) Umemura, A.; Diring, S.; Furukawa, S.; Uehara, H.; Tsuruoka, T.; Kitagawa, S. Morphology Design of Porous Coordination Polymer Crystals by Coordination Modulation. *J. Am. Chem. Soc.* **2011**, *133*, 15506–15513.

(240) Anderson, M. W.; Gebbie-Rayet, J. T.; Hill, A. R.; Farida, N.; Attfield, M. P.; Cubillas, P.; Blatov, V. A.; Proserpio, D. M.; Akporiaye, D.; Arstad, B.; Gale, J. D. Predicting Crystal Growth Via a Unified Kinetic Three-dimensional Partition Model. *Nature* **2017**, *544*, 456–459.

(241) Hughes, C. E.; Williams, P. A.; Keast, V. L.; Charalampopoulos, V. G.; Edwards-Gau, G. R.; Harris, K. D. M. New In Situ Solid-state NMR Techniques for Probing the Evolution of Crystallization Processes: Pre-nucleation, Nucleation and Growth. *Faraday Discuss.* **2015**, *179*, 115–140.

16 Graphical TOC Entry